NTNU – Trondheim
Norwegian University of
Science and Technology

High voltage wound-rotor induction machines - harmonic field effects and power quality issues

Torstein Kastet

Master of Energy and Environmental Engineering
Submission date: June 2015
Supervisor: Trond Toftevaag, ELKRAFT

Norwegian University of Science and Technology
Department of Electric Power Engineering

Abstract

The last few decades, harmonic content in the power system has increased dramatically, due to more complex power systems containing more power electronics and other nonlinear loads. The background for this work is a severe voltage quality problem causing lighting flicker at low voltage end consumers in a rural area in Norway. It is assumed that interharmonic components occurring close to the 5^{th} and the 7^{th} harmonic frequencies, creating a beat interaction with the associated integer harmonic components, resulted in the low frequent voltage disturbance. These interharmonic components occur during operation of three large high-voltage wound-rotor induction motors installed at a hydro pumping station. The main objective of this work is to investigate the source of the interharmonic components.

A mathematical description of a rotor-stator interaction is presented. Here, an integer harmonic component in machine rotor is reflected through the air gap over to machine stator. In machine stator reference frame, this component occur as an interharmonic component at a different frequency, due to machine slip. For this to happen, an integer harmonic component is required as the source for the interharmonic.

To investigate this, laboratory tests on an induction machine in the laboratory at NTNU is conducted. A six-pulse, diode rectifier is used as a harmonic source, feeding the motor with harmonics. In addition, a large upstream inductance is connected. This inductance reduces network strength and allow the machine and the rectifier to distort the voltage. Simulations and calculations are carried through to verify functionality of laboratory setup.

In the laboratory tests no interharmonic component occur when an external harmonic source feed the motor with harmonics. However, when the external harmonic source is disconnected, the induction motor generates interharmonic components by itself. It is noted that a weak grid is necessary for the interharmonic components to occur in machine voltage and that a stiff network do suppress the interharmonic components generated by the motor.

Test results indicate that the induction motors at the hydro pumping station are the harmonic sources themselves. It is considered very likely that induction machines at the pumping station generate harmonics in rotor. Then, a rotor-stator interaction reflects rotor harmonics to machine stator, occurring at an interharmonic frequency, due to machine slip. Calculations of the interharmonic frequencies are very close to verify a rotor-stator interaction. Deviations of around 1 % separate measured and calculated frequencies. It is concluded that these deviations could be caused by a combination of inaccuracy in measurement equipment, machine rotor speed and by data quality reduction during post processing of data.

Further, laboratory tests show that a beat phenomenon between two harmonic components could occur in any wound-rotor induction machine. A weak power grid or a harmonic resonance could result in power quality issues.

Sammendrag

De siste tiårene har harmonisk innhold i kraftsystemet økt kraftig, grunnet mer komplekse kraftsystemer med mer kraftelektronikk og annen ulineær last. Bakgrunnen for dette arbeidet er et alvorlig spenningskvalitetsproblem som skapte lysflimmer hos lavspennigskunder i et utkantstrøk av Norge. Det er antatt at interharmoniske komponenter som oppstår nært de 5. og 7. harmoniske frekvensene, samvirker med sine tilhørende heltallsharmoniske og lager en «beat», som resulterer i lavfrekvente spenningsforstyrrelser i nettet. De interharmoniske komponentene oppstår under drift av tre store høyspennings- induksjonsmaskiner med viklet rotor, installert på en pumpestasjon i forbindelse med et vannkraftverk. Hovedmålet med dette arbeidet er å undersøke kilden til de harmoniske komponentene.

En matematisk beskrivelse av en rotor-stator virkning er gitt. Den beskriver en heltallsharmonisk komponent i maskinens rotor som reflekteres gjennom luftgapet til maskinens stator. I statorens referansesystem vil denne komponenten oppstå som en interharmonisk komponent ved en annen frekvens, grunnet maskinens sakking. For at dette skal skje må det finnes en heltallsharmonisk komponent i maskinen som kan lage den interharmoniske komponenten.

For å undersøke dette er laboratorietester utført på en asynkronmaskin i laboratoriet ved NTNU. En sekspuls diodelikeretter er brukt som harmonisk kilde som mater motoren med harmoniske. I tillegg er en stor induktans installert oppstrøms for maskinen. Induktansen reduserer styrken på nettet og tillater maskinen og likeretteren å forvrenge spenningen. Simuleringer og utregninger er utført for å bekrefte lab-oppsettets funksjonalitet.

Laboratorieforsøkene viser at det ikke oppstår interharmoniske komponenter når en ekstern harmonisk kilde mater motoren med harmoniske komponenter. Når denne kilden er frakoblet genererer imidlertid asynkronmotoren interharmoniske komponenter selv. Det påpekes at et mykt nett er nødvendig for at de interharmoniske komponentene skal oppstå i maskinens spenning og at et stivt nett undertrykker de interharmoniske komponentene motoren genererer.

Testresultatene indikerer at asynkronmaskinene ved pumpekraftverket selv er kilde til de harmoniske komponentene. Det er vurdert som svært sannsynlig at asynkronmaskinene ved pumpekraftverket genererer harmoniske i rotor. En rotor-stator virkning reflekterer de harmoniske i rotoren over til maskinens stator, og oppstår ved en interharmonisk frekvens grunnet maskinens sakking. Utregninger av den interharmoniske frekvensen er svært nær å bekrefte en rotor-stator virkning. Avvik på rundt 1 % skiller målte og utregnede frekvenser. Det er konkludert med at disse avvikene kan skyldes en kombinasjon av unøyaktighet i måleutstyr, maskinens rotasjonshastighet og at kvaliteten på måledataene kan ha blitt svekket ved postprosessering av måledataene.

Videre viste laboratorieforsøkene at en «beat»-virkning mellom to harmoniske komponenter kan oppstå i enhver viklet asynkronmaskin. Et svakt kraftnett eller harmonisk resonans kan resultere i spenningskvalitetsproblemer.

Preface

This Master's thesis is a continuation of the Specialization project conducted in autumn 2014. Still, it is an independent work, not relying on the Specialization project. Therefore, some elements of the Specialization project have been reused in this work, to make the work complete. However, some knowledge of previous work performed regarding this phenomenon, including the Specialization project is beneficial for the reader.

The work is largely an investigation of a given voltage quality problem in a distribution network operated by a Norwegian utility, NTE Nett AS. Literature study, simulations and preparation and conduction of laboratory work has been conducted. Matlab, Simulink and Elspec Investigator have been used for simulations and post processing of measurement data. Basic understanding of electrical circuitry and induction machines is expected by the reader.

A lot of the already conducted work regarding this issue has been performed by my supervisor, Mr. Trond Toftevaag, which provided me with necessary information and support during the work. In preparation and designing of laboratory set-up, PhD student Atle Rygg Årdal was of great support. The laboratory set-up was built in cooperation with NTNU service personnel, Mr. Svein Erling Norum and Mr. Aksel Andreas Reitan Hanssen. In addition, Mr. Henrik Kirkeby and Mr. Helge Seljeseth at Sintef Energy Research contributed with support during laboratory work. Finally, professor Robert Nilssen at NTNU was an essential academic support for comprehension of harmonic fields in induction machines.

The work has been conducted in cooperation with NTNU and SINTEF Energy Research.

Trondheim, June 12, 2015

List of Figures

List of Tables

List of Equiment

All equipment with an ID number can be found in the NTNU archive, called Instrumentarkiv and is available online [18].

1. ELSPEC LTD, 4 ROGOWSKI AC- CURRENT COILS 0-300 A, ID NUMBER: H02-0167-01, -02, -03, -04
2. FLUKE, POWER HARMONIC ANALYZER, MODEL 41, ID NUMBER: H02-0079
3. ELSPEC LTD, ANALYZER NETWORK NOISE, ID NUMBER: H02-0194
4. FLUKE, CURRENT CLAMP AC, MODEL 801 - 5005, 1-500 A AC RMS, ID NUMBER: H02-0079-01
5. NTNU, SOFT START FOR TRANSFORMER AC 3 PHASE, ID NUMBER: R04-0166
6. TEKTRONIX, DIGITAL OSCILLOSCOPE, MODEL TDS 2014B, ID NUMBER: G04-0342
7. CARLO GAVAZZI, RPM MEASURING INSTRUMENT, MODEL MDI 40 TF1.D.2.A.XX.IX, ID NUMBER: N06-0075
8. NTNU, RECTIFIER 3 PAHSE BRIDGE, ID NUMBER: B02-0686
9. FLUKE, CURRENT CLAMP AC/DC, MODEL 80i-110s, ID NUMBER: I04-0521
10. SIEMENS, DC MACHINE USED AS LOAD FOR INDUCTION MACHINE, MODEL: 1GG5 116-OFK20, ID NUMBER: A01-0110
11. NEBB, INDUCTION MACHINE WOUND ROTOR, MODEL: MBUS 160 M4, ID NUMBER: A03-0060
12. TEKTRONIX, DIFFERENTIAL PROBE VOLTAGE, MODEL: P5200, ID NUMBER: I06-0486
13. NEBB, START UP RESISTANCE FOR INDUCTION MACHINE ROTOR, ID NUMBER: K01-0030
14. NTNU, 3 PHASE VARIABLE COIL, ID NMBER: K02-0072

Contents

Chapter 1

Introduction

1.1 Motivation and background

This Master's thesis is a continuation of the Specialization project conducted in autumn 2014. The background for the work is a severe voltage quality problem causing lighting flicker at low voltage end consumers in a rural area in Norway. Comprehensive investigations performed by the local network operator, Nord-Trøndelag Elektrisitetsverk (NTE), in cooperation with Sintef Energy Research eventually identified a nearby hydro pumping station as the disturbance source. The disturbance was caused by fluctuations in 5^{th} and 7^{th} harmonic components in the voltage at the pumping station. Further investigations showed that these fluctuations originated from interharmonic components occurring at frequencies close to the 5^{th} and 7^{th} harmonic frequencies. Interaction between the interharmonic component and the integer harmonic component caused a beat to occur in voltage and current.

It has been detected that harmonic resonance due to shunt connected capacitor banks connected at the hydro pumping station amplified the disturbance significantly. Therefore, capacitor banks were disconnected, improving voltage quality at low voltage end consumers dramatically.

However, the interharmonic component in voltage and current at the hydro pumping station is still present, and the source has not been identified. Providing an explanation for the harmonic source may help improve voltage quality at the hydro pumping station. In addition, understanding this disturbance phenomenon is important for improvement of network voltage quality in general.

1.2 Problem description

The Master's thesis work should comprise:

- Literature study, with focus on harmonic field effects in polyphase induction machines.
- Further analysis of already existing measurement data using amplitude spectrum plots or ELSPEC software.
- Modeling and simulation of harmonic generation in a power network, in order to clarify, among other things, the effect of grid stiffness on harmonic distortion and to prepare the (minimum) requirements that have to be put on a laboratory set-up for a proper laboratory-based analysis of this problem.
- Practical preparation and conduction of laboratory tests on wound-rotor induction machine supplied with voltage harmonics.
- Comparative analyses of laboratory results, simulations, calculations and already existing measurement data.

1.3 Limitations and scope of work

This work aims to provide an explanation for the origin of the harmonics causing the power quality disturbance reported by low voltage end users. Main focus will be to explain the existence of the interharmonic component. Further, an objective of the work is to investigate the described phenomenon through laboratory tests on an induction machine at NTNU. Necessary background work must be conducted, including literature study, simulations and preparation of laboratory work.

Laboratory tests performed in the laboratory at NTNU is performed on a machine that is not a replica of the machines at the hydro pumping station. Ideally, tests should have been performed on the machines at the pumping station, but they are in operation and are not available for testing. Earlier measurements from the hydro pumping station is available, and testing and measuring in this work is therefore limited to be performed on the machine in the laboratory at NTNU.

A computer simulation based investigation of harmonic generation by the motors at the hydro pumping station has not been attempted. That is largely due to lack of information about the machines. Winding structure and details about machine design has not been available, and machine supplier has not been willing to provide this information.

Chapter 2

Background

Since the 90's, harmonic content in the power system has increased dramatically [11]. This is due to more complex power systems containing more power electronics and other nonlinear loads [21]. The background for this Master's thesis work is a severe voltage quality problem first reported by end user customers in a rural area in Norway. The problem has been discussed in earlier papers, including an IEEEXplore-article from 2013 [9], and the Specialization project [12] working as a preliminary work for this Master's thesis. Customers complained about very poor lighting quality. The problem was described as slow, but distinct flicker, easily noticeable by the human eye. It was most severe in lighting equipment behind electrical dimmers. However, the problem only occurred at certain times during the day, without any obvious pattern.

The local grid company, Nord-Trøndelag Elektrisitetsverk (NTE), performed measurements to evaluate the situation. The first measurements did not reveal any large flicker levels or any rapid voltage changes that violates neither the Norwegian Power Quality Directive ('Forskrift om leveringskvalitet i kraftsystemet') nor the EN 50160 [15] [10]. However, the flicker was evidently there, as one of the complaining end users were able to record the clearly visible flicker on camera, while at the same time, only low disturbance levels were measured. The visible flicker had a frequency in the order of 2 Hz. Further investigations were therefore necessary and Sintef Energy Research was engaged. New measurements were now performed, using more advanced measurement instruments. Also, the customer

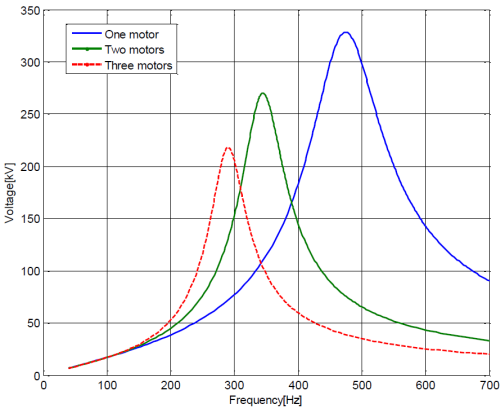

Figure 2.1: Frequency response of the local power grid (Simpow-simulation). Injection of 1 pu current on 6.6 kV node in hydro pumping station [23]

at the location of the measurements, was told to write down the time when the flicker occurred. In addition to the local measurements at end user, similar measurements were performed in the upstream distribution network.

The new measurements revealed voltage fluctuations dominated by the 7^{th} and partially the 5^{th} harmonic components. The 7^{th} harmonic magnitude was found to vary significantly in time. These observations resulted in even further investigations and measurements elsewhere in the grid. It turned out that the 7^{th} harmonic component could be observed in different parts of the network and that presence of the 7^{th} harmonic correlated 100 % with operation of a hydro pumping station nearby.

It soon became evident that the harmonics in some way was related to the three induction motors installed at the pumping station. However, the 2 Hz voltage variation remained a mystery and no obvious explanation were found in the literature. Each of the three motors are equipped with shunt-connected capacitor banks for reactive compensation. Simulations of the local power grid were performed to investigate the frequency response of the network. As can be seen from Figure 2.1, parallel resonance will occur in the frequency range around the 7^{th} harmonic component. In the simulation, injection of harmonic current is done in the upstream network. Therefore, in September 2013, the shunt capacitor banks installed at the pumping station were disconnected one by one, while measurements were performed. According to the measurements, the harmonic content was reduced by a factor of approximately 8 when all capacitor banks were disconnected. A schematic view of the hydro pumping station, where the induction machines are installed is depicted in Figure 2.2. Also, it is indicated where the measurements were performed.

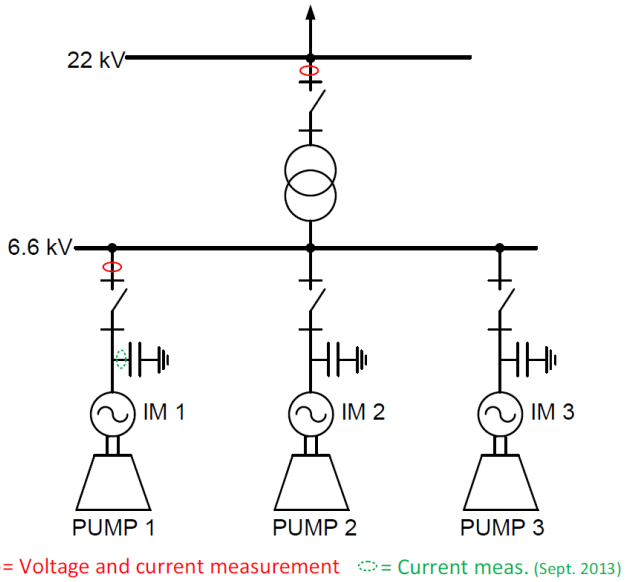

Figure 2.2: Schematic view of hydro pump station, indicating where measurements were performed.

7^{th} harmonic content and current resonance, mainly caused by the associated capacitor banks, was identified. However, this alone does not explain the pulsating disturbance. According to Elspec Investigator [4], the software associated to the measurement equipment that was used, RMS value of the 7^{th} harmonic varies in time with a frequency of 2 Hz. Further investigations indicated that the 2 Hz variation was caused by a beat interaction between a 7^{th} harmonic component and an interharmonic component at around 348 Hz. This is shown in Figure 2.3 and is discussed in detail in the Specialization project [12]. Also, a thorough description of the beat phenomenon is given in this work.

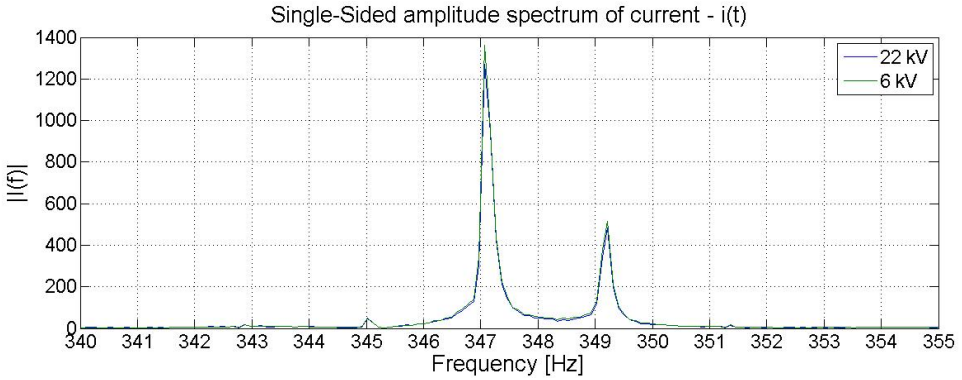

Figure 2.3: Amplitude spectrum of current at 6 kV side and 22 kV side of transformer for frequencies around the 7^{th} harmonic frequency. Data is taken from the 10 second interval 14:27:30 - 14:27:40, October 23, 2012. All three machines and capacitor banks are connected.

The 2 Hz variation is visible in the RMS value of the current at the hydro pumping station. In Figure 2.4, an Elspec Investigaor plot from October 2012 at the hydro pumping station, with all machines and capacitor banks connected, shows how the RMS value of the current vary. In addition to the 2 Hz variation depicted here, a 10 Hz wave in RMS current is observed when expanding the time window in Figure 2.4. This can be seen in the published article regarding this phenomenon from 2013 [9]. The 10 Hz waving is suspected to be related to an interaction between the three parallel connected machines at the hydro pumping station, since it only occur when all three machines are connected. Therefore, this phenomenon is not discussed in more detail here.

The source of neither of the harmonic components depicted in Figure 2.3 was determined in the work conducted in the Specialization project. Possible explanations were presented, but not tested or verified. A possible explanation for the interharmonic component is that a rotor-stator interaction transmit harmonics from rotor to stator in the induction machines. Due to machine slip, a harmonic component can occur at different frequencies in stator and rotor, creating the interharmonic component depicted in Figure 2.3. This was investigated in the Specialization project, but a conclusion was not given. Whether such interaction is present has not been determined, and the harmonic source is unknown. Therefore, further investigations are necessary.

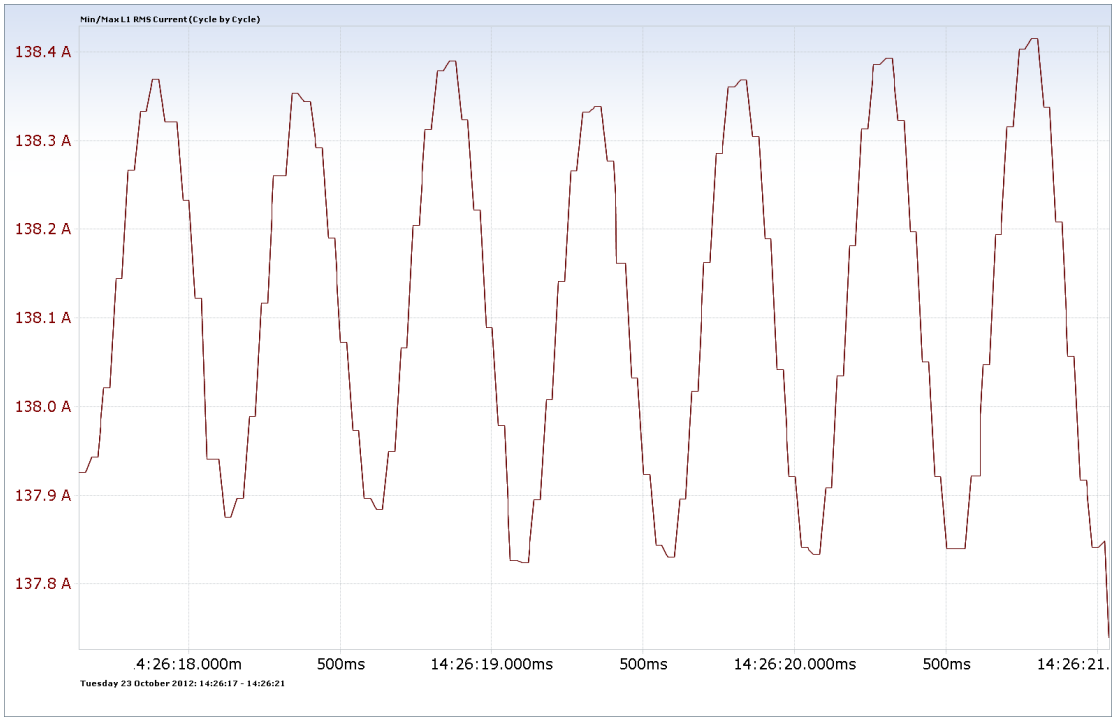

Figure 2.4: Elspec Investigator plot from October 2012 at the hydro pumping station, with all three machines and all three capacitor banks connected. The plot shows the RMS current at the 22 kV side over approximately 3.5 seconds. The RMS value varies from about 137.9 A to about 138.4 A. It is a small, but clear 2 Hz variation.

All three machines installed at the hydro pumping station are identical. Below, basic data for the asynchronous machines is given [23]:

- Nominal voltage: 6.6 kV
- Nominal frequency: 50 Hz
- Nominal power: 1.75 MW
- Nominal rotational speed: 742 rpm
- Rotor: wound rotor and slip rings connected to external resistance
- Starting method: External resistance in rotor circuit
- Capacitor banks for reactive compensation: 600 kVar (per machine)

Chapter 3

Harmonics in induction machines

Under most operating conditions, three phase current in the grid is not completely ideal. It contains a portion of harmonics which disturb the sinusoidal waves. In induction machines, flux waves are directly proportional to the input current. Therefore, harmonics in stator current can be seen both in the magnetic field of the machine and in the induced current in rotor, and vice versa. The grid is not necessarily the only harmonic source. The machine itself or power electronic equipment for controllability of the machine could create harmonic components. Normally, these harmonics are small relative to the fundamental current, but could still cause disturbances reducing machine efficiency and lifetime. In general, two kinds of harmonics could be present in an induction machine, time harmonics and space harmonics.

3.1 Time harmonics

Since the 90's, time harmonic content in the power system has increased dramatically [11]. This is due to more complex power systems containing more power electronics and other nonlinear loads [21]. If a sinusoidal voltage is applied to a nonlinear component, the current through the component will not be sinusoidal, as shown in Figure 3.1. This new waveform can be described by one cyclic waveform (the fundamental sinusoidal current) and a sum of sinusoidal functions with a frequency equal an integer multiple of the fundamental frequency [21]. These new functions are called integer harmonics, or simply harmonics. Time harmonics are functions of time and are simply a

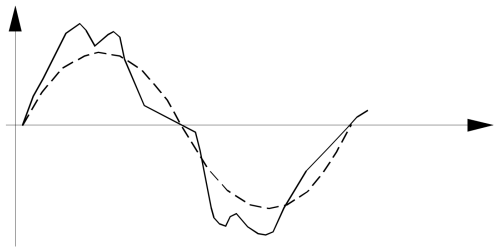

Figure 3.1: A perfect sinusoidal waveform (dotted line), and the same waveform with large harmonic content (solid line). [21, p. 3]

result of waveforms that do not vary completely sinusoidal in time. For a three phase induction machine, as considered in this work, different harmonic components have their own characteristics. Some harmonics are more often cause for concern than others, due to the nature of power systems.

A harmonic component occurring at a frequency that is not an integer multiple of the fundamental component is called an interharmonic component. In the Norwegian power system that means a frequency not a multiple of 50 Hz. Interharmonics are less normal than integer harmonics, but can be observed in an increasing number of loads. These loads include static frequency converters, cycloconverters, sub-synchronous converter cascades, induction motors, arc furnaces and all loads not pulsating synchronously with the fundamental power system frequency [8].

In a symmetrical and balanced three phase system (which more or less is the case for a normal power network) even harmonics cannot exist. For such system, the following relationship applies:

$$V(\omega t + \pi) = -V(\omega t) \tag{3.1}$$

, where $\omega = 2\pi f$ is the angular velocity and t is time. Now assuming the voltage contains a second harmonic component,

$$V(\omega t) = V_1 \times sin(\omega t) + V_2 \times sin(2\omega t) \tag{3.2}$$

, where the subscripts 1 and 2 denotes the first and second harmonics respectively. It is well known that if a waveform is shifted by θ degrees, its nth harmonic is shifted by $n\theta$ degrees [20, p. 42]. By using that relationship it can be seen that,

$$V(\omega t + \pi) = V_1 \times sin(\omega t + \pi) + V_2 \times sin(2\omega t + 2 \times \pi) \tag{3.3}$$

Now, the relationship from equation 3.1 can be used on equation 3.3,

$$V(\omega t + \pi) = -V_1 \times sin(\omega t) + V_2 \times sin(2\omega t) \tag{3.4}$$

Equation 3.4 should equal $-V(\omega t)$, as required by equation 3.1 for a symmetrical wave. Based on equation 3.2 it can further be said that

$$-V(\omega t) = -V_1 \times sin(\omega t) - V_2 \times sin(2\omega t) \tag{3.5}$$

It can be seen by comparing equation 3.4 and 3.5 (they should equal each other) that this can only happen if V_2 is zero, hence second harmonics cannot exist. This logic only holds as long as the three phase system is symmetric, which normally is the case. Exactly the same reasoning can be used for all even ordered harmonics, which therefore can be disregarded when considering harmonics in a three phase induction machine.

For 3^{th} harmonics the situation is different. We look at the following 3^{th} harmonic frequency components, one for each of the phases A, B and C.

$$V_{A3} = |V_3| \times sin(3w_1t) \tag{3.6}$$

$$V_{B3} = |V_3| \times sin(3w_1t - 3 \times \frac{2\pi}{3}) \tag{3.7}$$

$$V_{C3} = |V_3| \times sin(3w_1t - 3 \times \frac{4\pi}{3}) \tag{3.8}$$

It can be seen that phase B and C are one and two complete cycles, respectively, behind phase A. In other words, they are all in phase. Therefore, the total harmonic magnitude would be three times the magnitude of one 3^{th} harmonic. However, all three terminals would have the same potential (they are in phase) and current cannot flow from one phase to another. If the neutral point in a star connected system is grounded or connected to a return wire, the harmonic current can flow here. Inductions machines would normally have an isolated neutral and the machine would therefore be an open circuit to 3^{th} harmonics. If the machine is Δ-connected, all three 3^{th} harmonic components add together and drive a 3^{th} harmonic component around inside the Δ-winding of the machine. However, since the voltages drop across the internal impedance of the machine, there is again no significant 3^{th} harmonic component at the terminals of the machine [2, p. 646]. It can be shown that the same would apply to any triplen harmonic (whose order is a multiple of three), and these would therefore not affect the machine.

The 5^{th} harmonic is the lowest order harmonic component that often is problematic in asynchronous machines. Again, we look at three different 5^{th} harmonic components, one for each phase.

$$V_{A5} = |V_5| \times sin(5w_1t) \tag{3.9}$$

$$V_{B5} = |V_5| \times sin(5w_1t - 5 \times \frac{2\pi}{3}) = |V_5| \times sin(5w_1t - \frac{10\pi}{3}) = |V_5| \times sin(5w_1t - \frac{4\pi}{3}) \tag{3.10}$$

$$V_{C5} = |V_5| \times sin(5w_1t - 5 \times \frac{4\pi}{3}) = |V_5| \times sin(5w_1t - \frac{20\pi}{3}) = |V_5| \times sin(5w_1t - \frac{2\pi}{3}) \tag{3.11}$$

To obtain the last term of the equations, the same relationships and simplifications as used earlier were applied. It can be seen that these three voltages constitute a balanced three phase negative sequence system. In a negative sequence system, the phase order is reversed compared to a positive sequence system, so that phase C comes first, followed by phase B and then phase A. The voltages are therefore working in the opposite direction of the fundamental frequency. Hence, negative sequence currents and voltages contribute with negative torque.

7^{th} harmonic content could also be present in asynchronous machines. The equations are almost the same as for 5^{th} harmonic components.

$$V_{A7} = |V_7| \times \Big[sin(7w_1t)\Big] \tag{3.12}$$

$$V_{B7} = |V_7| \times \Big[sin(7w_1t - 7 \times \frac{2\pi}{3})\Big] = |V_7| \times \Big[sin(7w_1t - \frac{2\pi}{3})\Big] \tag{3.13}$$

$$V_{C7} = |V_7| \times \Big[sin(7w_1t - 7 \times \frac{4\pi}{3})\Big] = |V_7| \times \Big[sin(7w_1t - \frac{4\pi}{3})\Big] \tag{3.14}$$

It can be seen that these voltages constitute a balanced three phase positive sequence system, and will therefore contribute with a positive torque.

All higher ordered harmonics will behave equal to one of the foregoing harmonics. All even or triplen harmonics can be disregarded in induction machines, while harmonics of the order $n = 6k \pm 1$, where k is an integer greater than or equal to 1, can exist. Those harmonics generated by the plus-sign, 7, 13, 19 etc., rotates in positive direction, while those generated by the minus-sign rotates in opposite direction of the fundamental. Also, harmonics of higher orders are in general smaller and would therefore normally be less problematic than those of lower order [2, p. 646].

3.2 Space harmonics

Space harmonics are generated by a different source than time harmonics. Space harmonics in electrical machines are related to the slots distribution in space around the stator. Consider a single full-pitched coil connected to the power grid. The current in the coil and hence, the flux generated by the coil, would vary sinusoidally. If examined at one particular time instant, the MMF produced by this one coil, say coil 1 in Figure 3.2, would have a square waveform at the span of the coil, as depicted by the arrows [20]. When the current vary in time, the amplitude of this MMF would also vary sinusoidally in time.

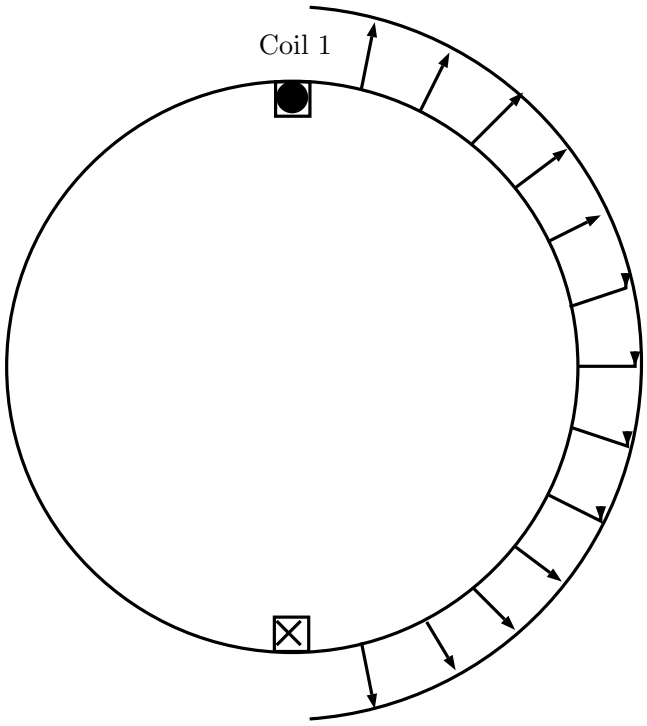

Figure 3.2: Single full-pitched coil, generating flux as depicted by arrows.

In a normal machine, the windings associated with each phase in stator are almost always distributed among several adjacent slots [2]. That means, new coils are connected in series with the first, still connected to the same phase. Say we have only one new coil, connected in series with the first. This second coil will be spatially displaced from the first one by a small angle, but their amplitude will vary identically in time. Thus, the MFF generated by this coil would be spatially displaced by the same angle. In Figure 3.3, these two MMFs are plotted together as a function of space angle along the air gap at a given time instant. These two MMF contributions will be superimposed and the resultant waveform will be as depicted in the blue graph in Figure 3.3. It can be seen that this waveform is far from a sinusoidal wave. Even if many more coils are connected close to each other, a perfect sinusoidal waveform will not be obtained. Other tricks, such as designing the rotor itself to distribute the flux in an approximately sinusoidal shape, or using fractional-pitch windings may be applied [2]. However, perfection is never obtained and this non sinusoidal distribution of flux in the air gap is what creates space harmonics in an asynchronous machine.

Space harmonics rotate in the same direction as time harmonics. Those harmonics generated by the plus-sign in $n = 6k \pm 1$, rotate in forward direction, while those generated by the minus-sign rotates in opposite direction of the fundamental [6, p. 121]. However, space harmonics in the magnetic field in the air gap of an induction machine rotate at a different speed than the fundamental component. The rotational speed of a space harmonic component is given as the rotational speed of the fundamental component divided by the space harmonic order. The

5^{th} harmonic component would rotate at $\frac{1}{5}$ of the fundamentals rotational speed, in the opposite direction of the fundamental. The 7^{th} harmonic component would rotate at $\frac{1}{7}$ of the fundamentals rotational speed, in the same direction as the fundamental.

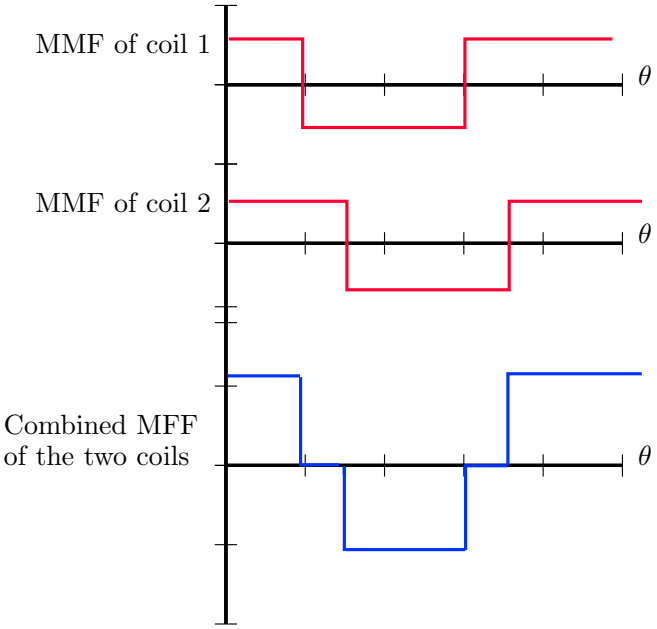

Figure 3.3: MMF of two series connected coils, spatially displaced by a small angle. The MMF is plotted as a function of space angle.

3.3 Mitigations

Some harmonic content in the power network is inevitable, but usually harmonics are very small in magnitude and cause little harm. Also, the magnitudes of the harmonics tend to decrease quite rapidly with the harmonic order. A rough rule of thump is that the harmonic magnitude decreases with the factor $\frac{1}{h}$, where h is the harmonic order. Therefore, the lowest order harmonics are usually of most concern. However, as described in the Specialization project [12], harmonic resonance could amplify the harmonic magnitude significantly and make even small harmonic components troublesome. To prevent resonance from happening, measures should be taken already in the planning phase. When designing networks, simulations should be performed to ensure that system resonance frequency does not occur at frequencies where harmonics are likely to be created. Also, filters that remove harmonics form the system can be created. For example, capacitors connected in parallel with a component could appear as a short circuit for high order harmonics. Such configurations are common in power systems to prevent harmonics from propagating through the network.

An important parameter for voltage quality in a power network is the short circuit level. High short circuit level means the impedance of the network is low. Low

network impedance result in less active and reactive power loss in power transmission, but also reduce voltage drop across the line. Seen from a voltage source perspective, downstream voltage drop will follow regular voltage division rules. If the voltage source can be regarded as stiff, the voltage will drop across the network impedance and the load impedance. If network impedance is very low compared to load impedance (high short circuit level), almost the entire voltage drop will be across the load, and the load will see almost the same voltage as generated by the stiff voltage source in the other end of the line. However, with a larger network impedance (relative to load impedance), voltage will drop significantly across the network, making the load see a lower voltage. Also, this voltage will be less stiff.

When voltage at load terminal is less stiff, the load is allowed more impact on the voltage. If this load draws harmonic current, voltage at the load terminal will be contaminated with these harmonics. In addition to affect that specific load, harmonics could propagate to nearby loads and affect them as well. If impedance between load terminals and the stiff voltage source is very small, load terminal voltage will not be influenced by the harmonic current. Therefore, high short circuit level is important to prevent harmonics in the voltage.

Even if harmonics are detected long after construction of the network, remedial actions could be performed. However, opportunities will be fewer and often more expensive. A measure that will always improve power quality is system reinforcement. Increasing short circuit level makes the system less vulnerable to all kinds of disturbance, reduce losses and increase voltage quality. However, at some point investments get to expensive and other measures must be considered.

Chapter 4

Beat phenomenon

Beating is a phenomenon most known from acoustics. The basic principle is that when two waves, traveling along the same medium, meet each other, they will interfere and create a new wave. The new wave will at all times be the sum, the superposition, of the two original waves. If the two original waves have different frequency, the time between each peak will be different for the two, and they will 'move' relative to each other, as shown in Figure 4.1. This is a plot created in Matlab, where a 50 Hz signal (red line) and a 60 Hz signal (blue line) is plotted together. The figure is only for illustration of the principle so the amplitude is set to be 1 and there is no unit on the y-axis.

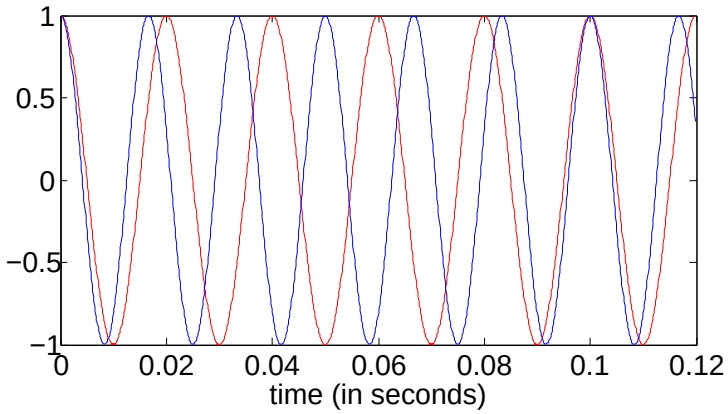

Figure 4.1: Two independent sinusoidal waveforms plotted together in the same graph over a period of 0.12 seconds. The red line is a 50 Hz wave. The blue line is a 60 Hz wave.

As Figure 4.1 shows, at some point two positive peaks will coincide and add together (at 0 and at 0.1 second in the graph in Figure 4.1). This is known as constructive interference [19]. However, if a positive peak from one wave coincide with a negative peak from the other wave, they will cancel each other out (at 0.05 second in the graph). This is known as destructive interference. From this it can be concluded that the resultant waveform will vary in amplitude as these two signals

alternate between interfering constructively and destructively. In acoustics, these variations in constructive and destructive interference makes themselves evident through volume variations. The volume rise and fall at what is called the beat frequency, which is the frequency of which constructive interferences occur, or the frequency of *beats* in the resultant waveform. The principle of signal superposition and beat does apply to all wave signals, including currents in a distribution line. The beat frequency is given by the absolute value of the difference in frequency between the two original waveforms, $f_{beat} = |f_1 - f_2|$. In this case, $f_{beat} = 60Hz - 50Hz = 10Hz$. The waves in Figure 4.1 are plotted over a time period of 0.12 seconds, to cover a full cycle (T) of the beat, which is $T = \frac{1}{f_{beat}} = \frac{1}{10} = 0.1$ seconds.

Figure 4.2 shows the two waveforms from Figure 4.1 superimposed into one new wave, which is the green line in Figure 4.2. The resultant wave is plotted over a longer time period (0.25 seconds) to show how the amplitude variation makes the signal beat repeatedly with a frequency of 10 Hz. In this simple example it is worth noting that during a beat, the resultant waveform reaches a magnitude equal the sum of the amplitudes of the original waves. Since both original waveforms have an amplitude of 1, the peak amplitude of the resultant waveform will be 2. A quick graphical examination of Figure 4.2 confirms both the beat frequency and the peak amplitude.

The black lines in Figure 4.2 are called the envelope of the beat. This is actually two sinusoidal waves, each with a frequency equal half the beat frequency and an amplitude equal two times the two original waves amplitude. They are added to show that the amplitude variation of the superimposed signal can be described by a sinusoidal function. As can be seen, these lines envelope the beat pattern created by the interference between the two waves and modulate the amplitude of the resultant wave.

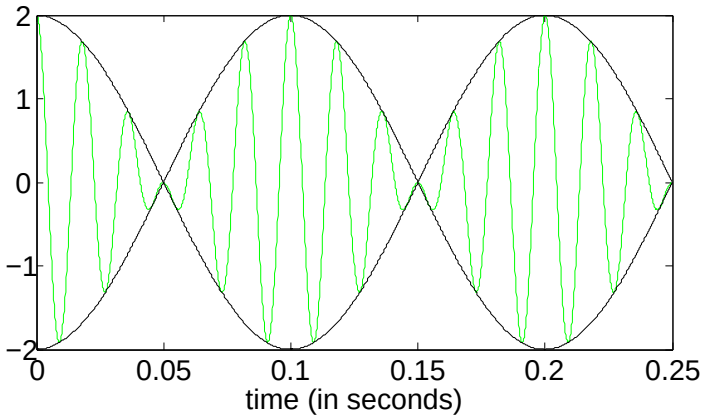

Figure 4.2: Two sinusoidal waveforms superimposed into one new waveform. The green line is the resultant wave. The black line indicates the envelope waveform.

The extremal points of this superimposed wave are simple to imagine, as a clean constructive interference double the amplitude, and a clean destructive interference cancel out the signal. However, in between these extremal points, the super-

imposed signal is also a sum of the two original waves, and it will have a value between the extremal values. The shape is smooth and looks similar to a sinusoidal shape varying in amplitude. In section A in the appendix, a wider examination of the beat phenomenon is given.

Chapter 5

Rectifiers

5.1 Rectifier concepts

A rectifier is a fairly simple an inexpensive electrical device that convert AC input to DC output by the use of diodes. This rectification is uncontrolled in the sense that the output is exclusively given by the input signal and there is no control circuit. Focus here will be on the three-phase rectifier. However, it is based on the even simpler single-phase rectifier, which also will be discussed.

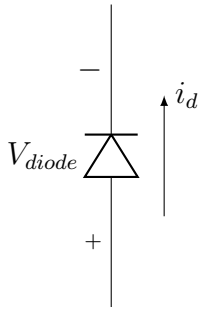

Figure 5.1: When the voltage potential V_{diode} across a diode is in the direction indicated, the diode allows a current i_d to flow. The diode is forward biased.

The concept of rectification is based on the operation of a diode, which we assume to be ideal. If the voltage across a diode is negative, the diode is reversed biased, and will not conduct current. When the voltage across the diode become positive, that is, the anode is at a higher potential than the cathode as indicated in Figure 5.1, the diode is forward biased and will allow current i_d to flow in the direction indicated. A diode only conducts current in one direction. This property of the diode can be exploited to convert AC input to DC.

5.2 Single-phase diode bridge rectifier

First, the basic operation of a simplified single-phase diode bridge rectifier will be described. In Figure 5.2, a single AC voltage source V_s is modeled as an ideal voltage source, without any internal impedance. Further, there are four ideal

diodes, D_1, D_2, D_3 and D_4, organized in a specific arrangement. We assume some load is connected to the DC side, so that DC current i_d can flow.

When V_s is positive, diode D_1 will see a positive voltage and be forward biased, hence conduct current. In contrast, there will be a negative voltage across D_4 which will block the current. Current from the source, i_s will therefore flow up through D_1. As the cathodes of diode D_1 and D_3 are at common potential and the anode of D_3 is connected to the negative side of V_s, D_3 will see a negative voltage V_s and be reversed biased. Anode side of D_2 has common potential with anode side of D_4. Cathode side of D_2 is connected to the negative side of V_s and will therefore see a positive voltage. Therefore, when V_s is positive, current i_s flow through diode D_1 and D_2. When polarity of V_s is reversed, voltage across all diodes switch and current flow will shift immediately. Now current will flow through diode D_3 and D_4, and i_s through the source will change direction. However, DC current i_d will flow in the same direction and the polarity of DC voltage V_d will not be reversed.

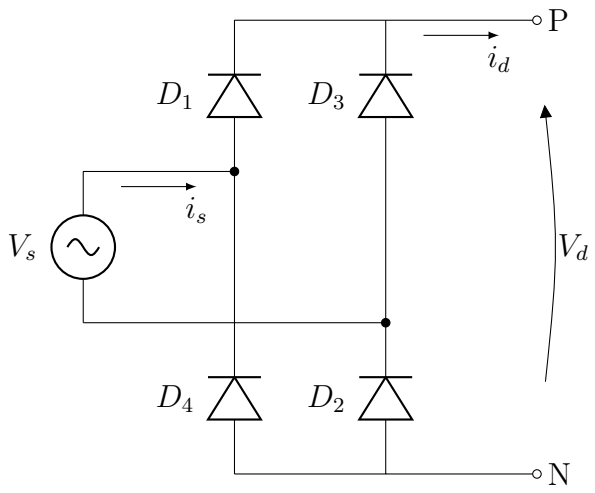

Figure 5.2: Single-phase diode bridge rectifier supplied by an ideal voltage source. Diodes D_1, D_2, D_3 and D_4 are arranged so that they convert the AC input to DC output.

The circuit in Figure 5.2 is idealized and several other factors would affect a real circuit. For example, the voltage source would in reality have an impedance, primarily inductive. This would affect the current commutation, the process of which current conduction shifts from one diode to another. This would no longer be instantaneous and a commutation interval would occur. Also, diodes are not ideal and will neither conduct without losses nor block all current, when being forward and reversed biased respectively. Also, the DC load, which is completely ignored in this example, could affect the operation of the rectifier.

5.3 Three-phase rectifier

A three phase rectifier is very similar to a single phase rectifier, only with a slightly more complex configuration. The three-phase, six-pulse, full bridge, diode rectifier shown in Figure 5.3, has only two more diodes than the single phase rectifier. Since it is a three phase rectifier, it is supplied by three ideal voltage sources, configured in a star connection. Again, diodes are assumed ideal and there is assumes some load connected to the DC side to allow a current i_d to flow.

The same rules for conducting applies to the diodes in a three-phase rectifier, as they did for a single phase rectifier. That means that at all times one diode in the top group, D_1, D_3 or D_5, and one in the bottom group, D_4, D_6 or D_2, will be conducting. In the top group, the diode with its anode at the highest potential will conduct, and the two others will be reversed biased. In the bottom group, the diode with its cathode at the lowest potential will conduct, while the other two become reversed biased. Current will commutate according to this rule and there will at all times flow a current i_d in the direction indicated in Figure 5.3 at the DC side.

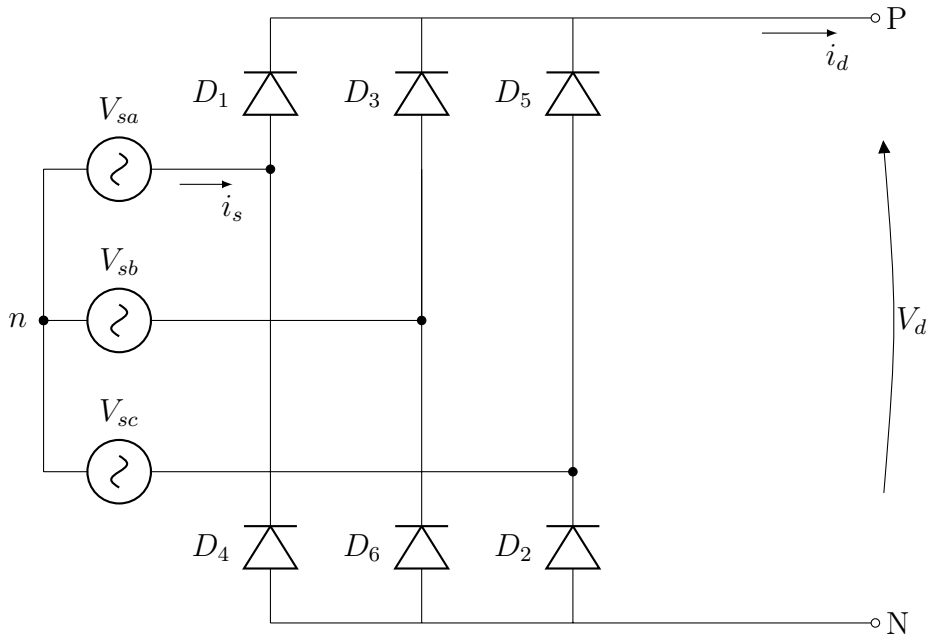

Figure 5.3: A three-phase, six-pulse, full-bridge diode rectifier supplied by three ideal voltage sources. Diodes D_1, D_2, D_3, D_4, D_5 and D_6 are arranged so that they convert the AC input to DC output.

The DC voltage V_d created by the rectifier in Figure 5.3 is not a flat DC voltage. In effect, the rectifier only cuts the top of the sinusoidal waves in the AC voltage. In Figure 5.4, the sinusoidal waves of an ideal three phase AC voltage system is sketched over a small time period. The rectifier in Figure 5.3 make sure that the potential at point P, with respect the neutral point n, called V_{Pn}, always is given

by the phase at the highest voltage potential. Similarly, the voltage potential at point N, called V_{Nn}, will at all times given by the phase with the lowest potential. The DC voltage will then be given by the difference, $V_d = V_{Pn} - V_{Nn}$.

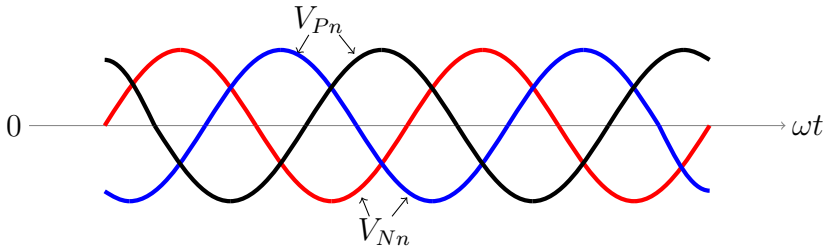

Figure 5.4: Three sinusoidal waves, red, blue and black line plotted together. They are 120 degrees out of phase of each other as in an ideal three phase power system.

The shape of the DC voltage created by the rectifier is depicted in Figure 5.5. It can be seen that V_d will consist of segments of sinusoidal waves, cut at the top. Per complete cycle of the AC voltage, 20 ms in a 50 Hz system, there will be six such sinusoidal segments, hence six-pulse rectifier. In a real rectifier there will be connected a large filter capacitor at the DC side to reduce voltage ripple. However, voltage from a rectifier will never be completely smooth. The current drawn by the DC load will depend on the voltage across it, though the current will be influenced by the load as well. An inductive load will smooth the current.

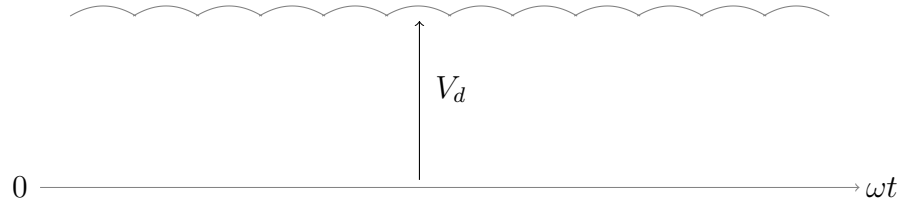

Figure 5.5: Depiction of the DC voltage V_d created by a three-phase, six-pulse rectifier. There is a significant voltage ripple.

5.4 Harmonic output by rectifiers

In the rectifier models described in the two previous sections, the voltage source has been described as an ideal voltage source. In reality this is not a complete model of an upstream power grid. There will always be some weakness in the network, making the voltage source less stiff. That means that the rectifier can potentially affect the voltage at AC side. It turns out that rectifiers do generate harmonics at AC side both in current and voltage, caused by the behavior of switching.

If the three-phase rectifier in Figure 5.3 or the single-phase rectifier in Figure 5.2 has a very large inductive load connected at DC side, DC current will be very

smooth. In such cases, it is possible to model the load as an ideal current source. If there is still no source impedance at AC side, there will at all times be a short circuit between DC load and AC source. A constant DC current i_d will then affect the source current i_s dramatically, making it a square wave. In Figure 5.6, this is illustrated for the single-phase rectifier in Figure 5.2. As described in more detail in section 3.1, harmonics occur when the voltage or current waves are non-sinusoidal in shape. The square wave i_s would create large harmonics in the AC side current.

Again, the analysis performed on the rectifier in Figure 5.2 is not completely accurate for a real system. Impedance in the voltage source or the rectifier itself, and other non-ideal conditions, will make the harmonic content look different. Distorted currents drawn by loads such as a diode bridge rectifier can result in distortion in the utility voltage waveform [17, p. 99].

In general it can be said that if line inductance is insignificant compared to the DC reactor inductance and DC current can be estimated as clean, the harmonic current frequencies created by a six-pulse three phase rectifier are some integer n times the fundamental frequency. The number n is given by the following formula:

$$n = 6k \pm 1 \tag{5.1}$$

, where $k = 1, 2, 3, 4, ...$ That means that there will be $5^{th}, 7^{th}, 11^{th}, 13^{th}...$ harmonic components created by the rectifier. The RMS values of the harmonic components decay by a factor of $\frac{1}{n}$. This means that harmonics of lower order usually are of most concern. These are all well known characteristics of the rectifier and are very important to be aware of when using a rectifier. [3, p. 9]

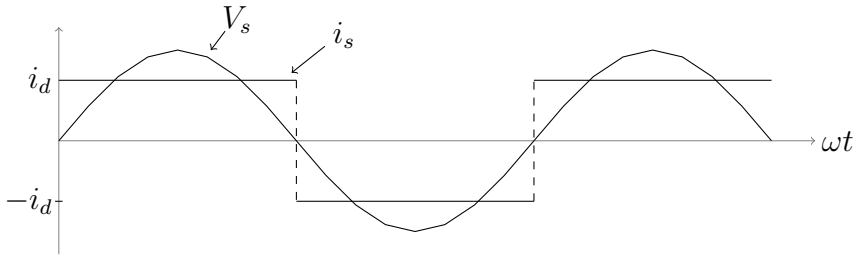

Figure 5.6: Voltage and current at AC side of a single-phase rectifier. The DC side is modeled as an ideal current source and there are no internal impedance in the voltage source. The squared waveform of the source current gives rise to harmonic content in the current.

Chapter 6

Fourier transform and representing signals in the frequency domain

6.1 Discrete Fourier transform

Discrete Fourier transform (DFT) is one of four categories of Fourier transform. For DFT to be applicable, the signal must be discrete and periodic. In the world of computers, all signals are represented in a discrete way, by some N number of values. The other categories of Fourier transform require either a continuous signal or a signal of infinite length [22]. A discrete signal in a computer can always be made periodic by imagining the signal has an infinite number of samples on the left and the right of the actual signal. If these points are duplications of the original signal, the signal is made periodic. Therefore, DFT is the only possible way to calculate a Fourier transform in a computer and this is the transform that will be focused here.

The principle of DFT is based on the Fourier theorem, which states that any continuous periodic signal can be represented as the sum of a series of sine or cosine terms, called Fourier series [13]. More specifically, if you have a discrete signal of N points, this can be decomposed into $\frac{N}{2}+1$ sine waves and $\frac{N}{2}+1$ cosine waves [22], each with a different frequency and amplitude. The sum of them will produce the original waveform. The frequency of these decomposed signals are not given in Hz, but in *number of complete cycles that occur over the N points of the signal*.

If the original discrete signal consists of 16 points, the decomposition would consist of nine cosine waves and nine sine waves. The first cosine wave would complete 0 cycles in the N points. This is often referred to as the DC offset. The next cosine wave would complete one cycle in the N points, then two, three and so on, up to 8, $\frac{N}{2}$, complete cycles. The same goes for the sine waves. These waves are commonly

called the *DFT basis functions* [22], an have unity amplitude. By assigning each of these basis functions the correct amplitude, the original signal is reproduced.

A precise mathematical description of how the frequency domain is obtained and the so called synthesis equation, which can be used to calculate the inverse DFT, can be found many places in the literature [22]. However, one more important point will be emphasized. The frequency domain is defined as a spectral density [22]. A spectral density describes how much signal (amplitude) is present per unit of bandwidth. To convert the sinusoidal amplitudes into a spectral density, divide each amplitude by the bandwidth represented by each amplitude. The point is that there is a difference between the value of the amplitudes of the sine and cosine waves needed to recreate the time domain signal and the values these frequency components are given in the frequency domain. This is only a simple normalization of the amplitudes, but it is important to be aware of.

6.2 Fast Fourier transform using MATLAB

The DFT can be calculated in different ways. However, the by far most efficient algorithm, and therefore the one almost always used, is called the Fast Fourier transform (FFT). The FFT algorithm itself is complicated and it is out of scope of this thesis to discuss the details in this algorithm. However, MATLAB has a built in FFT function that will be used in this work.

The FFT function is fairly straight forward to use and simply returns the DFT of the input vector. However, to process the data in a proper manner, it is important to be aware of how the data is returned. In this work the input vector will always be a vector containing the amplitude values of a signal in the time domain, with fixed time steps between the points. It should be noted that only the values on the y axis in a time domain signal are relevant to perform a DFT on the signal. The vector returned from the FFT function has a length equal the length of the input vector, call this length N. However, the returned vector contains a two-sided frequency spectrum, with values for both negative and positive frequencies. In reality, half of the signal has no real information because the two sides are completely symmetric and the negative frequency components are of no use for the purpose in this work. Therefore, the first half of the vector will be removed from the spectrum. What is left is a vector of length equal $\frac{N}{2} + 1$, where the 1 comes from frequency component 0, which is included and represent the DC component. Each object in the returned vector is a complex number where the real part represent the cosine amplitude, while the imaginary part represent the amplitude of the sine wave. These cosine and sine waves are the basis functions described in section 6.1.

As described earlier, the amplitude values given in the frequency domain is not the same amplitudes that the basis functions need to recreate the original time domain signal, a process called synthesis. A normalization based on the number of data

points in the time domain signal is required as described in section 6.1. It is noted that exactly what these amplitude values represent is not of great importance for this work, only that they are comparable with each other. To achieve this, it is essential that all spectrum plots are scaled in the same way.

Having this vector, the next step is to represent the data in a useful and clear manner. An easy representation would be to take the absolute value of each vector point, consisting of a complex number, and plot it against its position in the vector. The values on the y axis would not give any information about which of the sine and the cosine base function that give rise to the given value, only indicate the total contribution from the two. The x axis would represent the number of cycles each component complete over the N points. It could then easily be converted further into a frequency axis where it represents the number of complete cycles per second. It is recognized that a representation like this do remove some information regarding how the frequency spectrum of the signal is decomposed. However, given the purpose of the FFT analysis in this work, this information is not considered essential, and such a representation will be given.

Chapter 7

Hypothesis

7.1 Components interacting and creating a beat

There is large evidence indicating that an interaction between two frequency components in supply voltage create a *beat* in network voltage at the hydro pumping station terminals. This happens in accordance with the beat theory explained in chapter 4. In Figure 7.1 an amplitude spectrum plot created from data from a measurement performed at the hydro pumping station is given. Measurements were performed as depicted in Figure 2.2. Complete measurement data from measurements, performed with Elspec G4430 and G4500, have been retrieved into MATLAB and Fast Fourier Transform has been performed. Measurements were performed on October 23, 2012, and data is taken from the 10 second period from 14:27:30 - 14:27:40. This measurement was performed when all three capacitor banks and motors were connected. In the plot, the current content is given for frequencies from 340 Hz to 355 Hz, around the 7^{th} harmonic frequency. Two distinct spikes can be seen in the plot, which indicates that there are current components present at those frequencies.

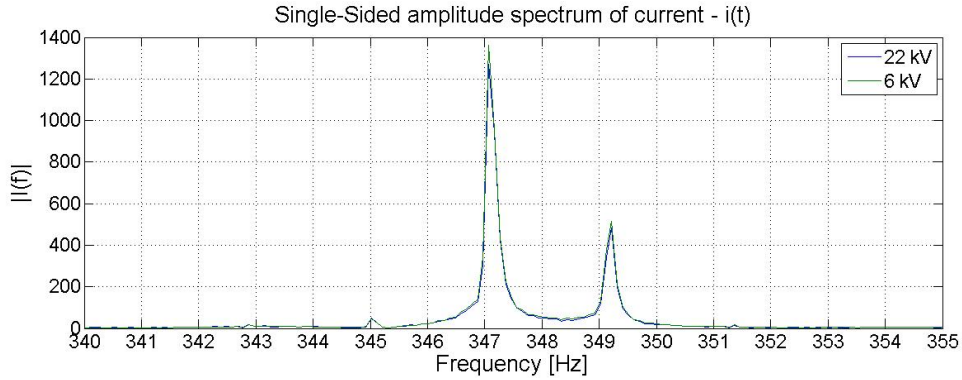

Figure 7.1: Amplitude spectrum of current at 6 kV side and 22 kV side of transformer for frequencies around the seventh harmonic frequency. Data taken from the 10 seconds 14:27:30 - 14:27:40, October 23, 2012. All three machines and capacitor banks connected.

The two components seen in Figure 7.1, do not exist independent of each other and will superimpose into one new wave, which has a frequency equal the average frequency of the two original components, and *beat* with a frequency equal the frequency difference between the two. In this case this would be at approximately 2 Hz. This could propagate to nearby end users and cause lighting disturbances, as those experienced. The Elspec monitoring equipment used for measurements, have integrated software that aims to extract all integer harmonic components from the measured voltages and currents. However, it does not provide a full analysis of interharmonics at frequencies between the real harmonics. This also explains why such phenomenon was not detected directly from the Elspec measurements. It is assumed that when harmonic components are extracted in Elspec Investigator, harmonic components in close proximity of the real harmonics can interfere with the real harmonic or even be interpreted as the real harmonic component itself. Therefore, a pulsating 7^{th} harmonic component can be seen in Elspec Investigator plots, without any indication of an interharmonic component present. Plots of pulsating 7^{th} harmonics can be found in the ieee-article written about the phenomenon [9].

7.2 Rotor-stator interaction

Further, explaining how these frequency components are created is essential. However, the internal physics of an induction machine is highly complex and understanding the exact behavior of voltage, current and magnetic field in a machine is very difficult. In the Specialization project, working as a preliminary work for this Master's thesis, a possible explanation for the creation of the interharmonic component was nevertheless presented. This was based on equations relating harmonic components in rotor to the stator reference frame, presented by Mr. Subhasis Nandi at University of Victoria [16, p. 565-580]. These equations were

not fully understood and definite calculations were not given. The relationship between rotor and stator reference frame has now been investigated further and the mathematical relationship has been deduced. This has been done in cooperation with professor Robert Nilssen at NTNU. It is emphasized that the following calculations are in accordance with the equations provided by Mr. Nandi.

The slip s (i.e. the relative difference in speed between rotor and stator magnetic field) in the machine makes it possible for a voltage appearing at a certain frequency in rotor reference frame to appear at a different frequency in stator reference frame. Multiplying rotor rotational speed ω (in rps) with number of pole pairs p, electrical rotational speed of rotor is obtained. This is somewhere close to fundamental frequency fs of 50 Hz, depending on machine slip. The difference between electrical rotational speed of the synchronous field (50 Hz) and rotor electrical rotational speed ($s \cdot 50\ Hz$), has to equal electrical frequency in rotor (fr_e), allowing the fundamental field generated by rotor ($B_{r,1}$) to rotate in synchronism with stator magnetic field ($B_{s,1}$). From rotor reference frame, the fundamental magnetic field generated by rotor ($B_{r,1}$), rotates in the same direction as the rotor with an electrical rotational speed equal electrical frequency in rotor (fr_e).

The n^{th} harmonic magnetic field component (B_n) move around the air gap at $\frac{1}{n}$ of the speed of the fundamental component of the magnetic field (B_1). However, the n^{th} harmonic magnetic field also has n times as many poles as the fundamental field. Say an induction machine has 2 poles ($p = 1$). The fundamental field ($B_{r,1}$) created by one rotor phase in this machine would have 2 poles. However, the 5^{th} harmonic field ($B_{r,5}$) would have $5 \cdot 2 = 10$ poles. This is illustrated in Figure 7.2, where the distribution of a 10 pole (5^{th} harmonic) field in the air gap around machine rotor is depicted. As indicated by arrows, the 5^{th} harmonic field rotates in the opposite direction of the rotor, and it rotates at $\frac{1}{5}$ of the speed of the fundamental magnetic field ($B_{r,1}$).

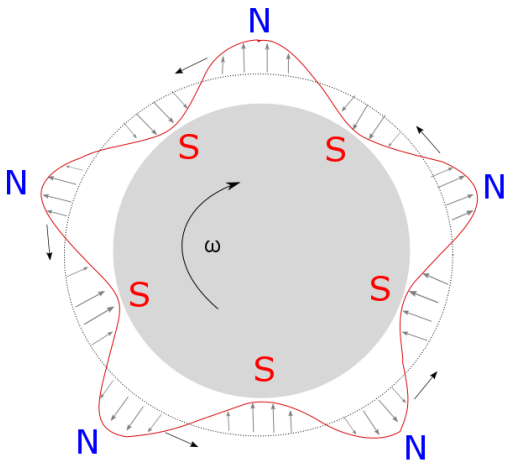

Figure 7.2: Illustration of a 10 pole magnetic field distributed around the air gap of an induction machine rotor (grey area). This field is the 5^{th} harmonic field of a 2 pole fundamental field. Rotor rotates in clockwise direction, indicated by the arrow, while the 5^{th} harmonic field rotates in counterclockwise direction, indicated by the small arrows.

Seen from rotor reference frame, all magnetic fields move slowly. The fundamental field (B_1) rotates fastest, given by machine slip. Speed of all harmonic fields can be measured relative to this component, and harmonics of higher order will rotate slower, either in the same direction, the opposite direction or they will not rotate at all. Rotational direction of different harmonic fields are explained in section 3.3. Seen from stator reference

frame, rotor fundamental field ($B_{r,1}$) rotates at rotor speed ω + the speed of the fundamental field seen from rotor ($B_{r,1}$). The same goes for the harmonic fields, which rotates at rotor speed ω + the speed of this harmonic component seen from rotor reference frame ($B_{r,n}$).

To perform calculations on the asynchronous machines at the hydro pumping station the following relevant data is necessary:

- Nominal frequency: $50Hz$
- Nominal rotational speed: $742\ rpm = 12.367\ rps \Rightarrow s = 1.067\ \%$
- Rotor: wound rotor
- Pole pairs: 4

It is assumed that machine rotates at nominal rotational speed 742 rpm. Then it is assumed that a 7^{th} harmonic component is present in machine rotor, not worrying about where the component originates from for now. At nominal rotational speed the asynchronous machines will have a slip of 1.0667%, which again gives a rotor frequency of $fr_e = fs \cdot slip = 50\ Hz \cdot 0.010667 = 0.533\ Hz$. In rotor reference frame, fundamental field rotates electrically at 0.533 Hz. The actual mechanical rotational speed of the field (physical rotation in space, disregarding number of poles in the machine) is only

$$\frac{0.533\ Hz}{4\ pole\ pairs} = 0.133$$

full rotations per second. From stator reference frame, this field rotates electrically at

$$12.367\ rps \cdot 4\ pole\ pairs + 0.533\ Hz = 50\ Hz$$

, which is strictly defined from synchronism. The 7^{th} harmonic field component seen from rotor reference frame ($B_{r,7}$) will rotate mechanically at

$$\frac{0.133\ Hz}{7} = 0.019048$$

full rotations per second in forward direction. Seen from stator reference frame, the mechanical rotation of this field is

$$12.367\ rps + 0.019048\ rps = 12.3857\ rps$$

However, this field has 7 times as many poles as the fundamental field, as illustrated by the principle in Figure 7.2. Therefore, electrical rotational speed of this field must be multiplied by the effective number of pole pairs, which is $4 \cdot 7 = 28$. Electrical frequency of 7^{th} harmonic magnetic field, seen from stator reference frame becomes

$$fs_7 = 12.3857 \cdot 28 = 346.80\ Hz. \tag{7.1}$$

Thus with a 7^{th} harmonic voltage component (350 Hz) present in machine rotor, a new interharmonic voltage component at 346.80 Hz will arise in machine stator. This frequency do not match exactly the frequency component depicted in Figure 7.1. Also, co-existing with a clean 7^{th} harmonic component, this would create a beat around 3.2 Hz, while the beat created from the pumping station is very close to 2 Hz. However, the difference is very small and the exact precision of the FFT plots created in MATLAB has been discussed and is doubtful. Also, exact rotational speed of the induction machines at the moment of measurement is unknown. The machine slip is essential for the calculations above, and could be a source for inaccuracy in the calculations. Therefore a further investigation of this desired and it was decided to perform a laboratory test of the phenomenon, using an induction machine at the laboratory at NTNU.

7.3 Harmonic source

For a rotor-stator interaction to occur, a 7^{th} harmonic component in the rotor is necessary. Whether there exist a 7^{th} harmonic component in the rotor of the machines at the pumping station is not known. If it exists, the source of this is not known either. However, some harmonic source must exist and two main hypothesis for this source is presented.

A possible explanation is that the machine creates all harmonics by itself. In general, the air-gap flux density distribution in an induction machine will not be completely sinusoidal. Machines are designed to produce as sinusoidal flux distributions as possible, but no design is perfect [2, p. 639]. Therefore, generation of some harmonics must be expected from an induction machine. Naturally, magnitude of the generated harmonics will depend on the size of currents drawn by the machine, and machine design. If the machine creates harmonics both in rotor and stator, independent of each other, that will explain how both harmonic components are created. Also, two individual harmonic sources (machine rotor and machine stator) could explain why the interharmonic component proved to have a larger magnitude than the integer harmonic component in almost every FFT plot created from the measurement data from the hydro pumping station, as shown in the Specialization project [12].

Another possibility is that there is an external source feeding the induction machines with harmonics from somewhere in the network. Earlier analysis has shown that a harmonic component arising from the network would see a resonance impedance caused by the shunt capacity banks that were connected before, as explained in chapter 2. Whether this could cause a rotor-stator interaction as described earlier is not known. However, applying the reasoning presented in section 7.2 from stator to rotor and back to stator will not give a frequency in the right order of magnitude. This is shown by Mr. Nandi, who shows that a 5^{th} harmonic in stator will appear at a much higher frequency in rotor [16]. If this component could be reflected back to stator it would appear at a frequency not

matching the measured frequency of the interharmonic component. Therefore, an additional explanation is required if the harmonic source is external.

Chapter 8

Windings of laboratory machine and general winding theory

Windings in a three-phase AC machine have the task to create a symmetrical 3-phase, balanced system of emfs of identical magnitude, wave shape and frequency. In a three-phase system, these phases should be displaced by 120 electrical degrees. A special group arrangement of the windings is necessary to achieve such system. [7, p. 219-220]

Armature windings in three-phase AC machines are open-type, which means that no closed path exist for the armature currents in AC windings. In one end they are connected to the voltage source, typically the grid or some regulating converter, in the other end, windings are brought together to form the neutral point for the star connection. Other winding types exist as well, but will not be discussed here. In Table 8.1 below, some of the most common characteristics of AC windings are summarized. [7, p. 219-220]

Type of coil	*Concentric, lap, wave*
Overhang	*Diamond, multiplane, involute, mush*
Layers	*Single, Double*
Slots	*Open, closed, semi-closed*
Connection	*Star, delta*
Phase spread	60°, 120°
Slotting	*Integral, fractional*
Coil span	*Full-pitched, chorded*
Circuits	*Series or parallel*
Coils	*Single-turn, multiturn*

Table 8.1: Characteristics of most commonly used windings in three-phase AC machines [7, p. 219-220].

It is not within scope of this work to give a description of all winding types and

the usage of them. This can be found in the literature. The windings in the laboratory machine at NTNU used for testing in this work will be described, and the most relevant theory regarding this type of winding will be discussed.

8.1 Winding structure of laboratory machine

The induction machine in the laboratory at NTNU was opened to investigate the winding structure. A picture of the open machine seen from the end is given in Figure F.1 in section F in the appendix. It is difficult to see the winding structure from the picture, but a sketch of stator and rotor windings is included in Figure 8.1 and Figure 8.3 respectively. In the drawings, each of the three phases are given a color, and each colored line represent a cluster of wires, constituting a coil.

Machine stator

As can be seen from Figure 8.1, the machine has four poles, or two pole pairs. Machine stator has 48 slots and there are 4 slots per pole per phase, which can be calculated, $q = \frac{48\ slots}{4\ poles \cdot 3\ phases} = 4$, or seen visually from the figure. This makes it an integral slot winding. Further, it can be seen that there are single layer windings, since it is not a second layer of windings on top of the first.

The windings are concentric. That means that the four windings that are grouped together and belonging to the same phase (same color in the drawing) is wound outside of each other. The outermost winding travels the furthest distance, while the innermost winding travels the shortest distance. It is the average span of all four windings that works as the efficient span of the phase. In this case, this distance is 12 slots.

The pole pitch equals the total number of slots divided by the number of poles, $pole\ pitch = \frac{48}{4} = 12$ slots per pole. This is the same number of slots that each phase spans over, which makes the the windings full-pitched as well. The coils are multiturn, since each coil in the machine (each line in the drawing) consists of many turns.

Each winding belt (group of four wires in the drawing) spread across 4 slots. 4 slots constitutes 30 mechanical degrees or 60 electrical degrees, since there are 2 pole pairs in the machine. That makes the phase spread 60 electrical degrees.

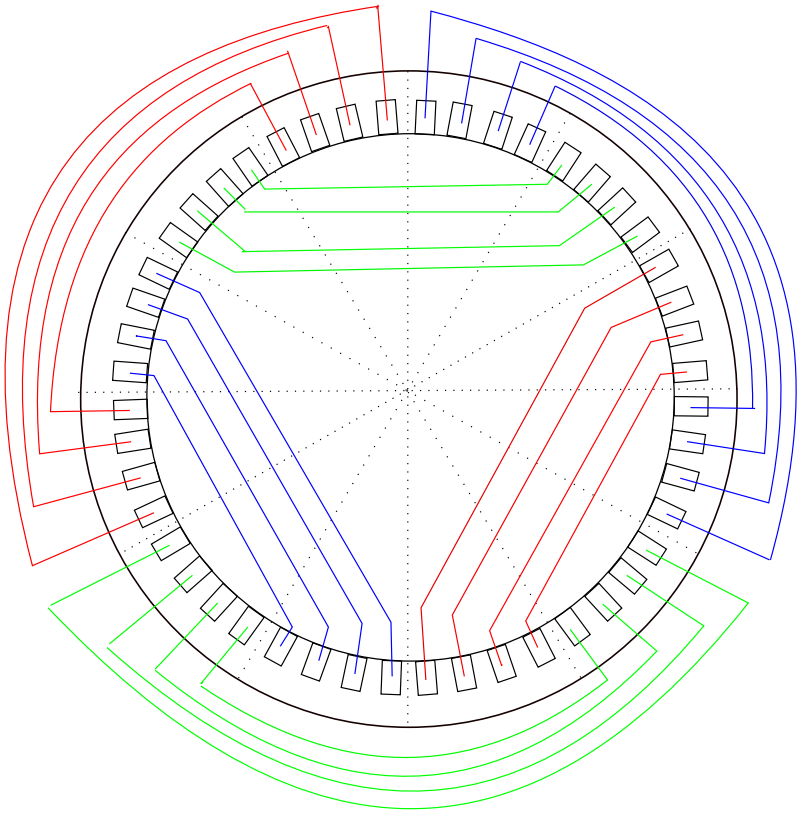

Figure 8.1: Drawing of stator windings. Each color corresponds to one of the three phases. The machine has four poles. There are 48 slots and integral slotting with 4 slots/pole/phase in machine stator. The windings are concentric, in a single layer and full-pitched.

Machine rotor

The machine rotor, shown in Figure 8.3, is a wound rotor. The other type of induction machine rotor is the squirrel cage rotor, which is the more common asynchronous rotor type. A cage rotor consists of series of conducting bars laid into slots carved in the face of the rotor and shorted at either end by large shorting rings. Unlike the squirrel cage rotor, the wound rotor has a complete set of three-phase windings that are similar to the windings on the stator. The usually Y-connected ends of the windings are tied to slip rings on the rotor's shaft, providing access to the rotor circuit at the stator brushes. [2, p. 309-310]

The rotor has many similarities with the stator, but also some differences. There are only 36 slots in the rotor, still distributed over 4 poles and three phases, which gives $q = \frac{36\ slots}{4\ poles \cdot 3\ phases} = 3$ slots per pole per phase. This makes it an integral slot winding. However, the winding structure is slightly more complex in rotor than stator. In the drawing in Figure 8.3, a solid line indicates a full coil, where the slot is filled up with conductors creating a coil, similar to the stator windings. A dashed line means that the line represents a coil with only 50 % of the turns of

a full coil, filling only half a slot. There are 3 slots per pole per phase, but they are distributed as 2 full and 2 half slots per pole per phase. The two fully filled slots are in the middle, while the two half filled slots are on each side, as shown in Figure 8.3. Then again, the next phase looks similar, with 2 full coils in the middle and on the sides there are two coils with only 50 % of the turns of a full coil, filling only half a slot. Together, two half coils from two different phases fill one slot. This principle is depicted in Figure 8.2 below. Here, seven slots in the rotor are seen from the end. The colored areas represent the area of the slot that is filled with conductors of that color's phase. The conductors goes into the paper.

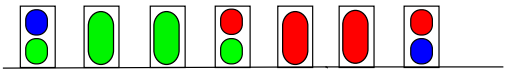

Figure 8.2: Scheme of rotor winding system. Each phase (color) consist of two full coils and 2 coils with only 50 % turns. In total, they constitute 3 coils and 3 slots per pole per phase.

By arranging the coils in this manner a more sinusoidal flux waveform is achieved, thus reducing harmonic content. The waveform is built up in smaller steps. This is very similar to the principle called reduced pitch, which requires double layer windings. In such arrangements there are two layers of wire upon each other and one of the layers are skewed slightly, relative to the other, obtaining a stair like winding arrangement. However, rotor windings in this machine is considered to be single layer windings.

Apart from this, machine rotor is wound very similar to the stator. Windings are concentric with an efficient coil span of 9 slots. There are integral slot windings and open slots. Each phase is spread over 60 electrical degrees, and the coils are multiturn. With 36 slots and 4 poles, the *pole pitch* $= \frac{36}{4} = 9$ slots per pole in the rotor. The rotor is Y-connected and all three phases are accessible at stator brushes.

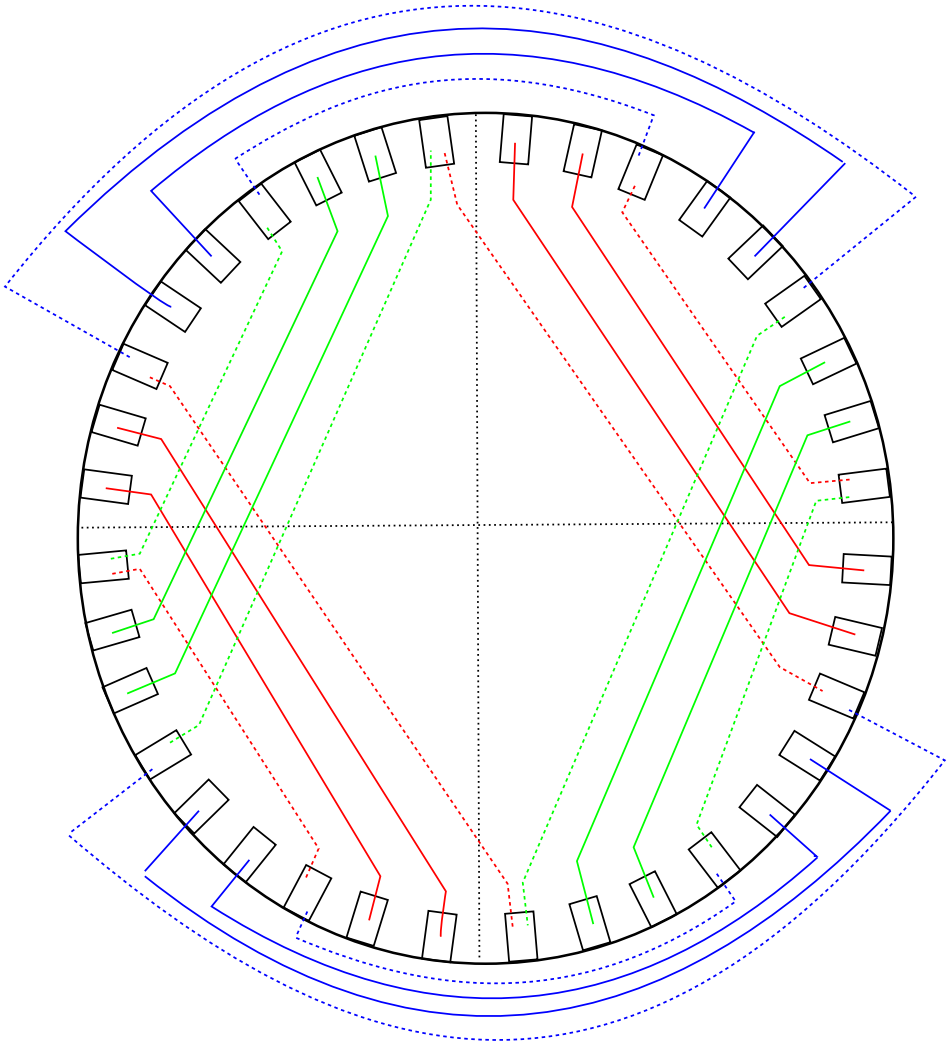

Figure 8.3: Drawing of rotor windings. Each color corresponds to one phase. The machine has four poles. There are 36 slots and integral slotting with 3 slots/pole/phase in machine rotor. For a single phase in a pole, 4 different slots are used. However, only two of these slots are filled with windings from that phase. The two last slots are split between two different phases. The third group of windings for a phase (dotted line) is split between in two coils and distributed over two different slots. The windings are concentric, in a single layer and full-pitched.

Chapter 9

Laboratory preparation

9.1 Purpose of laboratory tests

On basis of the mathematical relationship deduced in section 7.2, it was decided to perform a laboratory experiment with the purpose of recreating the interharmonic components around the 5^{th} and 7^{th} harmonic frequencies. The idea is to feed a wound rotor induction motor with voltage containing 5^{th} and 7^{th} harmonics, and continuously monitor stator voltage and current. When applying harmonic voltage on machine stator, the machine will draw harmonic current. Varying operational conditions, such as load (slip) and harmonic content in stator, can be used to investigate harmonic behavior of the machine.

The induction machine available for tests in the laboratory at NTNU is not a replica of the machines at the pumping station. Performing tests on the machine in the laboratory will therefore not give a complete picture of the behavior of the pumping station induction machines. Nevertheless, it is considered valuable to perform tests in the laboratory. Monitoring harmonic behavior in the induction machine at NTNU will provide basis for comparison. Independent of the result, this will provide information that can be used for further work. In lack of a true replica of the pumping station machine, this was considered the best available source of information.

Like the pumping station induction machines, the test machine has wound rotor and slip rings, as well as external resistance in rotor circuit used for start up. The machine at NTNU has switch that is used to choose star or delta connection to the network. Here a star connection is used. The laboratory machien has lower power and voltage rating than pumping station machines, and number of poles are different for the two. However, when investigating harmonic behavior, the most important feature of a machine is the winding structure. Unfortunately, a detailed description of the winding structure is not available neither for the machines at the pumping station, nor for the test machine at NTNU. However, the latter has been opened and investigated visually as explained in chapter 8. It should be mentioned

that this was done after laboratory tests were performed. Thus information on winding structure of the laboratory machine was not available when planning and conducting experiments.

In Table 9.1 a summary of the specifications of the induction machines at the hydro pumping station and the test induction machine at NTNU is given together.

	Pump station machines	**Test machine at NTNU**
Nominal voltage	66 kV	230 V
Nominal frequency	50 Hz	50 Hz
Nominal power	1.7 MW	7.5 kW
Nominal rotational speed	742 rpm	1430 rpm
Number of pole pairs	4	2
Rotor type	Wound, slip rings	Wound, slip rings
Starting method	External resistance in rotor circuit	External resistance in rotor circuit

Table 9.1: Comparison of induction machines at hydro pumping station and the test induction machine at NTNU used for the laboratory work.

9.2 Laboratory setup

Generating harmonics

To generate 5^{th} and 7^{th} harmonics, a six-pulse full-bridge rectifier is used. As described in chapter 5, a rectifier will draw harmonic currents from the source when a sinusoidal voltage is applied. If the applied voltage is not stiff, this current will in turn generate harmonic content in the voltage. Simulink simulations were performed as a part of preparing the laboratory work, and in chapter 10, it is shown how both voltage and current drawn by a rectifier contain 5^{th} and 7^{th} harmonics.

On DC side of the rectifier, a variable resistive load is connected. This will simply consume the power fed through the rectifier. By varying this resistance, power flow through the rectifier can be controlled. In addition, a large filter capacitor is connected in parallel with the resistance on the DC side. This is meant to reduce ripple in the DC voltage.

The rectifier will be connected in parallel with the induction machine. At the point of common coupling, the induction machine and the rectifier will see the same voltage. 5^{th} and 7^{th} harmonics generated by the rectifier will be present in machine stator voltage. Harmonic voltage will be applied to the machine which will therefore draw harmonic current.

Creating a weak grid

As three-phase voltage supply for the laboratory test the mains will be used. The power grid can more or less be regarded as a stiff voltage source for a small system, such as the laboratory setup used in this work. As shown in Figure 11.4 in section 11.2, using a stiff voltage source, the rectifier will draw a very ugly current without generating voltage harmonics, which is not useful for the purpose in this work. There will always be some natural inductance in the power grid, as all conductors will generate a magnetic field and contain some inductance, and there are many factors deciding the inductance in the grid. However, under normal circumstances, voltage supplied by the grid will be to stiff and the rectifier will not be able to generate voltage harmonics.

To ensure that the AC voltage is sufficiently distorted by the rectifier, a three phase inductance, L, will be connected between the mains and the rest of the laboratory setup. This inductance is variable and can be adjusted to different values between every machine run. The inductor has three legs, one for each phase. In each leg, there are five coils connected in series. When connecting the inductor, one can choose which coil to connect, hence how many coils to connect in series. Also, a crank handle can be used to adjust the air gap in the inductor, providing a non discrete regulation of the inductance.

Description of the arrangement

At the end of this section, a scheme of the complete laboratory setup is included. Directly from the mains, phases R, S and T are connected to the soft start equipment, number 5 in List of Equipment. Downstream of the soft start, a contactor, K101, is connected. This can disconnect the entire downstream circuit from the mains. After the contactor, the variable inductance is connected, number 14 in List of Equipment. Following the inductance the circuit is split at terminal block X22. This is the common point of coupling where both the rectifier and the induction machine is connected.

At the right hand side of the scheme, a new contactor K102 can disconnected the rectifier from the rest of the circuit. The rectifier, number 8 in List og Equipment, is downstream of this contactor. DC side capacitance is included in the rectifier unit in the scheme. This capacitance consists of four capacitors, each of $4.7mF$. These can be series or parallel connected as desired to achieve the required capacitance. The final element at DC side of the rectifier is the variable resistance. This consists of five water cooled resistances which can be connected independently or in parallel. The resistances have the following values: 22 Ω, 44 Ω, 80 Ω, 160 Ω and 320 Ω. Thus the smallest resistance possible to achieved is the parallel connection of all resistances, $R_{smallest} = 22||44||80||160||320 = 11.104\ \Omega$. The largest resistance that can be achieved is 320 Ω, and there is a number of variations in between.

Following the other path downstream of the point of common coupling X22, connection goes via another terminal block X2, which connect the circuit onto an already existing control unit that has been used to run the induction machine in previous laboratory experiments. Thereafter, there is another contactor K2. Before current is fed into the induction machine, a number of measurement connections for measuring RMS current, RMS voltage and active power fed into the machine are preinstalled. This setup can be found in scheme 205-4-A3 in section F.0.1 in the appendix. Connections go via terminal X1 where the induction machine stator is connected. Induction machine rotor has a variable start up resistance connected.

As a load for the induction machine, a DC machine (number 10 in List of Equipment) is connected on the induction machine shaft. This machine is controlled from a dedicated console, and the connection scheme for this console can be found in section F.0.1 in the appendix, scheme number 203-5-A3. When using the DC machine as a load for the induction machine, it is extremely important that the rotational direction of the two machines are the same. If the two machines are connected to the same shaft and pull in separate directions, tremendous strain will be applied to the machine shaft. Rotational direction is controlled from the console, but the direction is tested and visually inspected at forehand, before the conducting the experiments.

The laboratory setup was built in cooperation with service personnel at NTNU, Mr. Svein Erling Norum and Mr. Aksel Andreas Reitan Hanssen.

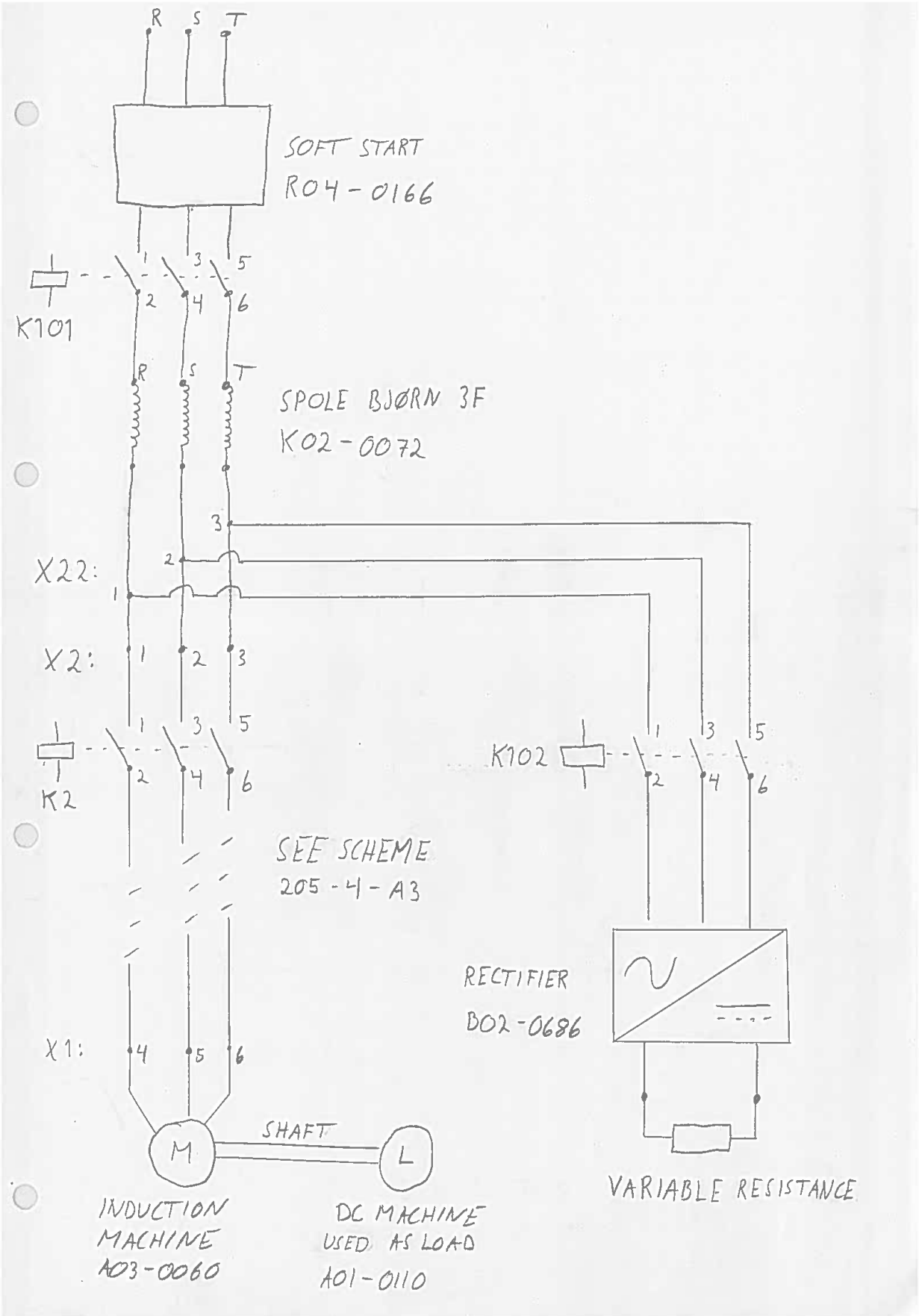
R S T
SOFT START
R04-0166
1 3 5
2 4 6
K101
R S T
SPOLE BJØRN 3F
K02-0072
3
2
1
X22:
X2:
1 2 3
1 3 5
2 4 6
K2
K102
SEE SCHEME
205-4-A3
RECTIFIER
B02-0686
X1:
4 5 6
SHAFT
M
L
INDUCTION MACHINE
A03-0060
DC MACHINE USED AS LOAD
A01-0110
VARIABLE RESISTANCE

9.3 Test of MATLAB code for FFT analysis

In the specialization project [12], working as a preliminary report for this master thesis, many FFT plots created from data from a measurement performed at the hydro power station were presented. In these plots there were seen two harmonic components around the 7^{th} harmonic frequency of 350 Hz. However, both of these components occurred slightly below 350 Hz in almost every plot. As commented in that report, it was expected to see a clean 7^{th} harmonic component in addition to an interharmonic component. It was not concluded whether that component was indeed an interharmonic or if there were some inaccuracy in measurement data or data processing, causing the 7^{th} harmonic to occur at a slightly lower frequency.

To further investigate this, a signal with a clean7^{th} harmonic component was created in MATLAB and used as input to the same MATLAB code as used to created the FFT plots in the specialization project. In Figure 9.1, the amplitude spectrum produced from this is given for frequencies from 340 Hz to 355 Hz. From this, it is evident that the MATLAB code used to produce the FFT plots do work properly, as the 350 Hz component in the input signal is given at exactly 350 Hz in the FFT plot. It can therefore be concluded that the deviation from 350 Hz is not caused by the FFT analysis of the data performed in MATLAB.

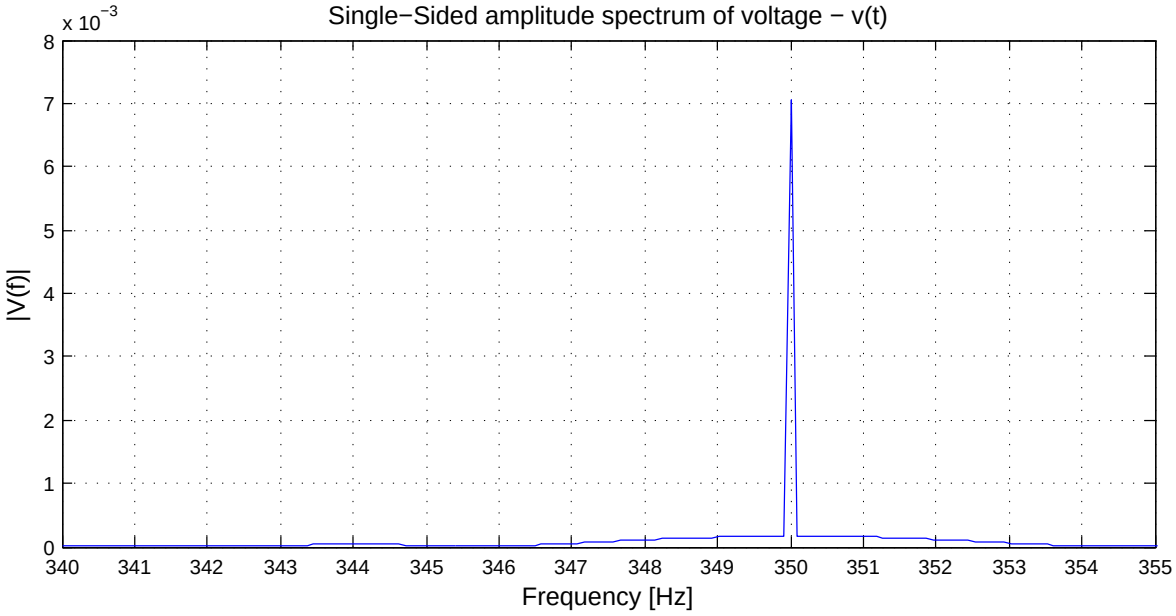

Figure 9.1: A signal containing a clean 7^{th} harmonic frequency component is given as input to the MATLAB code. The output is an FFT plot with one spike at exactly 350 Hz.

Based on this it seems very probable that some frequency shift occur either when the signal is measured or when the signal is exported from the ELSPEC database to MATLAB. How this happen is not yet known. However, based on the information available, the analysis method is considered reliable. The main purpose of the

FFT analysis is to look for different harmonic components, and it is considered very unlikely that any harmonic component can disappear from the signal when processing data. However, the analysis method used in this work cannot be used to verify the exact frequency of a harmonic component.

Chapter 10

Simulink model

10.1 Purpose of the Simulink simulation

Establishing a Simulink model of the system had multiple purposes. Primarily the objective was to confirm that harmonic components were created as expected. This includes investigating what network parameters is necessary for the harmonics to occur with a reasonable magnitude, and identifying circuit behavior in general, for example AC voltage collapse. Laboratory equipment has physical limitations, and power and voltage must at all times stay within these boundaries. Simulations will be used to look for very poor AC voltage quality that could prevent the machine from starting at all.

10.2 Scope of simulation

To keep analysis as simple as possible, it was decided not to include the entire laboratory set up in the Simulink model. The reason for this is that the rectifier in combination with the upstream network mostly decides the effects that will be examined in Simulink simulations. In addition, it was considered easier to identify which parameters caused the different responses in the circuit, in a small and simple model. Therefore, the induction machine itself was excluded from the Simulink model. The model consists of a stiff three-phase voltage source in series with an inductance, after which a three-phase, six-pulse, full-bridge diode rectifier follows. On the DC side of the rectifier there is a filter capacitor in parallel with a resistive load. This will be described in detail in section 10.3.

The Simulink simulation will be used to create Fast Fourier transform plots of voltage and current on AC side of the rectifier. Such plots are described in detail in section 6.2. The objective is to achieve around 5-10 % content of the 7^{th} harmonic component. This is to ensure that these harmonics are distinguished from any possible harmonic noise present in the power supply at the laboratory. Simulations

will be used to detect how different parameters influence harmonic content and how the desired values are best achieved within the physical limitations of the equipment.

It is useful to have a look on voltages and currents in the rectifier. Therefore, time plots of voltage and current will be made. It will be investigated what parameters most dramatically influence voltage quality. In a weak grid, voltage will collapse if the load draws too much current. Voltage stability under different circumstances will be examined. Although not a requirement for the laboratory work, RMS value of the voltage will be compared to the Norwegian Power Quality Directive ('Forskrift om leveringskvalitet i kraftsystemet'), which state that slow variations in voltage RMS value should stay within ± 10 % of nominal voltage [15].

10.3 Description of Simulink model

The Simulink model is shown in Figure 10.1. At the far left of the scheme, there are three star connected AC voltage sources, AC a, AC b and AC c for phase A, phase B and phase C respectively. These are 120 degrees shifted relative to each other as in a regular power system. These are perfect voltage sources and is therefore a good representation of the upstream power grid. In each phase an inductance is connected in series with the voltage source. These are named Ls a, Ls b and Ls c for phase A, phase B and phase C respectively and are all of equal magnitude. Following the inductance, there is connected a six-pulse, full-bridge diode rectifier. Each phase is connected to two diodes that control the current direction. In total there are six diodes, D a1, D a2, D b1, D b2, D c1 and D c2. This arrangement is a standard scheme which is described in more detail in chapter 5 and can be found in many text books [17].

In the right end of the scheme, the DC side, there is installed a large filter capacitor, C_d, and a resistive load, R_load, in parallel. Also, there are included some measurement devices in the model. The blocks named Voltage ab, Voltage ac and Voltage bc, measure the line voltages downstream of the inductance between the phases indicated by their names. The block I_d measure the direct current on the DC side of the model. In addition, voltage and current measurements are available from each Simulink component itself. For example, measurements of the current through the inductors Ls a, Ls b and Ls c are available. When running a simulation, the discrete time step is decided by the variable Ts=5e-06 s in the model. This means that the system state is calculated every 5^{th} micro second.

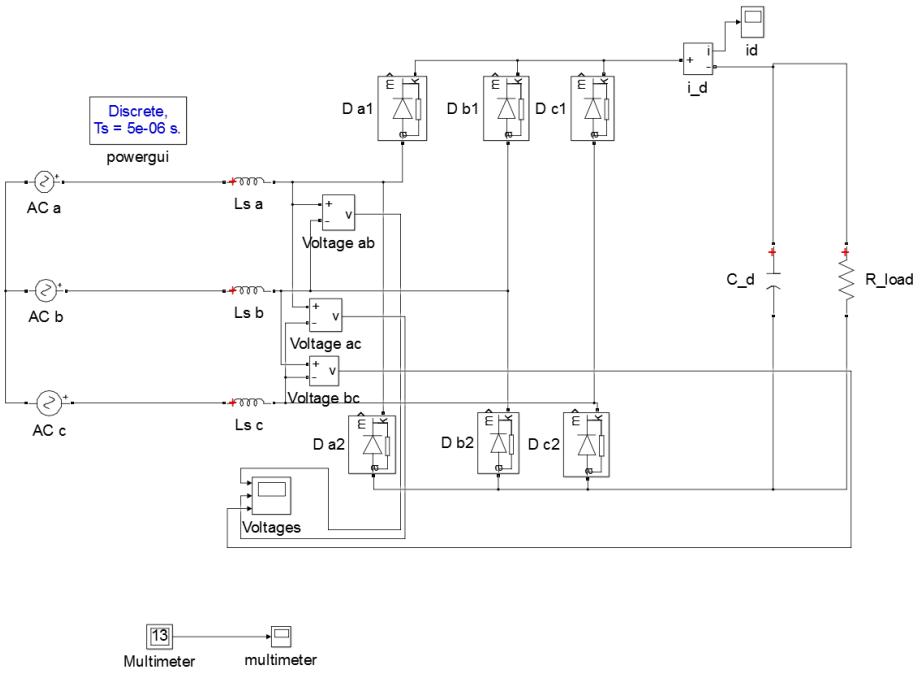

Figure 10.1: Simplified Simulink model of the laboratory setup. The induction motor is considered dispensable and is therefore not included.

10.4 Deciding parameter values

The Simulink model is meant to represent a specific part of the laboratory setup as good as possible and parameters should be chosen thereafter. For this, some simple assumptions and calculations were performed at forehand. Calculations were performed on a per-unit basis. The voltage source is given a value of 230 V RMS, as is customary in the Norwegian power grid. Therefore,

$$V_{base} = 230\ V = 1\ pu \tag{10.1}$$

The induction machine at hand in this laboratory work, number 11 in List of Equipment, has a power rating of 7.5 kW. When choosing base apparent power this power rating was considered. In addition, power will flow through the shunt-connected rectifier and be consumed by the resistor connected at the DC side. This resistor can consume at least 10 kW, and total power flow into the laboratory setup could therefore exceed 7.5 kVA by far. However, exactly how much power the rectifier should draw to achieve the desired harmonic content in the current, is not yet known. Therefore, base value for apparent power was chosen as a convenient round number,

$$S_{base} = 10\ kVA = 1\ pu \tag{10.2}$$

With these parameters set, base current, I_{base}, can be calculated according to equation (10.3).

$$S_{base} = \sqrt{3} \cdot V_{base} I_{base} \tag{10.3}$$

$$\implies I_{base} = \frac{S_{base}}{\sqrt{3} \cdot V_{base}} = \frac{10\ kVA}{\sqrt{3} \cdot 230\ V} = 25.10\ A = 1\ pu$$

Further, base value for impedance, Z_{base}, can be calculated from the same two parameters, by equation (10.4).

$$Z_{base} = \frac{V_{base}^2}{S_{base}} \tag{10.4}$$

$$\implies Z_{base} = \frac{(230\ V)^2}{10\ kVA} = 5.29\ \Omega = 1\ pu$$

Further, the value of the capacitor C_d must be decided. For this, the circuit time constant was used as an indicator, and a value of approximately 10 ms is attempted. The idea is that this will smooth DC voltage appropriate when one period of AC voltage is 20 ms. For the given circuit in Figure 10.1, the time constant can be calculated by equation (10.7).

$$\tau = \frac{1}{2} \frac{C\_dV_{DC}^2}{S_{base}} \tag{10.5}$$

To calculate C_d from this equation, DC voltage is required. An exact value of the DC voltage cannot easily be given, but the relationship given in equation (10.6) [17], can be used to estimate the DC voltage, given the line voltage on AC side. However, as will be shown later and presented in Figure 11.1 at page 50, DC voltage is affected by several parameters.

$$V_{DC} = \frac{3}{\pi}\sqrt{2}V_{LL} \approx 1.35V_{LL} \tag{10.6}$$

In a strong network V_{LL} would be 230 V. However, the upstream inductance makes the network weaker, and V_{LL} will decrease as current drawn by the rectifier increase. The capacitance value will be an estimation and there is some leeway as this is only a filter capacitor. Therefore, V_{LL} is estimated to 230 V. From this, V_{DC} can be calculated,

$$V_{DC} = \frac{3}{\pi}\sqrt{2} \cdot 230\ V = 310.6\ V$$

Now, equation (10.7) can be used to calculate the capacitans C_d,

$$C\_d = \frac{2 \cdot \tau S_{base}}{V_{DC}^2} = \frac{2 \cdot 0.01 \cdot 10000}{310.6^2} = 2.07\ mF \tag{10.7}$$

Circuit inductance

With these values established, it is now possible to estimate the desired inductance and resistance in the system. The purpose of the series connected inductance is to simulate a weak gird, which will increase magnitude of harmonic content in voltage. Similarly, the size of the resistance at DC side of the rectifier dictates power flow through the rectifier, thus affecting magnitude of harmonic content. The idea is that a small resistance (measured in ohms) and a large inductance will increase harmonic content, while a large resistance and a smaller inductance will reduce harmonic content. Therefore, a reasonable combination of these parameter values must be obtained.

In a very weak system, the reactance of the feeder line is large. For the simulations, a few different values for upstream inductance were tested, $X_L = 0.2\ pu$, $X_L = 0.3\ pu$ and $X_L = 0.4\ pu$. These values are rough estimations and simulations are meant to validate them. A reactance of $X_L = 0.4 \cdot Z_{base}$ is very much and constitutes a very weak grid. This should allow large harmonic components to arise. Inductance necessary to achieve this can be calculated by equation (10.8).

$$X_L = \omega L \tag{10.8}$$

$$\implies L_{0.4\ pu} = \frac{0.4 \cdot Z_{base}}{2\pi f} = \frac{0.4 \cdot 5.29}{2\pi \cdot 50} = 6.73\ mH$$

The same calculation can be performed to achieve a reactance of 0.3 pu,

$$\implies L_{0.3\ pu} = \frac{0.3 \cdot Z_{base}}{2\pi f} = \frac{0.3 \cdot 5.29}{2\pi \cdot 50} = 5.05\ mH$$

and again for a reactance of 0.2 pu.

$$\implies L_{0.2\ pu} = \frac{0.2 \cdot Z_{base}}{2\pi f} = \frac{0.2 \cdot 5.29}{2\pi \cdot 50} = 3.37\ mH$$

DC resistance

The final parameter that will have a large impact on the circuit behavior is the size of the resistive load at the DC side of the circuit. This can be adjusted to regulate power flow in the circuit, thus affecting the size of the harmonic content in voltage and current at AC side. Larger resistance will decrease current flowing, hence reduce power consumed by the resistance and therefore reduce power flow through the rectifier. A reasonable combination of upstream grid reactance and power flow through the rectifier must be chosen. It is estimated that physical limitations in laboratory equipment restricts power flow through the rectifier to approximately 10 kW.

Simple calculations by Ohm's law, show that a resistance of 10 Ω at the DC side of the rectifier will make the rectifier draw theoretical value of almost 10 kW, given a DC voltage of 310 V. Therefore, DC resistance should not be much smaller than 10 Ω according to these calculations. Higher DC side resistance will decrease power flow through the rectifier as a consequence of the relationship in equation (10.9).

$$P = \frac{U^2}{R} = \frac{310.6\ V^2}{10\ \Omega} = 9647.24\ W \approx 9.6kW \tag{10.9}$$

The value calculated in equation (10.9) works as a reference point, but different resistances will be tested in simulations.

10.5 Procedure of simulations

The Simulink model was made general with variable parameters that are set in a Matlab script. All data handling and processing are conducted in the same Matlab script. This makes parameter value adjustment and post processing of data simpler. This Matlab code is given in section G in the appendix.

There will be given FFT plots of the harmonic content from the simulations. How to create and interpret such plots is described in section 6.2. The code for performing the FFT of the signal is included in section G in the appendix as well. Current, voltage and power are plotted as a function of the variable resistance on DC side of the rectifier. This is done by running multiple Simulink run with different values of the resistance. Also, regular time plots of current and voltage waveforms are given from short time intervals of the simulation.

Chapter 11

Evaluating simulation results

For all Simulink simulations, the applied line voltage is 230 V RMS, and the frequency in the system is always 50 Hz. The large filter capacitor on DC side of the rectifier is 2.07 mF (see calculations in section 10.4), if not otherwise specified. Some parameter values are specified for each plot. Diode parameter values are given in the Matlab code for the rectifier simulation included in section G in the appendix.

11.1 Voltage behavior for different DC side resistances

Before FFT plots of current and voltage is presented, a documentation of the behavior of other circuit properties will be given. An important property for the circuit is to be able to control power flow through the rectifier. As mentioned earlier, this can be done by adjusting the load resistance. For a better understanding of the relationship between DC side resistance and power flow through the rectifier, the simulation was ran multiple times with different load resistance.

In Figure 11.1, DC current, DC voltage and DC power flow is plotted as a function of DC side resistance. The resistance is varied from 2 Ω to 24 Ω with increments of 2 Ω over 12 different simulations. Inductance was kept constant at $Ls = 6.7\ mH$ for all simulations.

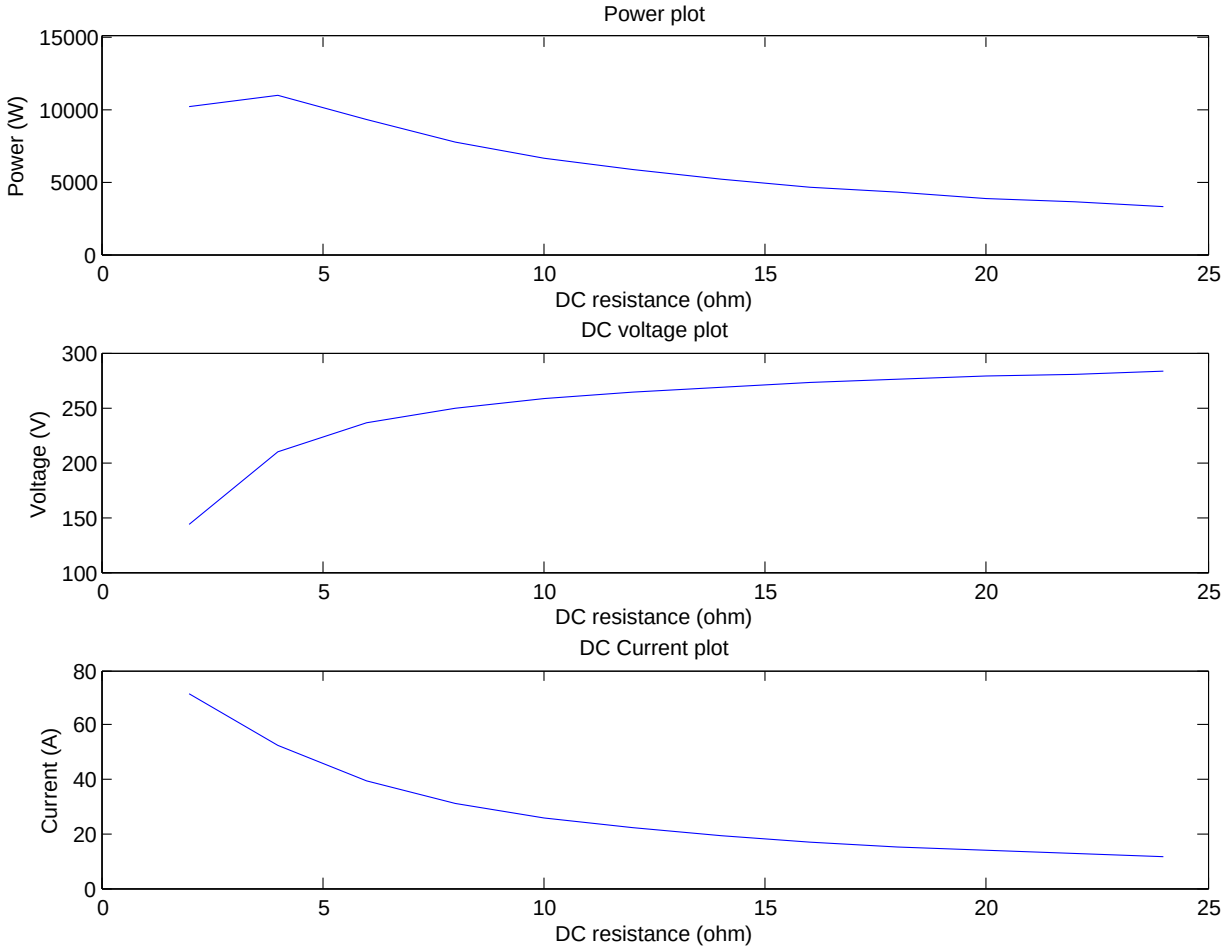

Figure 11.1: For a constant value of $Ls = 6.7\ mH$, R is varied from 2 Ω to 24 Ω with increments of 2 Ω. This is plotted against DC power, -voltage and -current respectively.

In the middle pane of Figure 11.1 it can be seen that DC voltage increase rapidly with DC resistance, starting from a value far below the theoretical DC voltage at 310 V. Also, this means that power flow through the rectifier at low resistances is substantially lower than the theoretical value presented in equation (10.9) at page 48, where $R = 10\ \Omega$ was calculated to give a power flow of 9.6 kW. Figure 11.1 shows that the power will peak at around $R = 4\ \Omega$ at a value of 11000 W. For further investigation of the DC voltage development for higher DC resistance, new simulations were performed. In Figure D.1 in the appendix, resistance is varied from $R = 10\ \Omega$ to $R = 300\ \Omega$ with a step of 10 Ω. A clear trend is evident from these plots. The DC voltage rises rapidly at first, before it flats out and increases slowly towards a value around to 310 V. Current drops as resistance increases. Power flow is the product of voltage and current, but current do drop more rapidly than voltage increases, hence DC power flow decrease.

As DC voltage depend on the voltage at AC side of the rectifier, a similar plot is created for the RMS line voltage. In Figure 11.2, DC voltage is compared to RMS

voltage. Also, the relationship $\frac{V_{DC}}{V_{LL,RMS}}$ is plotted in the lower graph. According to equation 10.6, at page 46, this relationship should have a value of 1.35.

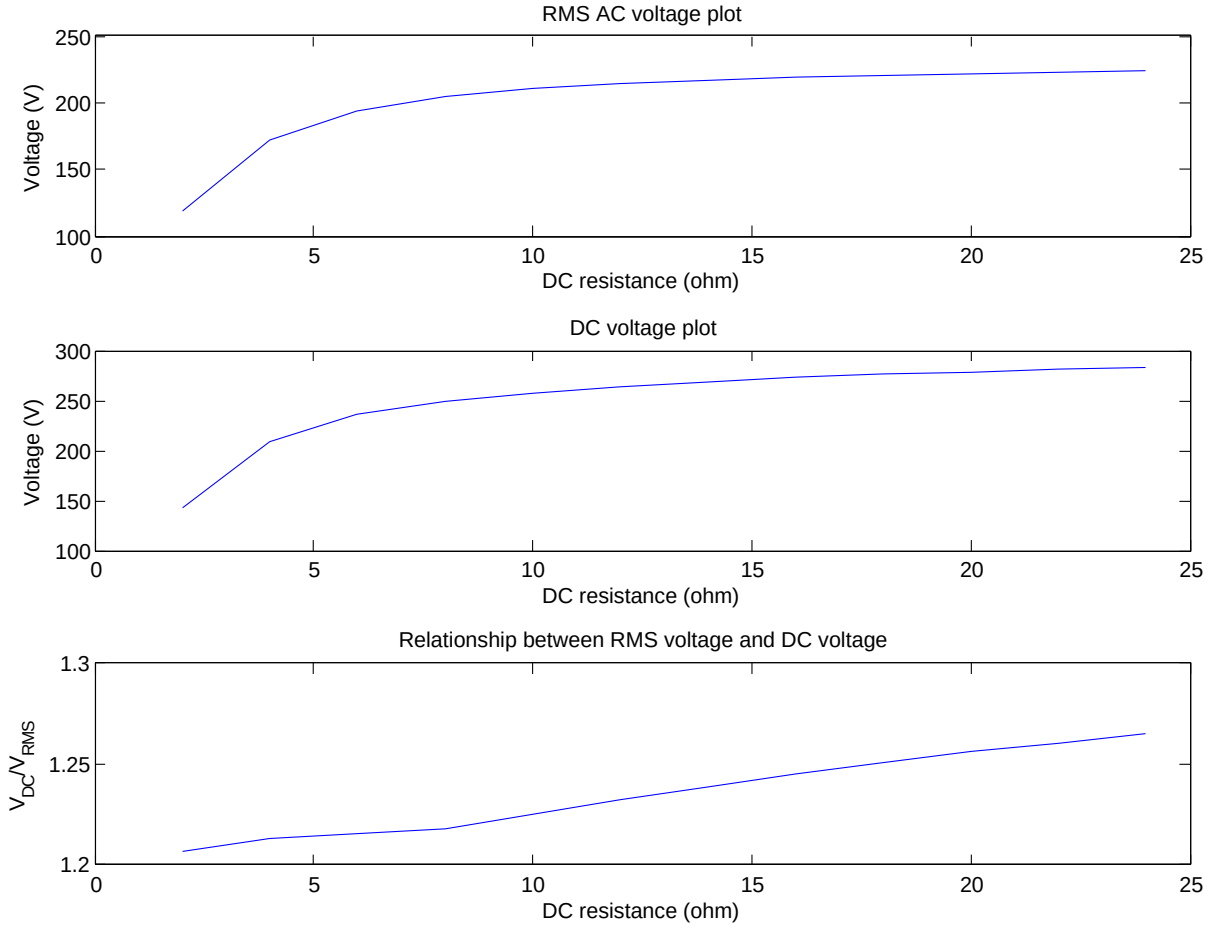

Figure 11.2: For a constant value of $Ls = 6.7\ mH$, R is varied from 2 Ω to 24 Ω with increments of 2 Ω. This is plotted against AC voltage, DC voltage and $\frac{V_{DC}}{V_{LL,RMS}}$ respectively.

As expected, RMS voltage behave very similar to the DC voltage as depicted in Figure 11.2. RMS voltage collapse at low DC resistance and in turn reduce DC voltage. At $R_{DC} = 2\ \Omega$, RMS voltage (in the upper pane) is only 118 V, a voltage drop of almost 50 % from the nominal voltage of 230 V. A DC resistance of 10 Ω gives an RMS voltage of 210 V, which is a voltage drop of less than 9 %.

The theoretical relationship between DC voltage and RMS voltage of $\frac{V_{DC}}{V_{LL,RMS}} = 1.35$ is not completely satisfied in the lower pane of Figure 11.2. The value rises slightly, but lies between 1.2 and 1.3. An explanation for this has not been found. However, considering that the purpose of the rectifier in this work is to generate harmonics, this is not considered to cause any problems, and further investigations are not necessary.

In stronger networks with lower upstream inductance, magnitude of AC voltage is less affected by power drawn by the rectifier. In Figure 11.3, a stronger grid is simulated. Here, upstream inductance is 3.37 mH. In the upper pane, DC power is plotted. This is now much larger than what is seen in Figure 11.1. DC resistance of 10 Ω gives a DC power flow of almost 7.8 kW. Reducing DC resistance any further gives a power flow of more than 10 kW. A strong network and a low DC resistance should be avoided in the laboratory set-up.

Power flow is increased due to the higher AC voltage depicted in the middle pane. For $R_{DC} = 2\ \Omega$, AC voltage is 173 V, a very large improvement from 118 V showed in Figure 11.2, where upstream inductance is 6.7 mH. A DC resistance of 10 Ω gives an AC voltage of 221.9 V, which is a voltage drop of only 3.5 % from 230 V at the source. In the lower pane, DC current is plotted. As expected, DC current is larger in Figure 11.3 than in Figure 11.1, and proves that a larger current will flow in a stronger network.

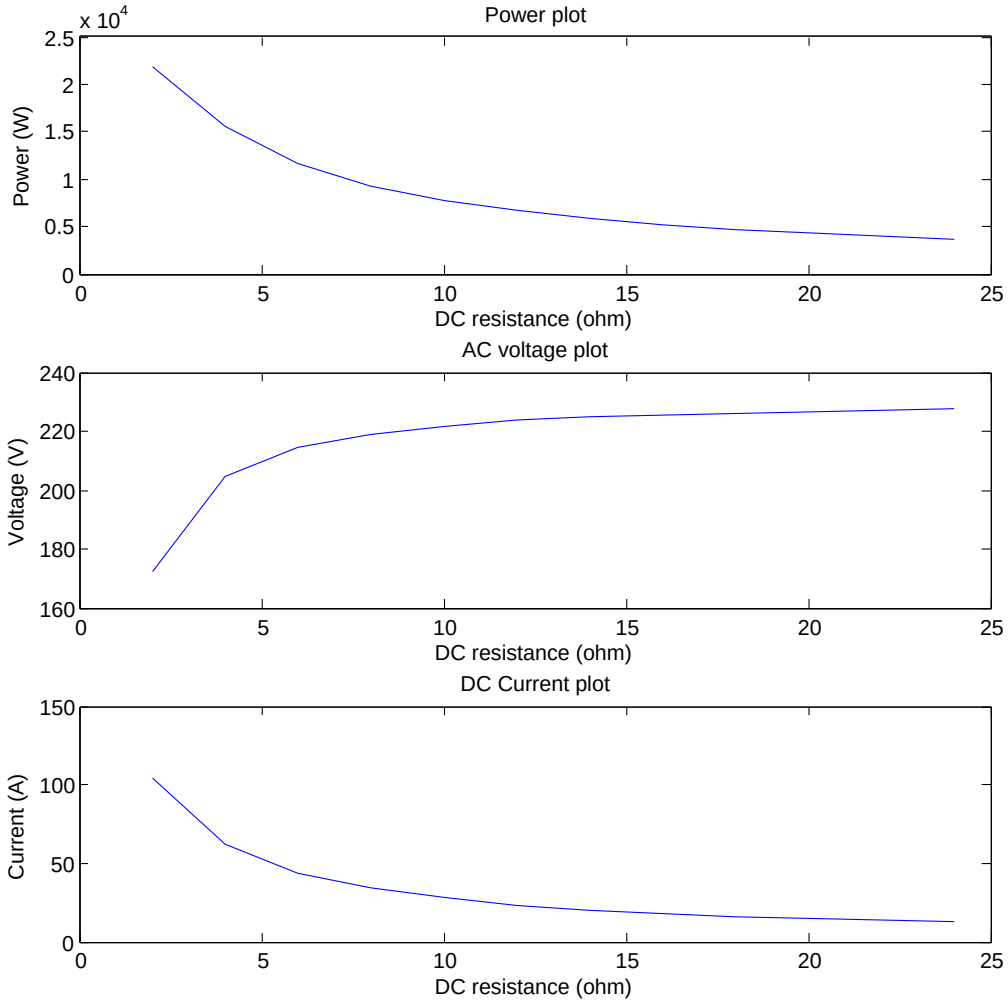

Figure 11.3: For a constant value of $Ls = 3.37\ mH$, R is varied from 2 Ω to 24 Ω with increments of 2 Ω. This is plotted against DC power, AC voltage and DC current.

11.2 FFT plots and waveforms

From the Simulink model at hand, FFT plots as well as voltage and current waveforms can be plotted. In section 11.1 it is shown that voltage do collapse at very low DC resistance, and a DC side resistance of 10 Ω is therefore tested first.

Base case

As a control, and to emphasize the need for upstream inductance, the very first simulation presented here is performed with a very low upstream inductance of $Ls = 1\ \mu H$, essentially a stiff grid. A time plot of voltage and current waveform from this run is given in Figure 11.4.

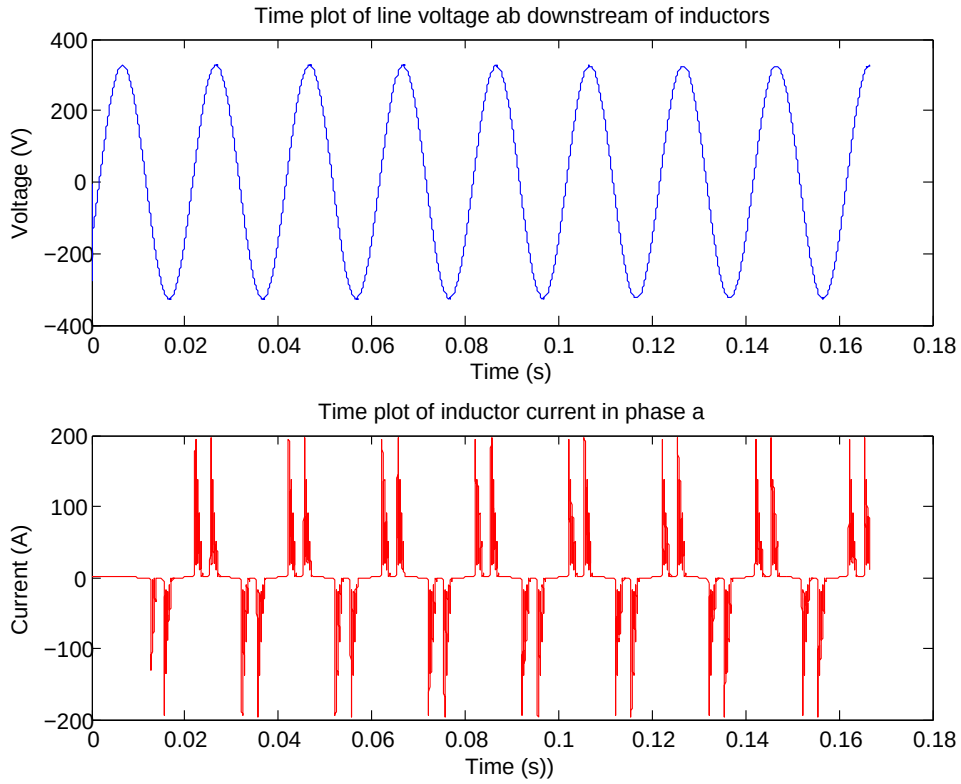

Figure 11.4: Time plot of voltage and current for the first eight periods of the simulation. $Ls = 1\ \mu H, R = 10\ \Omega$.

With a negligible inductance, the AC voltage is practically stiff. This gives a clean sinusoidal voltage in the upper pane in the figure, while the current in the lower pane looks horrible, with extremely large spikes and a waveform very far from a sinusoid. To generate the desired harmonics in the voltage and to avoid a terrible current waveform, upstream inductance is indispensable.

Introducing inductance

An upstream inductance of 6.7 mH was then tested. The simulation result is shown in Figure 11.5 and Figure 11.6, were a time plot of voltage and current waveform and an amplitude spectrum plot of the current is given respectively.

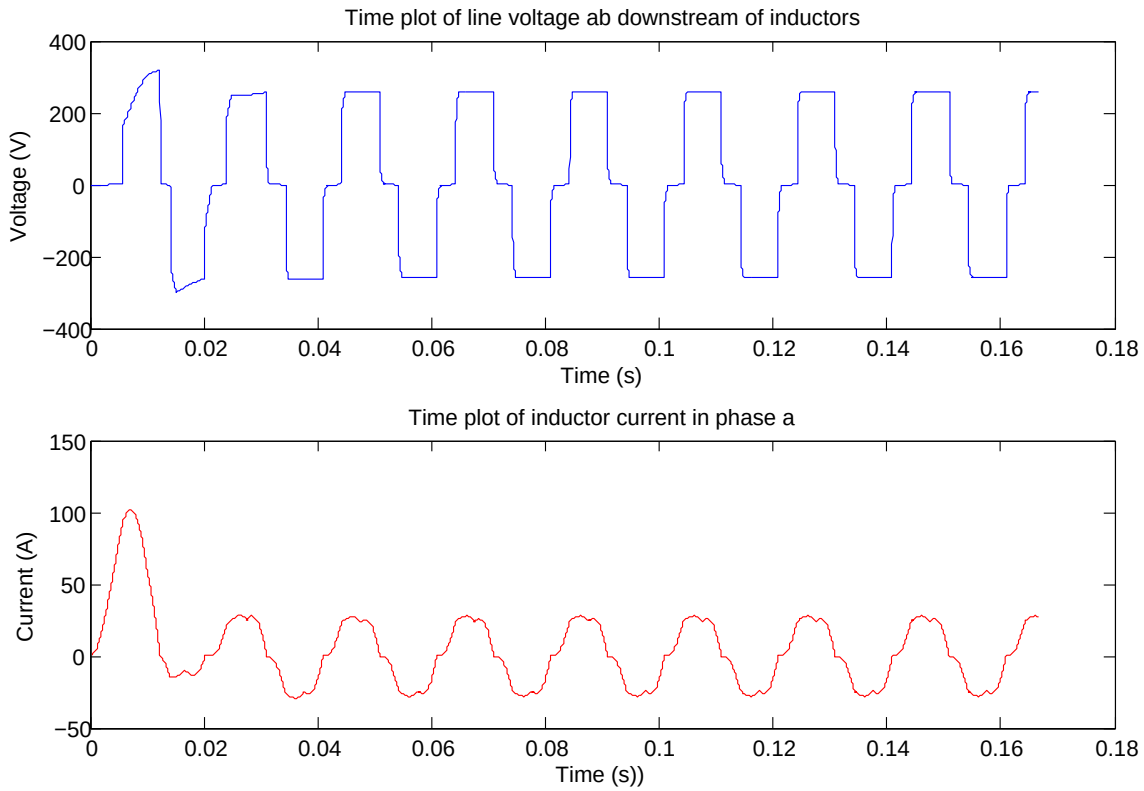

Figure 11.5: Time plot of voltage and current for the first eight periods of the simulation. $Ls = 6.7\ mH, R = 10\ \Omega$.

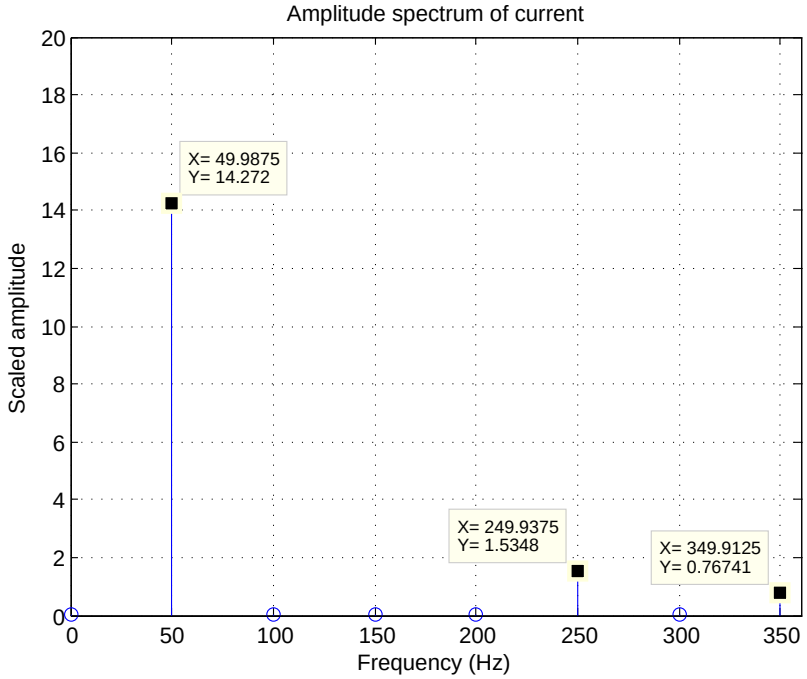

Figure 11.6: Amplitude spectrum plot of the current. The FFT analysis is performed on data from period number 6 in the signal given in Figure 11.5. $Ls = 6.7\ mH, R = 10\ \Omega$.

In Figure 11.5 a highly distorted voltage and current waveform is given, and the presence of harmonics is obvious. Current waveform is closer to sinusoidal than the voltage waveform. The inductance allow the rectifier more influence over the voltage, but at the same time it smooths the current. Also, a very large starting current is observed. In Figure 11.6 the mentioned harmonic content in the current can be seen. As expected, and desired, there are significant 5^{th} and 7^{th} harmonic components in the current. In Figure 11.7, a FFT plot of the line voltage is given as well. Harmonic content in voltage is even larger than harmonic content i current measured relative to the fundamental component.

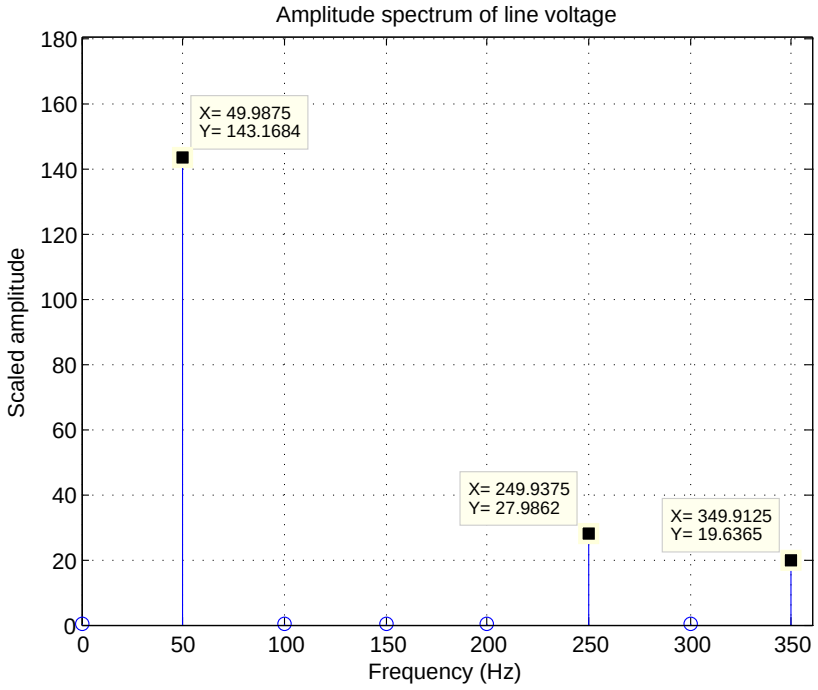

Figure 11.7: Amplitude spectrum plot of the voltage. The FFT analysis is performed on data from period number 6 in the signal given in Figure 11.5. $Ls = 6.7\ mH, R = 10\ \Omega$.

In Figure D.2 and Figure D.3 in section D in the appendix, another FFT plot of current and voltage respectively is given. The difference between these two plots and the plots in Figure 11.6 and 11.7, is that the filter capacitor on DC side of the rectifier is increased from 2.07 mF to 6.0 mF. As can be seen when comparing these figures, increasing the filter capacitor by this much has very little impact on the harmonic content. Although not shown graphically in this report, changing the capacitance even more in either direction has a very small impact on the system. Therefore, capacitance will be held constant at 2.07 mF for the rest of the simulations.

Summarizing results

To obtain a better understanding of 5^{th} and 7^{th} harmonic magnitude under different circumstances, a number of simulations were performed. The results are summarized in Table 11.1 and Table 11.2. In Table 11.1, harmonic content in current is given both in percentage of the fundamental frequency, as well as in absolute value. This is done for $R_{DC} = 10$, 20 and 80 Ω, and for each of those resistances, $L = 6.7$, 5.05 and 3.37 mH is tested (see calculations in section 10.4). The absolute value is unitless and can be used to compare harmonic content in different simulations with each other. Harmonic content given in percentage of the fundamental is a good measure on how disturbed a current or a voltage is.

Harmonic content in current

		$R_{DC} = 10\ \Omega$		$R_{DC} = 20\ \Omega$		$R_{DC} = 80\ \Omega$	
	Harmonic:	5^{th}	7^{th}	5^{th}	7^{th}	5^{th}	7^{th}
L=6.7 mH	*% of fund.*	10.75 %	5.38 %	16.89 %	7.05 %	27.28 %	7.86 %
	Abs. magn.	1.53	0.77	1.35	0.56	0.69	0.20
L=5.05 mH	*% of fund.*	13.39 %	6.34 %	19.60 %	7.26 %	30.40 %	9.74 %
	Abs. magn.	1.99	0.94	1.61	0.60	0.77	0.25
L=3.37 mH	*% of fund.*	17.29 %	7.17 %	23.43 %	7.26 %	35.80 %	14.34 %
	Abs. magn.	2.70	1.12	1.98	0.61	0.92	0.37

Table 11.1: Summary of harmonic content in current under different simulation conditions. For R_{DC} = 10, 20 and 80 Ω respectively, three different upstream inductances are tested. Results are given in absolute magnitudes that are directly comparable with each other, and as a % of the fundamental frequency component.

In Table 11.2, exactly the same information from the same simulations is given for the harmonic content in the voltage.

Harmonic content in voltage

		$R_{DC} = 10\ \Omega$		$R_{DC} = 20\ \Omega$		$R_{DC} = 80\ \Omega$	
	Harmonic:	5^{th}	7^{th}	5^{th}	7^{th}	5^{th}	7^{th}
L=6.7 mH	*% of fund.*	19.55 %	13.72 %	16.16 %	9.47 %	7.80 %	3.13 %
	Abs. magn.	27.99	19.64	24.78	14.52	12.54	5.04
L=5.05 mH	*% of fund.*	18.50 %	12.30 %	14.20 %	7.38 %	6.56 %	2.94 %
	Abs. magn.	27.40	18.22	22.15	11.51	10.59	4.74
L=3.37 mH	*% of fund.*	16.14 %	9.41 %	11.47 %	4.97 %	5.21 %	2.92 %
	Abs. magn.	24.76	14.43	18.19	7.87	8.44	4.72

Table 11.2: Summary of harmonic content in voltage under different simulation conditions. For R_{DC} = 10, 20 and 80 Ω respectively, three different upstream inductances are tested. Results are given in absolute magnitudes that are directly comparable with each other, and as a % of the fundamental frequency component.

In the appendix, a time plot of current and voltage waveforms as well as an FFT plot of voltage and current is given for two selected simulations. Figure D.4, Figure D.5 and Figure D.6 are from the simulation with an upstream inductance of 5.05 mH and 20 ohm DC side resistance. Figure D.7, Figure D.8 and Figure D.9 are from the simulation with an upstream inductance of 3.37 mH and 80 ohm DC side resistance. From the two waveform plots, it can be seen that inrush current is larger when inductance is low. Also, in Figure D.7, a startup effect makes the current zero for the first couple of periods, as explained in the figure caption. What is interesting to notice from this is that when current is zero; voltage waveform is a perfect sinusoidal. This shows that harmonics in the voltage is created by

harmonics in the current. The FFT plots only confirm what is summarized in Table 11.1 and Table 11.2.

Discussing simulation results

There are a few interesting trends worth noting from the above tables. Without exception, 5^{th} harmonic component is larger than 7^{th} harmonic in an individual simulation, for both current and voltage. This is expected, as the magnitude of harmonics produced by a rectifier decreases with the harmonic order [17, p. 485].

Further, considering the *absolute magnitude* of the harmonics, without exception this decreases for higher DC side resistance. Again, this is expected, as a smaller current through the rectifier should reduce harmonic magnitude in both current and voltage.

However, when looking at harmonic magnitude measured relative to its fundamental component, voltage and current harmonics have different development for larger DC side resistance. Magnitude of harmonic current actually increase relative to its fundamental component for larger resistance, while harmonic voltage decreases relative to its fundamental. When resistance increase, current flow decreases. When there is less current flowing (hence smaller absolute magnitude of current harmonics), there is less harmonic current available to distort the voltage. Fundamental component of the voltage actually increases for larger resistance, as shown in section 11.1, and the relative magnitude of voltage harmonics will therefore decrease even if relative magnitude of current harmonics increases.

Looking at one table column at the time and comparing harmonics for decreasing inductance, L, current and voltage harmonics develop differently again. Current harmonics increase for decreasing inductance while the voltage harmonics decrease for decreasing inductance, both in absolute magnitude and measured relative to the fundamental. Circuit inductance smooth current and explain why current harmonics are smaller for larger inductance. For the voltage, less upstream inductance gives a stronger network. The voltage source at the far left of the Simulink model in Figure 10.1 is stiff, and the inductance between the source and the rectifier allows harmonics to exist in the voltage at AC side of the rectifier. Reducing this inductance, allow less harmonic content in the voltage. However, it is noted that even with an inductance of only 3.37 mH, significant voltage harmonics are generated.

11.3 Conclusion of Simulink simulation

To avoid voltage collapse and too large power flow in the circuit, resistance at DC side of the rectifier should not be any lower than $5-10\ \Omega$, depending on upstream inductance. As long as R_{DC} is kept above this minimum value, voltage magnitude and power flow through the rectifier should not be of any concern.

From the waveforms depicted in Figure 11.5 in section 11.2 and Figures D.4 and D.7 in section D in the appendix, it can be seen that a large inrush current occur. When starting an induction machine in parallel with the rectifier in the laboratory, inrush currents are expected to become very large. Therefore, installing a soft start equipment upstream of the point of common coupling is preferred.

For the induction machine in the laboratory to draw harmonic current, harmonics must be present in the voltage. Therefore, voltage harmonics measured relative to the fundamental component are the most important harmonics from these simulations. Table 11.2 shows that voltage harmonics decrease from upper left to bottom right. In the laboratory work, a resistance between 10 Ω and 20 Ω will be attempted. The inductance will be adjusted to reach desired harmonic levels, but based on the information from Table 11.2, a value around 4 mH is expected to be sufficient.

When generating harmonics by the use of a rectifier, 5^{th} harmonic component will be larger than 7^{th} harmonic, and the difference seen in Table 11.1 and Table 11.2 is substantial. At the pumping station where the harmonics are present, the 7^{th} harmonic is the largest harmonic. However, for the purpose of this work it is not considered essential which harmonic component is largest, as long as both components can be measured and distinguished from any possible harmonics present in supply voltage in the laboratory.

Chapter 12

Laboratory Work

12.1 Procedures

The laboratory work will be conducted as individual runs, where some parameters will be adjusted during a run, while the upstream inductance L can only be adjusted when the circuit is disconnected and de-energized. Therefore, inductance L is always constant for a single machine run. Parameters that can be adjusted during a run, is induction machine loading and rectifier loading. In addition, both these components can be totally disconnected and reconnected during a run. Machine loading can be continuously regulated during operation, by use of the DC machine. However, when adjusting the DC side resistance, rectifier will be disconnected from the circuit and reconnected with a different load.

As shown and described in section 9.2, there are several places where power can be interrupted and reconnected in the laboratory set up. Contactors can be controlled from the control desk (depicted in Figure F.2 in section F in the appendix). In addition to the three contactors $K101$, $K2$ and $K102$, the soft start equipment has a switch that can connect the circuit. To reduce inrush current at start-up of a machine run, the soft start should be the last switch to be turned on. If both the rectifier and the induction machine shall be connected from start, contactor $K101$, $K2$ and $K102$ should be in *on* state, before the soft start is turned on and energize the complete circuit. In rush current is then reduced by the soft start equipment. Alternatively, only the induction machine or the rectifier can be connected from the beginning of a machine run.

When de-energizing the circuit, disconnecting $K2$ and $K102$ first is preferred. Disconnecting these contactors first, means a smaller current is interrupted and stress on equipment is reduced. However, contactor $K102$ is dimensioned to interrupt the complete load current. When conducting a machine run, measurement information available from Elspec measurements is very limited. Only RMS values of current and voltage are live streamed to a screen. Therefore, it is extremely important to note the exact time of the day (to the second) for every action per-

formed from the control desk. This allows post processing of the data in Elspec Investigator [4]. In addition, the oscilloscope and the Power Harmonic Analyzer from FLUKE is used for a live feed of current waveform. The current clamps can be connected as desired, usually at induction machine stator. This is used as a control of Elspec measurements, and to ensure that the circuit behave as expected. As these measurements are not particularly well looking, they are not included in the results.

Many machine runs were conducted and the general procedure is the same for every run. Before a machine run, all switches are in *off* state and the main fuse is disconnected, leaving the circuit de-energized and finger-protected. Machine rotor resistance is set to *start* mode and resistance on DC side of rectifier is selected by buttons on the control desk. The water supply to the water cooled resistance is switched on and all measurement equipment is turned on. First step in energizing the circuit is to connected the main fuse. Then, rectifier and the induction machine is connected to the circuit by the use of contactors $K2$ and $K102$ (or only one of them if desired), and contactor $K101$ is set to *on*. Current start flowing into the circuit when the *on* button is pushed on the soft start equipment. Exact time of the day is noted and machine rotor resistance is switched from *start* to *operation* immediately.

This leaves the machine running idle and the rectifier drawing power. From this point, every run is slightly different. However, at some point, the DC machine is energized from the control desk. For the DC machine to work as a load it must be operated on a lower rotational speed that the induction machine. Then, loading can be adjusted by controlling armature current in the DC machine from the control desk. When changing rectifier load, the rectifier is first disconnected by the use of contactor $K101$. The desired combination of DC side resistances is chosen from the control desk and the rectifier is then reconnected by the use of contactor $K101$. Again, for every connection, disconnection or change in machine loading, the exact time of the day is noted.

When shutting down the machine, the two contactors $K101$ and $K2$ are switched off first, one at the time. All current has then been interrupted. Finally, the last contactor and the soft start equipment is turned off. Time of the day is noted, main fuse is disconnected and rotor resistance is switched back to *start*.

12.2 Base case

To establish a reference point for comparison of machine runs with different operational conditions, a base case machine run was performed. It should be mentioned that due to practical circumstances regarding the building process of the laboratory setup, the base case was the last machine run performed in the laboratory. However, this is not expected to affect the result at all. In the base case, the upstream inductance connected between the machine and the grid is removed. In

addition, the rectifier is removed from the circuit and the induction machine is connected directly to the mains. Despite being the last machine run performed, this is the first being presented here.

In Figure 12.1, waveforms of machine stator voltage and current is given in an Elspec Investigator plot [4]. As expected, these are both smooth and sinusoidal. The network is stiff and does not allow large voltage disturbances. In Figure C.2 in the appendix, 5^{th} and 7^{th} harmonic voltages and currents are shown. Harmonic content is indeed small and none of the two harmonics are significantly larger than the other. Also, a plot of voltage and current RMS values during the machine run is included in Figure C.1 in the appendix. As expected, voltage is stiff at around 230 V and only slightly affected by increased current flowing into machine stator. When increasing and reducing machine loading, stator current increase and decrease respectively.

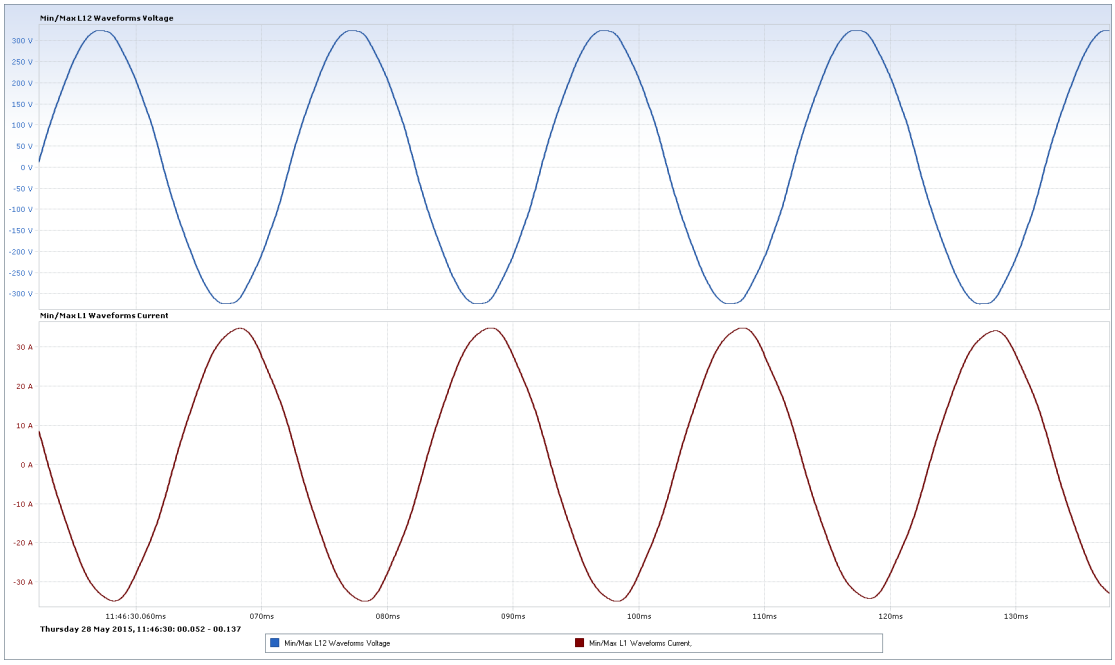

Figure 12.1: Elspec Investigator plot of voltage and current waveforms from machine run performed on May 28, 2015. In the upper pane, machine stator voltage V_{12} is given. In the lower pane, machine stator current I_1 is given. This machine run works as the base case and the induction machine is connected directly to the network. No upstream inductance is connected, neither is the rectifier.

For a proper investigation of interharmonics occurring in proximity of the 7^{th} harmonic frequency, an FFT plot is made in Matlab from the 10 second interval 11:46:30 - 11:46:40 in Figure C.1. This is shown in Figure 12.2. From this is becomes clear that there is a 7^{th} harmonic frequency component present in the voltage, and that there is no interharmonic component.

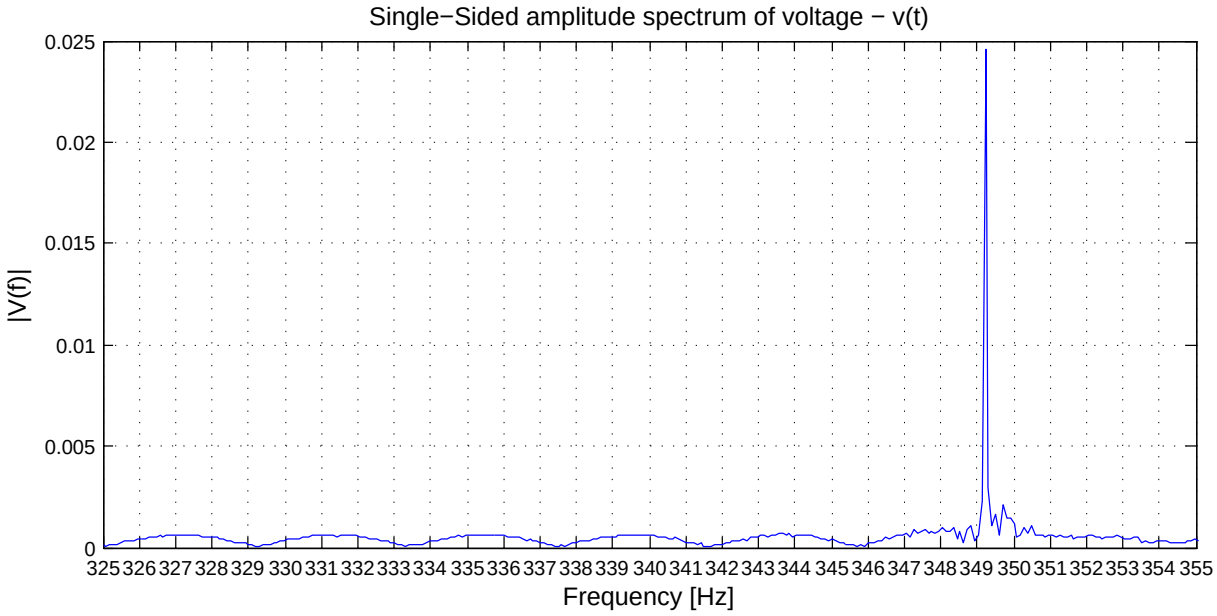

Figure 12.2: Amplitude spectrum of machine stator line voltage V_{12} for frequencies around the 7^{th} harmonic frequency. Data is taken from the 10 second interval 11:46:30 - 11:46:40, May 28, 2015. The machine is loaded and run at 1450 rpm, a slip of 3.33 %. The induction machine is connected directly to the network without any extra inductance and no rectifier connected.

In Figure D.10 in the appendix, a similar FFT plot for the machine stator current in given. Again, there is only a clean 7^{th} harmonic component present, without any interharmonic.

12.3 Voltage measurements of machine run

For a proper and tidy examination of the harmonic content in the laboratory setup, several machine runs under different operational conditions must be performed. To do this, several parameters in the laboratory setup can be adjusted. By adjusting machine loading, the slip of the machine is controlled. This is important for investigating how the machine slip affects the harmonics in the machine. Further, there are two parameters that are expected to affect harmonic content in machine stator winding - the power drawn by the rectifier and the upstream inductance. These effects have already been studied in the laboratory preparations by the use of a Simulink simulation in chapter 10.

In the first machine run, ensuring that all equipment work as expected, including measurement equipment is important. Together with the calculations and simulations performed at forehand, the first machine run can be used to tune parameter settings to reasonable values. In Figure 12.3, a new plot from Elspec Investigator [4] is included. In this plot there is used a large upstream inductance. For a given air gap in the inductor, three coils are connected in series creating an inductance

of 6 mH per phase. In the upper pane, the RMS line voltage V_{12} in the induction machine stator is shown. In the lower pane, the green line is the 5^{th} harmonic component and the orange line is the 7^{th} harmonic component, of machine stator voltage V_{12}. The time of the day can be read along the x axis, and is the same for both panes. Arrows are drawn in the plot to clarify the connection and disconnection sequence, which is summarized in Table 12.1.

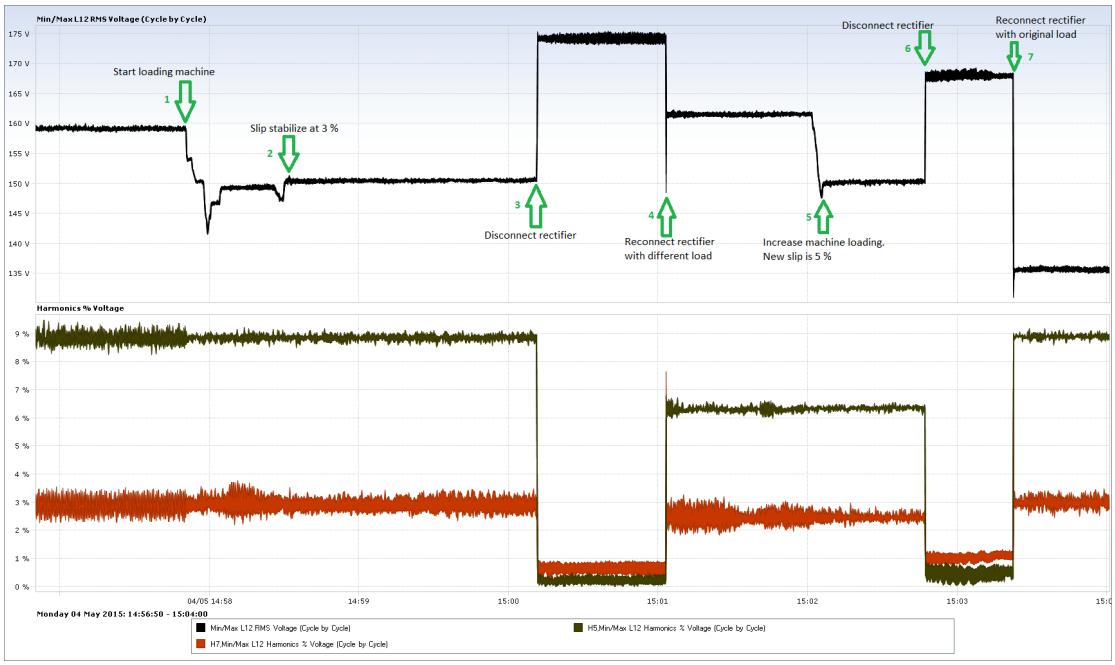

Figure 12.3: ELSPEC Investigator plot of machine run performed on May 4, 2015. In the upper pane, machine stator voltage V_{12} is given. In the lower pane, green line is the 5^{th} harmonic component and the red line is the 7^{th} harmonic component of the voltage, given in percentage of the fundamental component. The inductance L during the machine run is 6 mH. Connection and disconnection sequence is given in Table 12.1.

The connection sequence begin with both the rectifier and the induction machine connected. On DC side of the rectifier there is connected three resistances in parallel, $R = 22\ \Omega$, $R = 44\ \Omega$ and $R = 80\ \Omega$, in total constituting a resistance of $R = 12.394\ \Omega$. However, there is no load connected to the machine, and it runs idle. In the lower pane it can be seen that the 5^{th} harmonic component is about 9 % of the fundamental, around three times the 7^{th} harmonic at only 3 %. As indicated in the plot, load is connected and adjusted so that the machine runs at 3 % slip, which equal a rotational speed of 1450 rpm. This does not seem to affect the harmonic components much.

Parameter / Zone	Machine load	Rectifier load
start - 1	idle	$R_{DC} = 12.394\Omega$
1 - 2	increasing	$R_{DC} = 12.394\Omega$
2 - 3	$s = 3\%$	$R_{DC} = 12.394\Omega$
3 - 4	$s = 3\%$	disconnected
4 - 5	$s = 3\%$	$R_{DC} = 22\Omega$
5 - 6	$s = 5\%$	$R_{DC} = 22\Omega$
6 - 7	$s = 5\%$	disconnected
7 - end	$s = 5\%$	$R_{DC} = 12.394\Omega$

Table 12.1: Overview of the connection sequence in the first machine run. The zones correspond to the numbers indicated in Figure 12.3

At around 15:00:15 the rectifier is disconnected from the circuit. This is indicated in the plot and the circuit responds as expected. Harmonic content immediately drop to almost zero and the stator voltage of the machine rises. When the rectifier reconnects, harmonic content rises again, and machine voltage drops. This time the rectifier has a larger resistance connected at DC side, and the rectifier draw less power. This can be recognized in stator voltage which stabilize at a slightly higher level than before. Then machine loading is increased further and stator voltage drops again. When the rectifier is disconnected again, the voltage does not reach the same level as earlier, due to its larger loading. Finally, rectifier is reconnected with its original loading, making the total circuit loading the highest during the whole run. This can be seen in the voltage which reaches a level of only 136 V. The connection and disconnection sequence is summarized in table 12.1

There are a few points worth noting from this plot. Varying machine slip is an important part of this laboratory exercise because a possible rotor-stator interaction should be affected by the machine slip. The view presented in Figure 12.3 does not indicate that harmonic content is affected by machine loading, hence machine slip. However, power drawn by the rectifier do affect the harmonic content. 5^{th} harmonic component is reduced, as expected. That is because the induction machine, which draws a more sinusoidal current, now draws a larger share of the total current drawn from the network, and to a larger extent determine the voltage at point of common coupling. Since the harmonic current drawn by the rectifier, which draws a very disturbed current, now draws a smaller share of total current, it is less able to generate harmonics in the voltage. However, the 7^{th} harmonic only have a very small drop in magnitude and looks almost unaffected by the change in rectifier current.

It is noted that harmonic content, both 5^{th} and 7^{th} voltage harmonics, is large enough to distinguish it from potential network harmonics or small measurement inaccuracies, which is very important. Finally, it is noted that due to large upstream inductance, the machine stator voltage is very low. Even with rectifier disconnected and a slip of 3 %, the voltage reaches only 175 V. That is 24 % less

than network voltage in the area (230 V) and way outside the accepted voltage in the Norwegian grid, which is $230 \pm 10\%$, according to FoL [15].

In Figure 12.4, a view of voltage and current waveform from a part of the machine run depicted in Figure 12.3 is given. This shows that when the rectifier is connected, both waveforms are distorted and the presence of harmonics is obvious. The waveforms are typical when 5^{th} and 7^{th} harmonics are present.

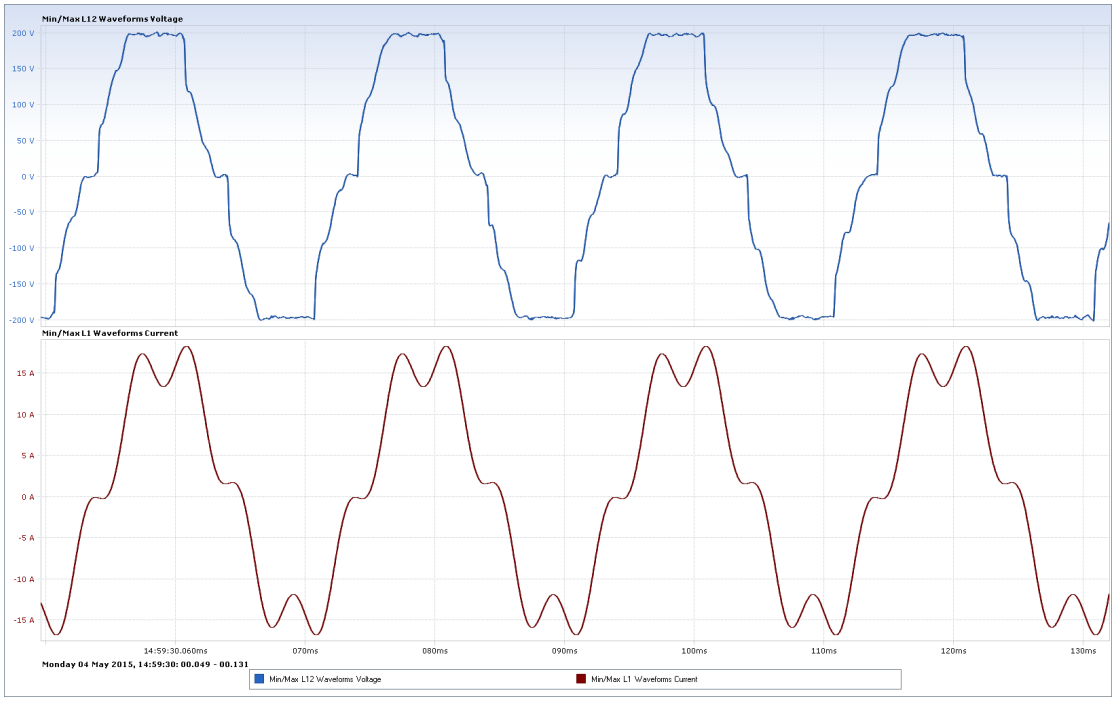

Figure 12.4: Elspec Investigator plot. Waveform of machine stator voltage V_{12} is given in the upper pane, while machine stator current I_1 is given in the lower pane. The view is from four periods while the rectifier is connected in Figure 12.3.

FFT analysis of voltage

In the Specialization project, working as a preliminary work to this Master's thesis, several FFT analyzes of already measured data were performed and presented [12]. The same Matlab code, written by Mr. Leif Warland at Sintef Energy Reaserch, will be used in this work to perform similar analyzes of data from the tests performed in the laboratory. In Figure 12.5, an FFT analysis performed on the voltage data from the test run presented in Figure 12.3 is presented. The frequency interval goes from 325 Hz to 355 Hz on the x axis, while the voltage content for each frequency can be read at the y axis.

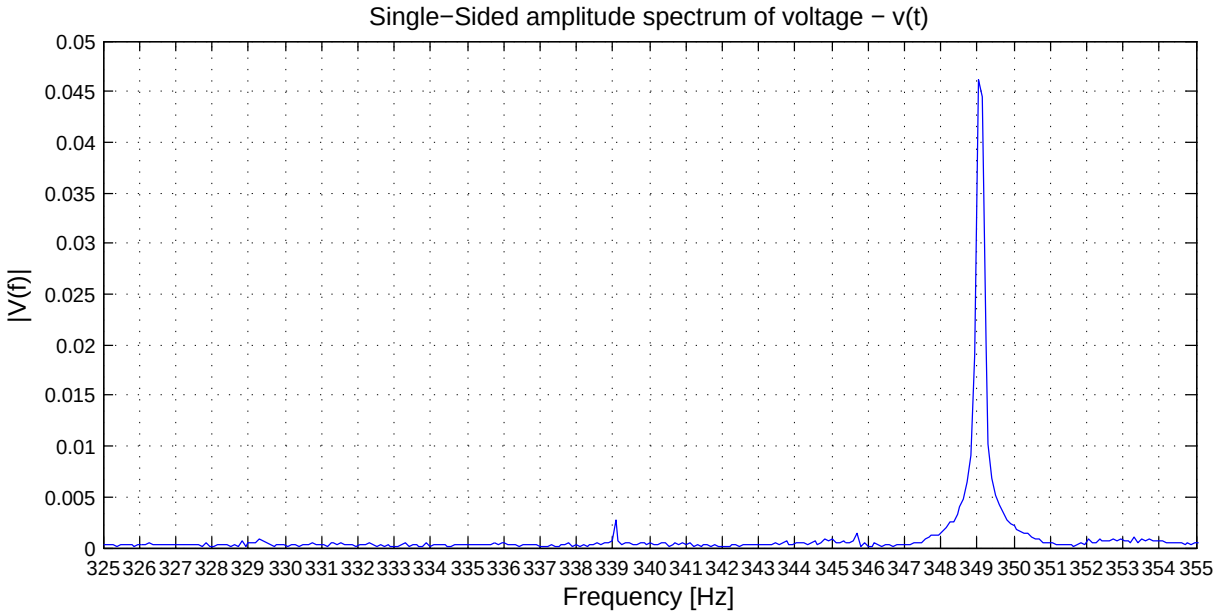

Figure 12.5: Amplitude spectrum of machine stator line voltage V_{12} for frequencies around the 7^{th} harmonic frequency. Data is taken from the 10 second interval 14:59:30 - 14:59:40, May 4, 2015 in Figure 12.3. The machine is loaded and run at 1450 rpm, a slip of 3.33 %. The shunt-connected rectifier has a resistance of $R = 12.394\Omega$.

In the time interval that the FFT plot in Figure 12.5 is made from, the rectifier is feeding 5^{th} and 7^{th} harmonics to the machine. It is clearly shown in this plot that there is only a 7^{th} harmonic component present, which means that no visible interharmonic component has been created by the induction machine. Since there is only one frequency component present, it is not possible for any beat to occur in this voltage.

In Figure 12.6, a similar FFT plot for frequencies around the 5^{th} harmonic frequency is given. This shows exactly the same as Figure 12.5, that there is no interharmonic component for the 5^{th} harmonic to interact with.

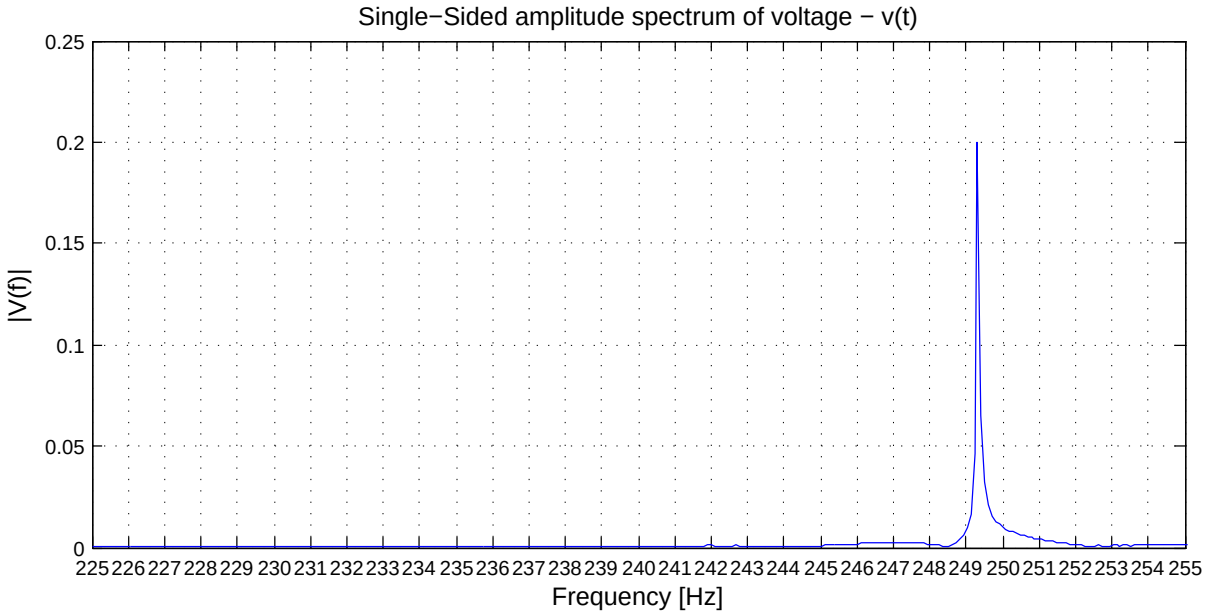

Figure 12.6: Amplitude spectrum of machine stator line voltage V_{12} for frequencies around the 5^{th} harmonic frequency. Data is taken from the 10 second interval 14:59:30 - 14:59:40, May 4, 2015 in Figure 12.3. The machine is loaded and run at 1450 rpm, a slip of 3.33 %. The shunt-connected rectifier has a resistance of $R = 12.394\Omega$.

From the two plots presented in Figure 12.5 and Figure 12.6, one more thing should be noted. Machine stator voltage does contain 5^{th} and 7^{th} harmonics, provided on purpose and in a controlled manner, by the use of a rectifier. Also, Elspec Investigator [4], the software provided with the measurement equipment delivered by ELSPEC, number 3 in List of Equipment, shows 5^{th} and 7^{th} harmonics present. Despite of this, both the 5^{th} and the 7^{th} harmonic in Figure 12.6 and Figure 12.5 respectively, are shifted by between 0.5 Hz and 1 Hz. This looks very similar to the plot presented in Figure 2.3 in chapter 2 and every FFT plot presented in the Specialization project. In section 9.3, the MATLAB code used to create these plots where tested and proved to give a correct representation of the frequency components. Therefore, Figure 12.5 and Figure 12.6 strengthen the assumption that there are clean 5^{th} and 7^{th} harmonics present. For the rest of this work it will be assumed that either measurements are slightly inaccurate or data processing distorts the signal slightly, making the components occur at different frequency in the FFT plots.

In section D in the appendix, two more FFT plots of stator voltage is included in Figure D.11 and Figure D.12. These only confirms that no interharmonic component appear in the machine voltage.

12.4 Current measurements of machine run

In the plots presented earlier in section 12.3, stator voltage and stator voltage harmonics are shown. However, current measurements performed did not always look completely trustworthy. In Figure 12.7, this is illustrated with data from the same machine test and the same time interval as presented in Figure 12.3. In the upper pane, machine stator voltage V_{12} is plotted exactly as in Figure 12.3. In the lower pane, stator 5^{th} and 7^{th} harmonic current is given in ampere. As indicated in the lower pane, the 7^{th} harmonic component (light green line) is zero at all times, independent of the rectifier. The 7^{th} harmonic current is not expected to be zero as there is a 7^{th} harmonic voltage present, shown in Figure 12.3. The 5^{th} harmonic current component is present, and the magnitude looks reasonable. However, there is a peculiar mismatch between the disappearance of the 5^{th} harmonic and disconnection of the rectifier. As indicated by arrows and circles in Figure 12.7, the 5^{th} harmonic disappear before the rectifier is actually disconnected, at both disconnections.

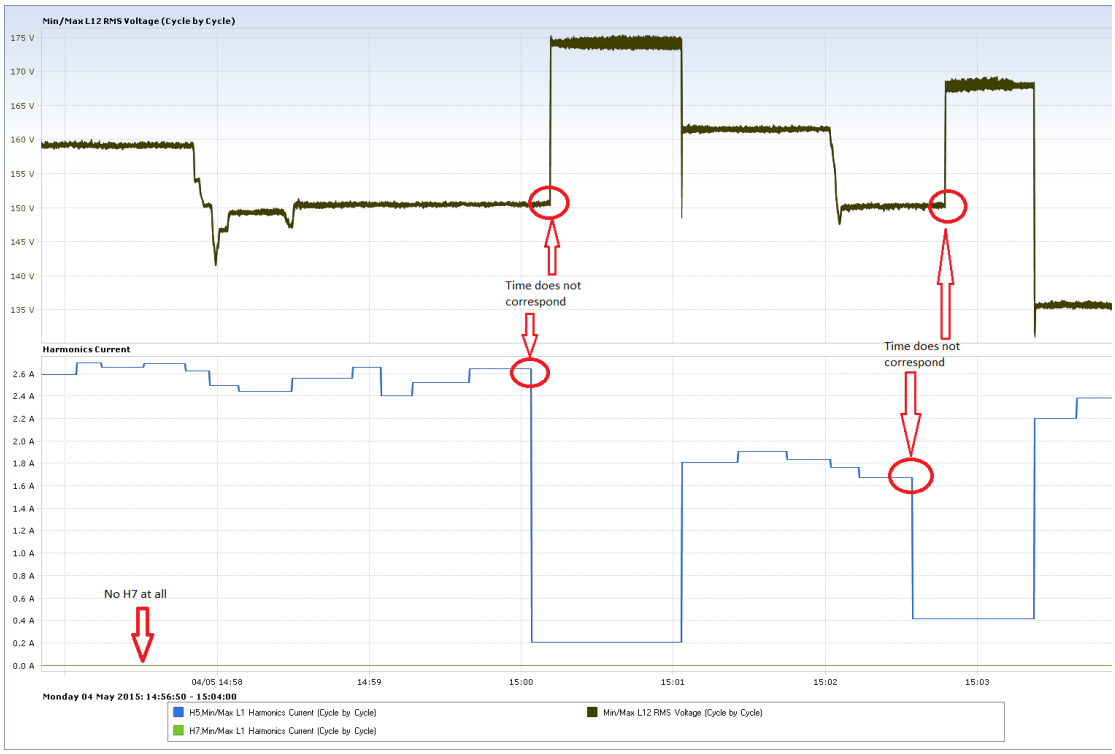

Figure 12.7: ELSPEC Investigator plot of machine run performed on May 4, 2015. In the upper pane, machine stator voltage V_{12} is given. In the lower pane, stator 5^{th} and 7^{th} harmonic current is given in ampere. The inductance L during the machine run is 6 mH. Connection and disconnection sequence is given in Table 12.1.

It is assumed to be a coincidence that the 5^{th} harmonic disappear just prior to disconnection of the rectifier at both occasions. There should be no sign in the

circuit of the disconnection before it happens, so it is not possible for the current to respond to the disconnection in advance. Also, plots from other machine runs support the assumption that the 5^{th} harmonic sometimes disappear at random. One such plot is presented in Figure C.3 in the appendices.

The stator current is measured using three Rogowski coils for AC current measurements of current from 0-300 A, number 1 in List of Equipment. A possible explanation for the questionable current measurement is that the current rating of these Rogowski coils are too high, and that the coils therefore are unable to precisely measure currents of very small magnitude. In addition, these Rogowski coils should ideally be tuned for the analyzer equipment that is used. This is not done and could contribute to the reduced measurement precision.

To investigate this, new tests were performed. A single phase Power Harmonic Analyzer by FLUKE, number 2 in List of Equipment, was used in addition to the ELSPEC analyzer, to verify the current. This uses a current clamp, number 4 in List of Equipment with rated current 1-500 A. In addition, one of the Rogowski coils was twisted one extra turn around the current conductor to measure double current. In Figure 12.8, a segment of a recording from Elspec Investigator from this machine run is shown. In the upper pane the RMS stator current of phase 1, where the Rogowski coils is twisted one extra turn, is shown. In the middle pane, 5^{th} and 7^{th} harmonic components of current in phase 1 (dark red and light green respectively) is shown. Also, 5^{th} and 7^{th} harmonic of current in phase 2, both dark green, is given in the middle pane. In the lower pane, the 5^{th} and 7^{th} harmonic component of stator voltage are given to show that they do exist.

Currents are given in ampere to visualize how the current in phase 1 is reduced when the Rogowski coil is removed and replaced with only one turn around the conductor. In the upper pane, a 50 % reduction in current is clear around 11:52:35. This is when the Rogowski coil in phase 1 is rearranged from 2 to only 1 turn around the conducting wire. In the middle pane, the same reduction is seen in the 5^{th} harmonic component of phase 1. However, the 7^{th} harmonic component of phase 1 is not reduced by 50 %, but disappear completely. In addition, it should be noticed that the 7^{th} harmonic of phase 2 is absent during the whole plot and that the 5^{th} harmonics of both phase 1 and phase 2 are very similar after the Rogowski coil of phase 1 is twisted only one turn. This strongly indicates that when the 7^{th} harmonic gets very small in magnitude, it is simply too small for the Rogowski coils to measure it and it is recorded as zero. In addition, the measurements performed with the Power Harmonic Analyzer by FLUKE, did show a small 7^{th} harmonic component in the current during the entire machine run.

The conclusion from this test is that the Rogowski coils are considered trustworthy for their purpose in these experiments if the measured current is large enough. Therefore, current will be measured with the Rogowski coils twisted three turns around the conducting wire in future experiments. Three turns are the most turns practically feasible to achieve.

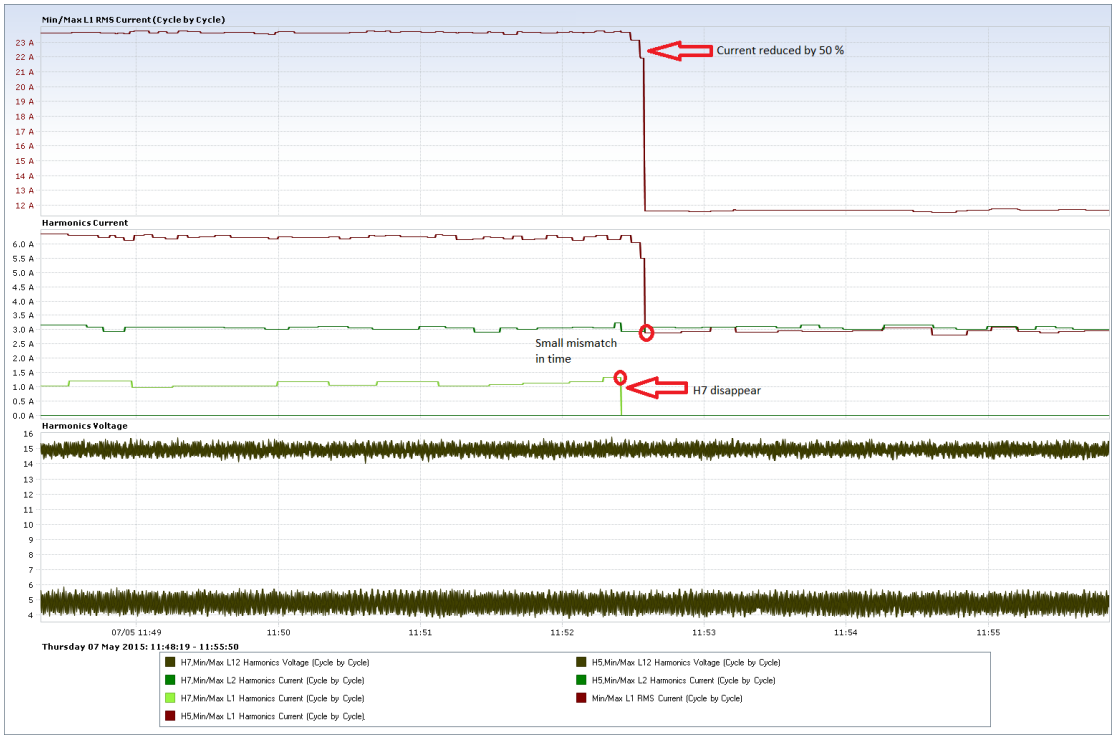

Figure 12.8: Elspec Investigator plot. In the upper pane the RMS stator current I_1 is shown. In the middle pane, 5^{th} and 7^{th} harmonic components of current I_1 and I_2 are given. In the lower pane, 5^{th} and 7^{th} harmonic component of stator voltage V_{12} are given. Inductance L during this machine run is 4 mH. DC side resistance is $R_{DC} = 12.4\ \Omega$.

12.5 New current measurements

In Figure 12.9, a recording from Elspec Investigator of a new machine run is included. In this run, all Rogowski coils are entangled three turns around its respective conductor, thus measuring three times as large current. When importing data from the measurement equipment, a reduction factor of 3 is added to the data, so that currents in the plot are scaled correctly. In the upper pane of Figure 12.9, all three phases of stator current is included. In the lower pane, 5^{th} and 7^{th} harmonic (red and blue line respectively) of current in phase 1 is shown. The inductance L in this run is 4 mH and the connection procedure is given i Table 12.2.

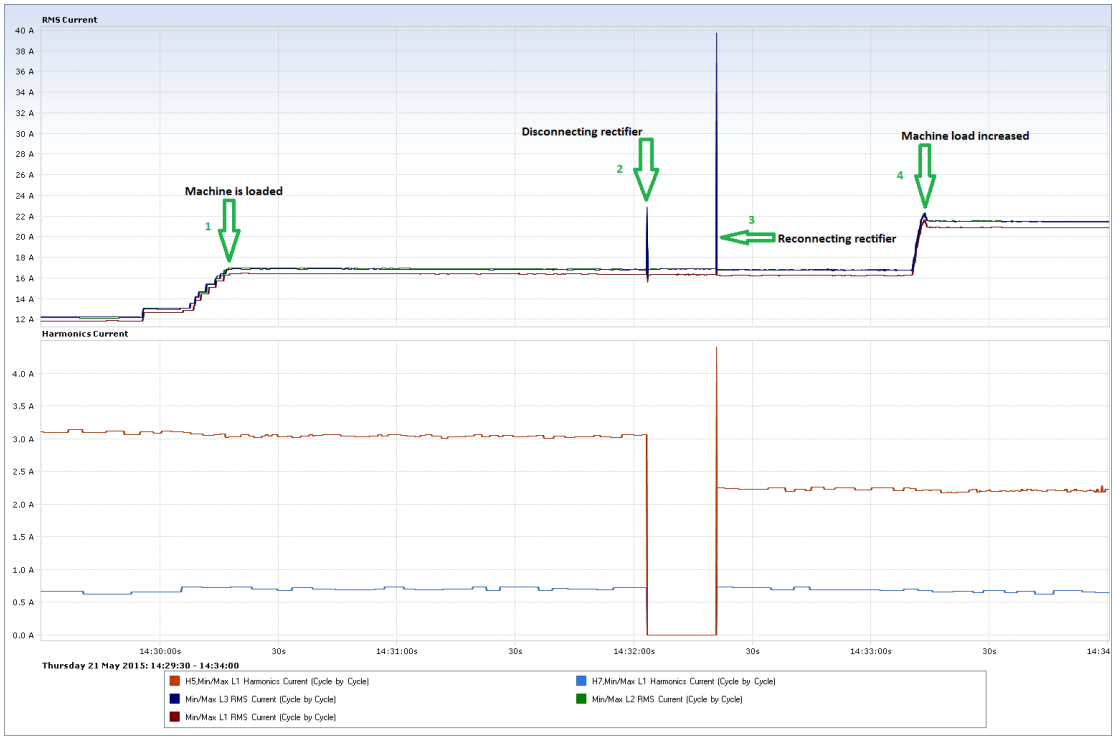

Figure 12.9: ELSPEC Investigator time plot, $L = 4\,mH$. In the upper pane, stator current of three phases is plotted. In the lower pane, 5^{th} (red line) and 7^{th} (blue line) harmonics of stator current are given. The connection and disconnection sequence is given in Table 12.2.

Parameter / Zone	Machine load	Rectifier load
start - 1	increasing	$R_{DC} = 12.394\Omega$
1 - 2	$s = 3.33\%$	$R_{DC} = 12.394\Omega$
2 - 3	$s = 3.33\%$	disconnected
3 - 4	$s = 3.33\%$	$R_{DC} = 22\Omega$
4 - end	$s = 4.7\%$ (rated)	$R_{DC} = 22\Omega$

Table 12.2: Overview of the connection sequence in the machine run. The zones correspond to the zones indicated in Figure 12.9 and Figure C.4.

Current in Figure 12.9 behaves as expected. 5^{th} and 7^{th} harmonics are present when the rectifier is connected. When disconnecting the rectifier, both harmonic components disappear. The 5^{th} harmonic is significantly larger than the 7^{th} harmonic. That is expected and in accordance with the voltage harmonics. Similar to the voltage harmonics in Figure 12.3, current harmonics are slightly reduced when rectifier load is decreased (measured in power), but the reduction of the magnitude is clear only for the 5^{th} harmonic component. No real change can be seen in the 7^{th} harmonic. In addition, changing machine loading has no visible influence on harmonic content. In section D in the appendix, a similar plot for a

weaker grid is given in Figure C.4. Stator current and current harmonics are given for a machine run where inductance is increased to $L = 6\ mH$. The two current plots look very similar, and harmonic behavior in Figure C.4 is not significantly different from what is seen in Figure 12.9. However, a slight reduction in current harmonic content is seen when upstream inductance is increased.

FFT analysis of current

Again, an FFT analysis of the data is performed in MATLAB. In Figure 12.10, a spectrum plot of frequencies from 325 Hz to 350 Hz for the current in phase 1 is given. The data is taken from the ten seconds from 14:31:30 to 14:31:40 in Figure 12.9, where the rectifier is connected. The FFT analysis do agree with the Elspec plot that a 7^{th} harmonic component exist. Again, the FFT analysis show no interharmonic component in proximity of the 7^{th} harmonic frequency.

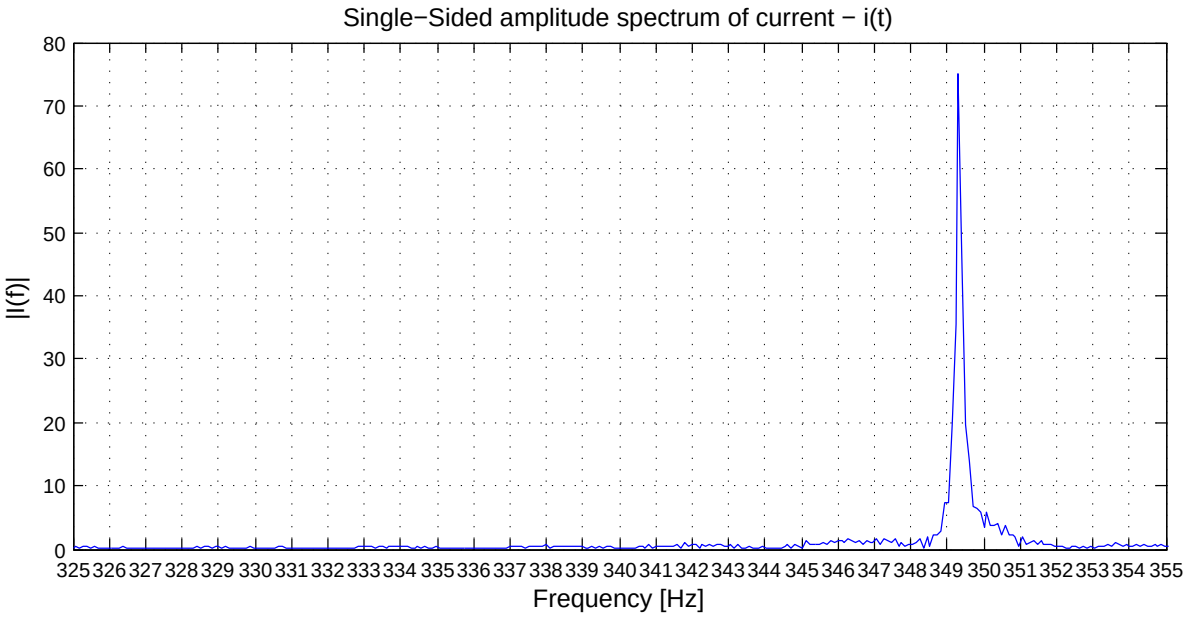

Figure 12.10: Amplitude spectrum of machine stator current I_1 for frequencies around the 7^{th} harmonic frequency. Data is taken from the 10 second interval 14:31:30 - 14:31:40, in Figure 12.9. The machine is loaded and run at 1450 rpm, a slip of 3.33 %. The shunt-connected rectifier has a resistance of $R = 12.4\ \Omega$.

In Figure 12.11 a similar FFT plot is given for the same data as in Figure 12.10, but for the frequencies around the 5^{th} harmonic frequency. Again, the presence of a 5^{th} harmonic is clear, while no interharmonic component is present.

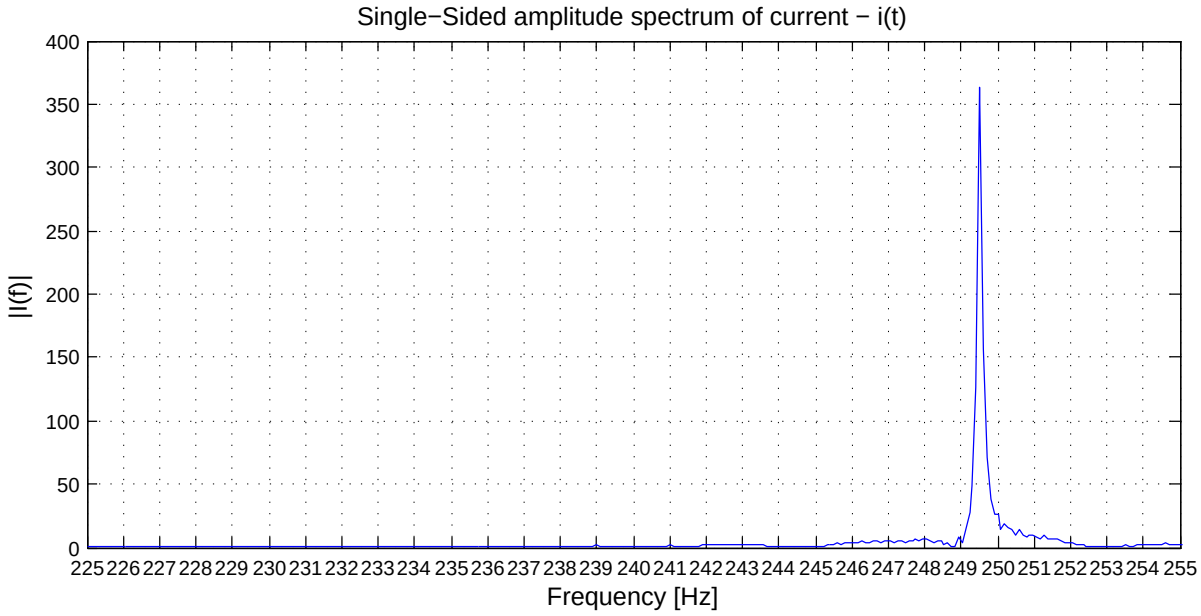

Figure 12.11: Amplitude spectrum of machine stator current I_1 for frequencies around the 5^{th} harmonic frequency. Data is taken from the 10 seconds 14:31:30 - 14:31:40, in Figure 12.9. The machine is loaded and run at 1450 rpm, a slip of 3.33 %. The shunt-connected rectifier has a resistance of $R = 12.4\ \Omega$.

Given the operational conditions where a rectifier is feeding the machine with 5^{th} and 7^{th} harmonics, many FFT plots have been created of both current and voltage, and no interharmonic component is visible in any of them. Two more FFT plots of current are included in section D in the appendix, in Figure D.13 and Figure D.14. Here data is taken from a machine run with $L = 6\ mH$, a smaller rectifier load (measured in power) and larger machine loading. These plots confirm that when harmonics are fed by the rectifier, no interharmonic component appears in the machine current, even if circumstances are slightly changed.

12.6 Interharmonic components without rectifier

During most machine runs, there are periods where the rectifier is disconnected and power flows through the inductance and directly into the machine. In Figure 12.3 in section 12.3, the rectifier is disconnected between 15:00:10 and 15:01:00. An FFT plot of voltage made from data from this time interval is given in Figure 12.12. Unlike every FFT plot made from measurement data with the rectifier connected, the plot in Figure 12.12 has an interharmonic component present around 341 Hz, in addition to a smaller 7^{th} harmonic component.

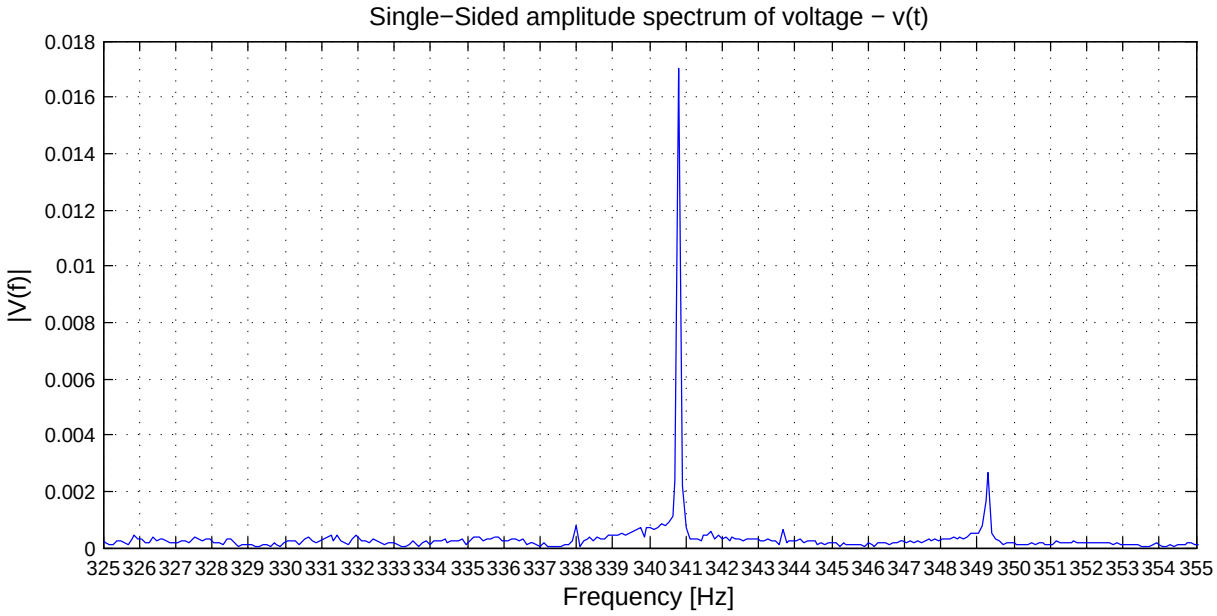

Figure 12.12: Amplitude spectrum of machine stator voltage V_{12} for frequencies around the 7^{th} harmonic frequency. Data is taken from the 10 seconds 15:00:30 - 15:00:40, in Figure 12.3. The machine is loaded and run at 1450 rpm, a slip of 3.33 %. The rectifier is disconnected and inductnace $L = 6\ mH$.

It is expected that the 7^{th} harmonic component in Figure 12.12 is much smaller than it was in the FFT plots presented in section 12.3, because the machine is no longer fed with harmonics by the rectifier. However, the interharmonic component occurring in Figure 12.12 was not present under similar condition with the rectifier connected. It should be emphasized that all FFT plots of voltage are scaled by exactly the same factor. Also, FFT plots of current are scaled by a common factor, but they are scaled differently from voltage plots. Therefore, the value on the y axis in a voltage FFT plot can be compared to the same value in other voltage FFT plots.

In Figure 12.13, another FFT plot from the same time interval is presented, this time of the current. Here, no interharmonic component is present. Again, the 5^{th} harmonic component is much smaller than it was in the FFT plots of current presented in section 12.3.

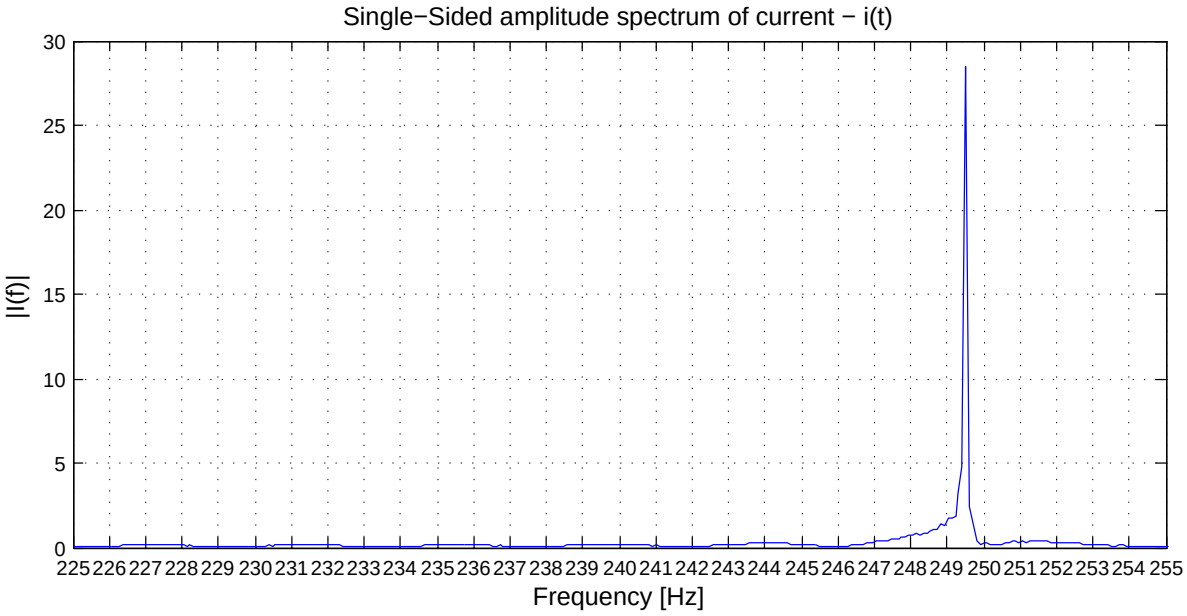

Figure 12.13: Amplitude spectrum of machine stator current I_1 for frequencies around the 5^{th} harmonic frequency. Data is taken from the 10 seconds 15:00:30 - 15:00:40, in Figure 12.3. The machine is loaded and run at 1450 rpm, a slip of 3.33 %. The rectifier is disconnected and inductnace $L = 6\ mH$.

In Figure 12.14, another FFT plot of machine stator voltage is given. Data is now taken from the 10 second interval 15:03:00 - 15:03:10, in Figure 12.3. The difference in operational conditions in Figure 12.14 and Figure 12.12, is the machine loading, hence the machine slip. Slip is increased from 3.33 % in Figure 12.12, to 5.0 % in Figure 12.14, and the intarharmonic component has moved from around 341 Hz to approximately 337 Hz. In section B in the appendix, calculations based on the assumption that a 7^{th} harmonic component exists in rotor and is transmitted to stator, occurring at a different frequency is given. According to these equations, the interharmonic component appearing in Figure 12.12, should have a frequency of 340.0 Hz (equation B.1), while the component appearing in Figure 12.14 should have a frequency of 335 Hz (equation B.2).

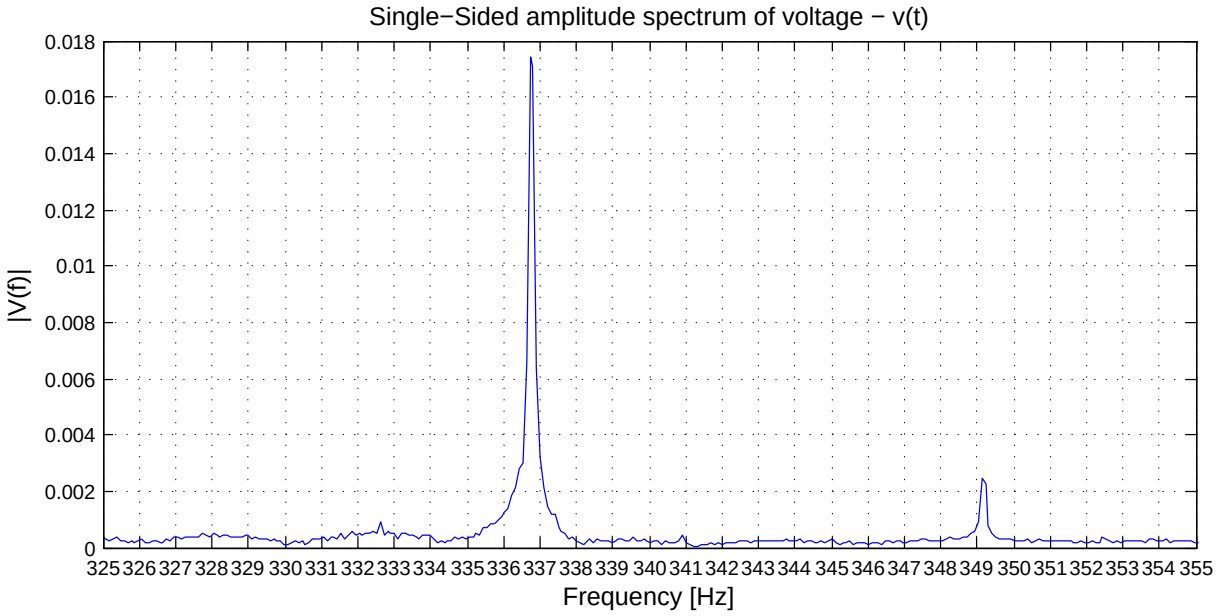

Figure 12.14: Amplitude spectrum of machine stator voltage V_{12} for frequencies around the 7^{th} harmonic frequency. Data is taken from the 10 seconds 15:03:00 - 15:03:10, in Figure 12.3. The machine is loaded and run at 1425 rpm, a slip of 5.0 %. The rectifier is disconnected.

In Figure 12.15, an FFT plot of machine stator voltage for frequencies around the 5^{th} harmonic frequency is given. Data is taken form the same time interval, 15:03:00 - 15:03:10, in Figure 12.3 where the rectifier is disconnected. Calculations in section B in the appendix show that the interharmonic component should occur at 240 Hz (equation B.3).

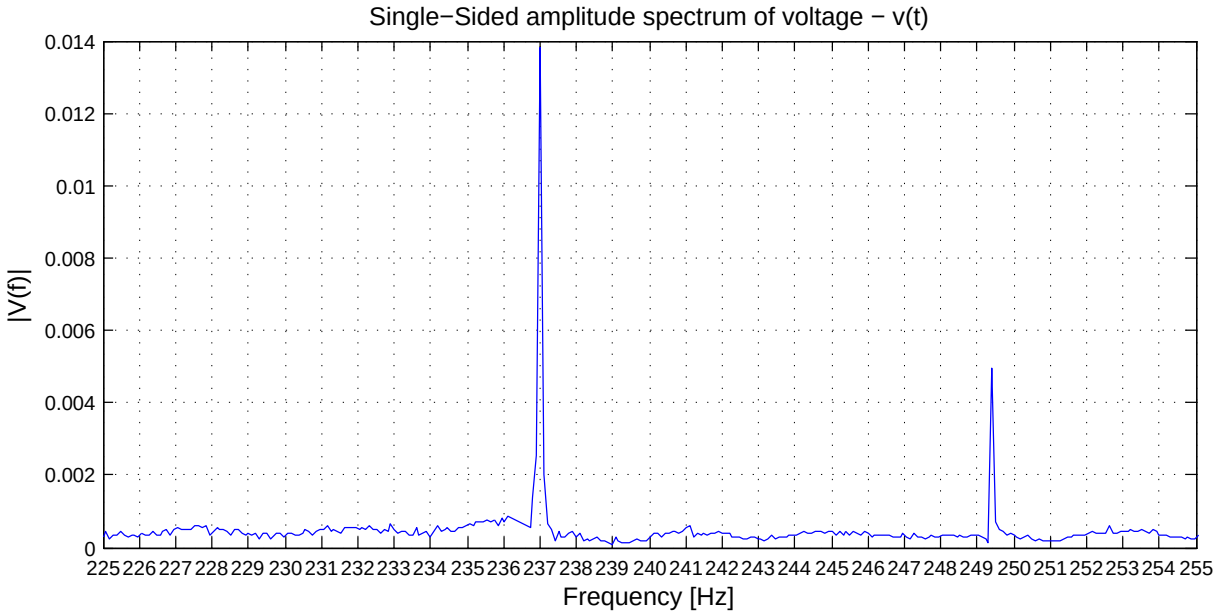

Figure 12.15: Amplitude spectrum of machine stator voltage V_{12} for frequencies around the 5^{th} harmonic frequency. Data is taken from the 10 seconds 15:03:00 - 15:03:10, in Figure 12.3. The machine is loaded and run at 1425 rpm, a slip of 5.0 %. The rectifier is disconnected.

The calculated frequencies do not match the measured frequencies completely. The mismatch is about 0.2 % - 0.8 %. Though calculations are slightly off, general behavior of the interharmonic components is in accordance with the idea of a rotor-stator interaction. When slip is increased, the frequency difference between the integer harmonic component and the interharmonic component do increase, which indicates that slip is decisive for the frequency of the interharmonic component.

In Table 12.3 calculated values and measured values for the different interharmonic components are summarized. In addition, the deviation between the two values is given.

Terms for calculations	**Calculated frequency**	**Measured frequency**	**Deviation**
s = 3.33 %, 7^{th} harmonic, Figure 12.12,	340.0 Hz	340.8 Hz	0.2 %
s = 5 %, 7^{th} harmonic, Figure 12.14	335.0 Hz	336.8 Hz	0.5 %
s = 5 %, 5^{th} harmonic, Figure 12.15	235.0 Hz	237.0 Hz	0.8 %

Table 12.3: Summary of calculations performed in section B in the appendix.

In Figure 12.16, a view of voltage and current waveforms from a part of the machine run depicted in Figure 12.3 is given. The waveforms are taken from an approximately 80 ms wide time window around 15:00:30 in Figure 12.3, where the rectifier is disconnected. This shows that when the rectifier is disconnected, both waveforms are much smoother and closer to a perfect sinusoid, compared to the waveforms when the rectifier is connected, depicted in Figure 12.4. However, the voltage waveform is still slightly disturbed, and the presence of smaller voltage harmonics is obvious.

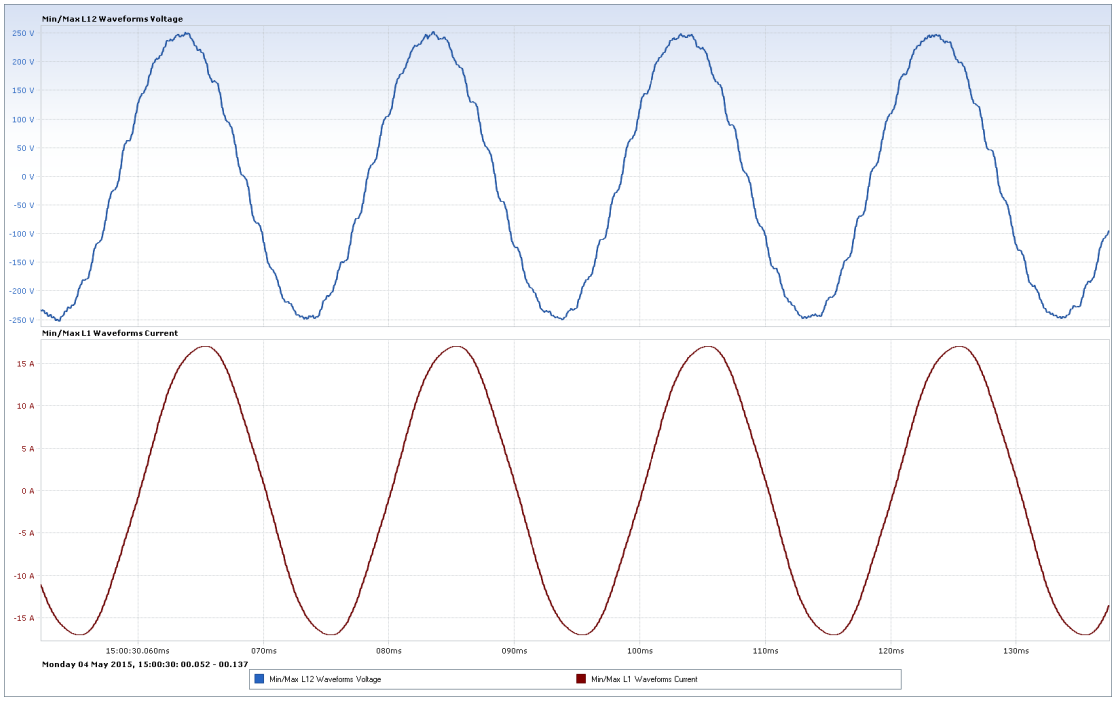

Figure 12.16: Elspec Investigator plot. Waveform of machine stator voltage V_{12} is given in the upper pane, while machine stator current I_1 is given in the lower pane. The view is from four periods while the rectifier is disconnected in Figure 12.3.

Comparing Figure 12.16 to the waveform of the base case, given in Figure 12.1 is interesting. The main difference in operating conditions between the two cases is the upstream inductance $L = 6\ mH$ connected in Figure 12.16. This inductance makes network voltage less stiff and allows the induction machine more influence over the voltage. Voltage harmonics generated by the machine is no longer suppressed by the network. While in the base case, the voltage is stiff and harmonics generated by the machine is suppressed. However, machine stator current is not much different in the two cases. Upstream inductance smooths the current, and remove harmonic content from the current.

In Figure C.5 in the appendix, the largest harmonic voltage components present in the waveform in Figure 12.16 are given. Figure C.5 shows that 16^{th}, 17^{th}, 18^{th} and 19^{th} harmonic components in the voltage are significant. These high order

harmonics explain the bumps seen on the voltage waveform in Figure 12.16.

In Figure C.6 in the appendix, the same harmonic components are given for the voltage waveform from the base case, presented in Figure 12.1. Figure C.6 confirms that the high order harmonics have almost disappeared in the base case voltage. That makes the waveform much cleaner and more sinusoidal.

In Figure C.5, total harmonic distortion of the voltage waveform in Figure 12.16 is given in the lower pane. In Figure C.6, total harmonic distortion of the voltage in the base case waveform in Figure 12.1 is given. Total harmonic distortion confirms that larger harmonic content is present in the weak grid. Since the high order harmonics are not present in supply voltage, this suggests that the source of these harmonics must be the induction machine itself.

Chapter 13

Discussion

13.1 Simulations

The Simulink model of the rectifier and the upstream inductance that was made worked as a preparation for the laboratory tests and gave a good indication on the amount of harmonics the rectifier would generate. Calculations estimated that an upstream inductance of $4-6\ mH$ was reasonable, and simulations largely confirmed that. In addition, simulations showed that caution should be taken to avoid very low voltages at machine stator terminals. Drawing large currents through the series connected inductance will give a low voltage in machine stator terminal, which may cause the machine to operate undesirably. That was useful knowledge when building the laboratory setup, to ensure a good combination of inductance and rectifier load.

Regarding generation of harmonics by the rectifier, some interesting points from the simulations should be noted. Simulation results are summarized in Table 11.1 and Table 11.2 in section 11.2. When increasing power flow through the rectifier (reducing ohmic resistance at DC side of the rectifier, which increases power delivered to DC load) absolute magnitude of harmonic content increased, both in voltage and current. When the magnitude of the current fundamental increases, it is natural that the magnitude of the current harmonics increase as well, in turn increasing magnitude of voltage harmonics. However, measured relative to the fundamental, harmonic content in current is reduced when increasing power flow. This is mainly due to a larger current flowing, and when flowing through a large inductance, current is smoothed. Voltage magnitude changes differently than current magnitude. Voltage magnitude is reduced when current flow increases, due to increased losses. Therefore, voltage harmonics increase relative to its fundamental for increased power flow through the rectifier.

Harmonics in the induction machine at the laboratory are created by harmonics in supply voltage, making the machine draw harmonic current. Therefore, harmonics in the voltage are the most important harmonics in the simulations. Table 11.2

shows that harmonics in the voltage is increased by increasing power flow through the rectifier and by increasing upstream inductance.

13.2 Functionality of laboratory setup

In general, the behavior of the laboratory setup was as expected. When increasing machine load or rectifier load (measured in power), current flow increased and machine terminal voltage dropped. As expected, increasing upstream inductance did reduce voltage quality and machine stator voltage dropped even more, hence an even larger current had to flow to supply the same power. Voltage level did drop to a very low level of only 136 V when an upstream inductance of 6 mH was chosen and both rectifier and machine were heavily loaded. That is an even lower voltage than any simulation showed at forehand. However, simulations were performed with only the rectifier drawing current. As Figure C.4 shows, under the given operational conditions and when loaded at rated slip, the induction machine draw a current of approximately 16 A in addition to the rectifier. It is therefore very expected that the voltage dropped significantly more with the machine connected in parallel with the rectifier. Even under these conditions, machine operated as it should and measurements could be made as planned. In addition, the rectifier did generate the expected harmonics in machine terminal voltage, and the machine did draw harmonic current. 5^{th} and 7^{th} harmonics were measured in machine terminal voltage and stator current and the laboratory setup must therefore be considered successful.

Upstream inductance prove to have a very large influence on both voltage level and voltage quality in the tests. Looking at the RMS value of the voltage in Figure 12.3 in zone 3-4, when the rectifier is disconnected, the voltage is just below 175 V. In the base case, where no inductance is connected, the RMS value of the waveform showed in Figure 12.1 is very close to 230 V. Voltage drops by more than 20 % when connecting the upstream inductance.

13.3 Interharmonic component

When feeding machine stator voltage with 5^{th} and 7^{th} harmonics, no interharmonic components around these frequencies were detected, neither in voltage nor in current. However, when disconnecting the rectifier, still having a weak grid created by the upstream inductance, an interharmonic component did arise in the voltage. This is a very interesting result, indicating that the induction machine itself could be the source of the interharmonic component. Suppose the harmonic source is somewhere in the network around the hydro pumping station, and that an external harmonic source could created the interharmonic components in the machines; it would then be expected to see such interhamonic component in machine stator

when feeding external harmonics into the machine by the use of a rectifier, in the laboratory.

It should be emphasized that all FFT plots of voltage are scaled by exactly the same factor. Also, FFT plots of current are scaled by a common factor, but they are scaled differently from voltage plots. Therefore, the value on the y axis in a voltage FFT plot can be compared to the same value in other voltage FFT plots. Looking at the magnitude of the interharmonic component in Figure 12.12, 12.14 and 12.15, these would have been visible in all FFT plots created, if they were present.

Another interesting point to notice is that the interharmonic component only appears in machine voltage, not in the current. This could be explained by the series connected inductance creating a weak grid. The inductance allows the machine more influence of terminal voltage, but at the same time it smooths the current. This becomes evident in the Simulink simulations, summarized in Table 11.1 and Table 11.2. The current harmonics in Table 11.1 is reduced, both in absolute magnitude and relative to the fundamental component, when the inductance increases. However, the voltage harmonics in Table 11.2 increases, both in absolute magnitude and relative to the fundamental. With small harmonics present, it seems plausible that current harmonics are suppressed by the inductance, and reduced to a magnitude where the measurement equipment could not measure it.

Harmonic component is reduced

Further, in section 12.6, the waveform from the base case (network is strong), given in Figure 12.1, was compared to the waveform shown in Figure 12.16, where the grid is weak. In the weak grid, a clear increase in harmonic content was proven, generated by the machine.

Then, FFT plots created from the same data, for frequencies around the 7^{th} harmonic frequency, can be compared. The FFT plot created from the base case, presented in Figure 12.2, shows that a 7^{th} harmonic component is present in the voltage, when the machine is connected directly to the grid. However, no interharmonic component is present, indicating that network rigidity suppress the interharmonic. The FFT plot shown in Figure 12.12, where the grid is weak, shows that an interharmonic component has occurred, but that the magnitude of the 7^{th} harmonic is dramatically reduced. Why the magnitude of the 7^{th} harmonic component is reduced, is not known.

Suppose the power supply in the laboratory at NTNU is the source of the 7^{th} harmonic component in Figure 12.2, and that the induction machine itself do not generate any (or a very small) 7^{th} harmonic component. Then, the large inductance between the network and the machine may simply remove the harmonic from machine stator voltage, in the sense of allowing the machine to dictate harmonic content in the voltage. This should be investigated further.

In addition, it is observed that when feeding a large 7^{th} harmonic into machine stator, the interharmonic component disappear. This disappearance is similar to the base case, but might be for another reason. Whether there is some interaction between the two components, suppressing one of them, is not known. This should be investigated further.

Harmonics in supply voltage

The source of the 7^{th} harmonic component present in the voltage in the base case is not verified. The magnitude of this component is only 0.7 % as shown in Figure C.6 in the appendix. It is considered most likely that the component is present in the supply voltage. 7^{th} harmonics of this magnitude is common in a regular power network and numerous potential sources can be found in the network.

13.4 Validating results

If the interharmonic component measured both at the hydro pumping station and in machine stator in the laboratory at NTNU origins from a clean 7^{th} harmonic in machine rotor, reflected in machine stator at another frequency, calculations should be able to confirm the frequency of this interharmonic component. However, calculations presented in this work are not matching the measured frequencies perfectly, and several possible sources of inaccuracy should be considered when interpreting these results. Calculations are based on a strict mathematical relationship. Therefore, if the small deviation between calculated and measured frequencies observed cannot be explained by other factors, a rotor-stator interaction cannot explain the presence of the interharmonic component.

As discussed briefly in section 9.3 and in more detail in the Specialization project [12], FFT plots created in MATLAB from measurement data seem to slightly misplace the frequency of the components. This is largely confirmed for the 5^{th} and the 7^{th} harmonic components, which seem to occur at about 1 Hz lower than they should. The source of this inaccuracy is not known.

Calculation of the interharmonic component in the measurement from the hydro pumping station was based on a slip that is not verified. Nominal rotational speed of the machine was assumed. There is no reason to believe that motors in a hydro pumping station are operating far from their nominal operating conditions. Still it is considered possible that the slip used in the calculation is slightly inaccurate. From Figure 7.1 it can be seen that the interharmonic component occur at approximately 347 Hz.

Also, it is worth noting that the frequency difference between the two components is just above 2 Hz, since the 7^{th} harmonic component occur just above 349 Hz. The 2 Hz frequency difference between the components is substantiated by other data. Fluctuations in the 7^{th} harmonic magnitude in Elspec Investigator plots occur

close to 2 Hz, and the visual lighting flicker occur at around 2 Hz. According to the beat theory, explained in chapter 4, this means that the frequency difference between the two components is 2 Hz. This in turn indicates that the 1 Hz deviation in the FFT plots apply to the interharmonic component as well. If that is the case, the frequency difference between the harmonic components, is more important to consider than the frequency of the two components individually.

Calculated frequency of the interharmonic component is 346.8 Hz, shown in equation 7.1. This is calculated under the assumption that the 7^{th} harmonic frequency is 350 Hz, hence calculations indicate a frequency difference of 3.2 Hz. If 7^{th} harmonic frequency is reduced by 1 Hz, frequency of the interharmonic component should be reduced by roughly the same, and calculations would give a frequency of less than 346 Hz. This means a larger deviation between calculated and measured frequency, but it is still well within 1 % deviation.

Assuming the frequency difference between the two harmonic components depicted in Figure 7.1 is correct, a specific rotational speed of the motors at the hydro pumping station is required to generate this frequency by the rotor-stator interaction described in section 7.2. This can be calculated by reversing calculations of the interharmonic frequency. In section B in the appendix, this is done, assuming an interharmonic component at a frequency of 347.9 Hz. Figure 7.1 is visually inspected and the frequency difference between the components is approximated to 2.1 Hz, making 347.9 Hz the real interharmonic frequency, given the 7^{th} harmonic occur at exactly 350 Hz. To achieve this interharmonic frequency, a rotor speed of 744.8 rpm is calculated, given in equation B.4. Nominal speed of the motors at the hydro pumping station is 742 rpm. That is less than 0.4 % less than what calculations show is the required speed necessary to generate an interharmonic component at 2.1 Hz less than the 7^{th} harmonic frequency. A rotational speed of 744.8 rpm constitutes a very small slip of only 0.7 % in the motors at the hydro pumping station.

In Table 12.3 in section 12.6, calculated frequency and measured frequency for some interharmonic components occurring in laboratory tests are compared. Again, calculations are based on the 5^{th} and 7^{th} harmonic components occurring at exactly 250 Hz and 350 Hz respectively. Deviation between measured and calculated values are between 0.2 % and 0.8 %. Due to uncertain precision in FFT plots, this comparison is difficult, but all calculations predict a lower frequency than what the measurements show. Also, this difference would increase if calculations were performed with the integer harmonic occurring at a lower frequency. However, deviation between calculated and measured frequencies in general seems to be less than 2 %.

During machine runs in the laboratory, rotor speed was continuously monitored. However, some very small variations in rotor speed could occur. It is considered plausible that actual rotational speed could vary ± 5 rpm from the specified value during a machine run. Therefore, in section B in the appendix, an additional calculation has been performed. Here it is assumed that for one of the machine

runs, actual rotor rotational speed was 1455 rpm instead of 1450 rpm, as used for earlier calculations. According to original calculations, the interharmonic component should have a frequency of 340 Hz, shown in equation B.1. New calculations show a frequency of 341 Hz, shown in equation B.5. An increase of 0.3 %. This means that a deviation of 0.8 % between measured and calculated values cannot be explained exclusively by misalignment of rotor speed.

Elspec measurement equipment, using Rogowski coils and banana plugs for current and voltage measurements respectively, should be able to measure voltage and current with high accuracy. However, measurements from the laboratory work presented in section 12.4 showes that Rogowski coils had to be twisted extra turns around the conducting wires to measure the small 7^{th} harmonic current components. This, and the small deviations detected in the data used to create FFT plots, indicate that some inaccuracy or offset could be present in the measurements. Also, the Rogowski coils used for current measurements were not tuned for this specific Elspec instrument. Ideally, these coils should be tuned to achieve highest possible accuracy.

Some current measurements were performed with a power harmonic analyzer by Fluke, in addition to the Elspec equipment. The power harmonic analyzer used a current clamp delivered by Fluke, and measurements were largely in accordance with Elspec measurements. However, due to small continuous variations in current and disturbed current waveforms, an exact comparison of the two measurements were difficult. Absolute accuracy and precision cannot be guaranteed from any measurement equipment. Accuracy and precision of measurements must therefore be considered a source of error. Also, voltage measurements, performed with banana plugs, should be extremely accurate and precise. According to Elspec, uncertainty of voltage measurements is 0.1 % of nominal voltage [5].

The Elspec instrument used for measurements perform 1024 samples of voltage per cycle in a 50 Hz wave. The amount of data becomes very large. Therefore, integrated software in the Elspec instrument compress data by converting signals to the frequency domain. Then, all harmonic components proving too small for the instrument to measure them precisely, are deleted. This reduces storing space significantly. However, the algorithm compressing data in the Elspec instrument, could potentially reduce data quality when data is downloaded to Matlab for further post processing. This is considered as a possible source of error and may explain the detected deviation in 5^{th} and 7^{th} harmonic frequency in FFT plots. Apart from this, there is no specific indication that other post processing of data is a source of error.

Another very small possible source of error is the fundamental frequency of the supply voltage. This should be 50 Hz, and rarely varies more than $\pm 0.1\ Hz$ [14]. Any deviation here will give n times larger deviation in the n^{th} harmonic frequency. Also, it will change synchronous speed of the induction machine slightly. However, it should be emphasized that supply frequency should deviate equally much above and belove 50 Hz. Any consistent deviation in one direction should not occur

from this. Therefore, variations in supply frequency is regarded as an insignificant source of error.

13.5 Evaluating hypothesis

Despite deviations between measured and calculated frequency of the interharmonic component occurring both at the hydro pumping station and in the laboratory tests, a relationship between machine slip and frequency of the interharmonic component seems evident. This substantiates that a rotor-stator interaction is the source of the interharmonic component. As described in section 7.3, applying the mathematical reasoning presented in section 7.2 to an integer harmonic component reflecting from stator to rotor and back to stator, will not give a frequency in the right order of magnitude. If the harmonic source is external, a different reasoning for the rotor-stator interaction is necessary. Alternatively, a completely different explanation for the interharmonic component must be presented. It should be emphasized that rotor slip rings only are connected to external resistances for start-up, and no harmonic source should be present here.

In general, the air-gap flux density distribution in an induction machine will not be sinusoidal. Machines are designed to produce as sinusoidal flux distributions as possible, but no design is perfect [2, p. 639]. Therefore, some harmonic generation must be expected from an induction machine. Naturally, magnitude of the generated harmonics will depend on the size of currents drawn by the machine, and machine design. However, phenomenons such as the flicker observed in connection with this hydro pumping station is not very common. Important reasons for this is probably that network rigidity usually undermine the generated harmonics and that harmonic resonance was an important contributor to the large magnitude of the harmonics in this case.

If machine rotor generate a harmonic component due to windings and machine geometry, machine stator could do the same. Having two separate harmonic sources (rotor and stator), provides an explanation for the difference in magnitude between the two harmonic components. The larger magnitude of the interharmonic component can originate from larger harmonic generation in machine rotor. Whether rotor generates larger harmonics than stator has not been investigated in this work. Alternatively, a 7^{th} harmonic component can easily origin from supply voltage as well, as there are many possible sources for 7^{th} harmonics.

Earlier work has shown that when capacitor banks were connected, harmonic resonance occur at the hydro pumping station around the 5^{th} and 7^{th} harmonic frequencies, as explained in chapter 2. This analysis is performed by the use of a network model of the nearby network in the computer software Simpow. In this model, it is assumed that the harmonic source is in the nearby network, propagating through the grid. The frequency analysis shows that parallel resonance will occur at frequencies around the 5^{th} and 7^{th} harmonic frequencies, depending on

the number of capacitor banks connected [23]. Disconnecting capacitor banks at the actual pumping station reduced harmonic content significantly, proving the existence of harmonic resonance. If induction motors at the hydro pumping station are the harmonic source themselves, a resonance impedance must be seen by harmonics originating from the machines as well. A new frequency response simulation, performed with induction machines as the harmonic source could clarify whether machines can be the harmonic source.

According to SINTEF Energy Research, there are in total three known cases in Norway where a beat phenomenon, similar to the one discussed in this work, has occurred. These have caused flicker in lighting or other disturbances. Two plots from one of the other cases are included in Figure E.1 and Figure E.2. Measurements are performed somewhere in western Norway. Figure E.1 shows the magnitude of the different harmonics in the system. The 17^{th} (turquoise) and the 19^{th} (magenta colored) harmonics are the ones causing disturbance in this case. In Figure E.2 the voltage waveform is given. The small waves creating the bumpy surface on the sine-waves are the 17^{th} and the 19^{th} harmonics. Over time, these small waves move relative to the larger sinusoids. This indicates an interaction between two different harmonic components in close frequency proximity [1].

Chapter 14

Conclusion

An external source feeding the induction machines at the hydro pumping station with harmonics, causing the interharmonic component to occur in machine stator, is considered unlikely. Assuming the harmonic source is external, no mathematical explanation for the generation of the interharmonic component by the induction machines has been found. Also, feeding an induction machine with external harmonics in laboratory tests did not create any interharmonic components in machine stator voltage or current.

Experiments in the laboratory show that interharmonic components associated with the 5^{th} and the 7^{th} harmonic frequency do occur in induction machine stator when upstream grid is sufficiently weak. This is observed when no external source is feeding harmonics into the machine. The frequency of these interharmonic components are around 10 Hz lower than the frequency of their associated integer harmonic. Assuming induction machine rotor generates harmonic components, calculations based on a rotor-stator interaction in the induction machine are very close to verify the frequency of the interharmonic component, thus largely verifying the hypothesis of a rotor-stator interaction. However, some deviation between calculations and measured values are evident. Considering the magnitude of the deviations, it is concluded that these deviations could be explained by a combination of inaccuracy in measurement equipment, machine rotor speed and by data quality reduction in post processing of data.

Laboratory tests have been performed on a machine that is not a true replica of the machines at the hydro pumping station. This fact, combined with lack of technical information of the machines at the hydro pumping station, makes it impossible to draw a definite conclusion on what caused the voltage disturbance at the hydro pumping station. However, based on the available information and laboratory tests, it is considered very likely that induction machines at the hydro pumping station are the harmonic sources themselves. Also, it is likely that the interharmonic components origin from integer harmonic components in machine rotor, appearing at a different frequency in machine stator.

Further, laboratory tests show that a beat phenomenon between two harmonic

components could occur in any wound rotor induction machine. A weak power grid or a harmonic resonance could result in power quality issues.

Chapter 15

Further Work

Induction machines generate harmonics based on winding structure and machine geometry. For the machine at the laboratory at NTNU, this is all known. Therefore, it should be possible to perform a computer based analysis of the induction machine, using software like COMSOL. This could verify whether stator, rotor or both generate 5^{th} and 7^{th} harmonics. Time did not permit such investigation in this work, but performing this would definitely improve understanding of the phenomenon at the laboratory, in turn improve understanding of the phenomenon at the hydro pump station as well.

As discussed earlier, when feeding a large 7^{th} harmonic into machine stator, no interharmonic component is present. When the interharmonic component occur (when no 7^{th} harmonic is fed to the machine), the 7^{th} harmonic is suppressed (compared to the base case). Magnitude of the 7^{th} harmonic component decrease dramatically when a large inductance is connected between the network and the machine. Explaining these two phenomenon would improve understanding of the laboratory circuit and improve interpretation of results. Investigation of harmonic cancellation may be considered.

In earlier work, a SIMPOW-simulation indicating harmonic resonance around the 7^{th} harmonic frequency was performed. This simulation injected harmonic current in the upstream network. A similar analysis where the harmonic current is injected in the induction machines would clarify whether a similar resonance will still occur. It has been proven that resonance did occur at the pumping station, and it should be investigated whether this happens when machines are the harmonic source also.

For a definite conclusion on the source of the interharmonic component, more information about the motors at the hydro pumping station is required. Knowing details about motor windings and design would allow computer simulations of these machines, and it would expand interpretation possibilities of results from the laboratory work conducted in this Master's thesis work.

Bibliography

[1] Sintef energy reaserch.

[2] Stephen J. Chapman. *Electric machinery fundamentals*. Fifth edition, 2012.

[3] ABB Drives. Technical guide no. 6 - guide to harmonics with ac drives.

[4] ELSPEC. Elspec investigator. http://www.elspec-ltd.com/PQInvestigator. Accessed: 2015-05-08.

[5] ELSPEC. G4500 blackbox pqa. http://www.elspec-ltd.com/G4500BLACKBOX. Accessed: 2015-06-08.

[6] Mohammad A. S. Masoum Ewald F. Fuchs. *Power Quality in Power Systems and Electrical Machines*.

[7] S. Ghosh. *Electrical Machines*. Pearson Education India.

[8] Cigré/CIRED CC02 Working Group and IEEE Interharmonic Task Force. Interharmonics in power systems.

[9] Trond Toftevaag Helge Seljeseth, Rune Paulsen. Harmonic voltages and lightning equipment flicker caused by pumping station – measurements, analysis and mitigation. *ieee.org*.

[10] Antoni Klajn Henryk Markiewicz. Voltage disturbances - standard en 50160 - voltage characteristics in public distribution systems.

[11] POWER QUALITY INTERNATIONAL. The harmonics problem. http://www.powerqualityinternational.com/resource-center/the-harnomic-problem. downloaded December 15, 2014.

[12] Torstein Kastet. Low-frequency power quality problems in distribution grid caused by pump station equipped with high voltage wound-rotor induction machines. Specialization project, NTNU.

[13] E. Kreyszig. *Advanced Engineering Mathematics*.

[14] Eivind Lindeberg. Automatisk frekvensregulering i det nordiske kraftnettet. *NEF Teknisk møte, 2014*.

[15] Lovdata. Forskrift om leveringskvaliteti kraftsystemet - krav til leveringspålitelighet og spenningskvalitet.

https://lovdata.no/dokument/SF/forskrift/2004-11-30-1557. Accessed: 2015-03-31.

[16] Subhasis Nandi. Space and time harmonics related problems and their mitigation for position and speed sensorless slip-ring induction motor drives applications.

[17] William P. Robbins Ned Mohan, Tore M. Undeland. *POWER ELECTRONICS - Converters, Applications and Design.*

[18] NTNU. Instrumentarkiv. http://semper5.itea.ntnu.no/baa/www.elkraft.ntnu.no/elkraft3/instr pm10c/.

[19] The physics classroom. Interference and beats. http://www.physicsclassroom.com/class/sound/Lesson-3/Interference-and-Beats. Accessed: 2014-11-19.

[20] Prof P. Sasidhara Rao Prof. Krishna Vasudevan, Prof G. Sridhara Rao. *Electrical Machines 2.*

[21] Kjell Sand. Overharmoniske i kraftnett.

[22] Ph.D. Steven W. Smith. The scientist and engineer's guide to digital signal processing. http://www.dspguide.com/ch8/1.htm. Copyright 1997-2011 by California Technical Publishing, accessed: 2015-04-23.

[23] Trond Toftevaag. Resonansproblem i fordelingsnett knyttet til kondensatorer for fasekompensering - målinger, simuleringer og analyser. *NEF Teknisk møte, 2014.*

Appendix A

Beat

In chapter 4 a review of the beat phenomenon was given. In this section a wider examination of superposition of to signals is given to support understanding of the beat observed in this work.

Superposition of signals around the 7^{th} harmonic frequency

In the specialization project that formed the basis for this work, a probable interaction between two frequency components with approximately two hertz frequency difference occurring around the 7^{th} harmonic frequency was described [12]. Below, a Matlab-plot of two waveforms at 348 Hz and 350 Hz respectively is plotted together over a short time interval. As can be seen in Figure A.1, the blue line (348 Hz) is very slowly drifting away from the red line (350 Hz) from their starting point where both signals were in phase. The sum of the two signals will gradually decrease as they drift out of phase and eventually cancel out each other completely. Then again the sum will gradually increase until the signals are back at the starting point relative to each other, and the cycle repeat itself. This pattern is shown in Figure A.2. Here the two waves are superimposed over a time interval of 1.5 seconds to clearly show the pattern that appears. The plot is constructed in the same way as the one in Figure 4.2, only the frequencies are different. Again, the black line that envelopes the superimposed signal consists of two sinusoidal waves. These show that the amplitude variation of the superimposed signal follow a perfect sinusoidal path for this superposition. The green line is the superimposed signal.

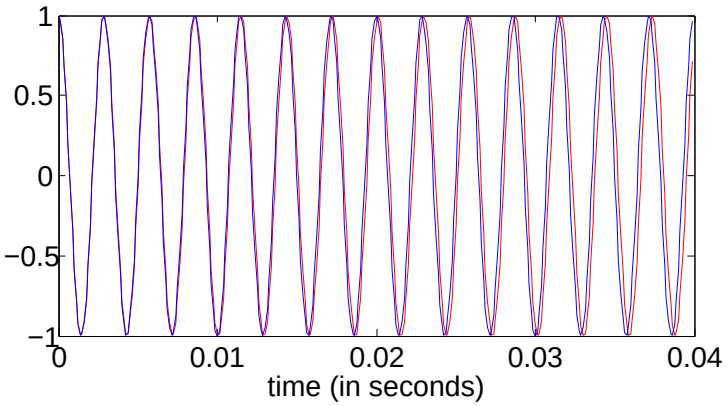

Figure A.1: A 348 Hz signal (blue) and a 350 Hz signal (red) is plotted together over 0.04 seconds. Amplitudes are one and unitless. The waves are completely in phase at t=0, but move slowly apart from each other during the 0.04 seconds.

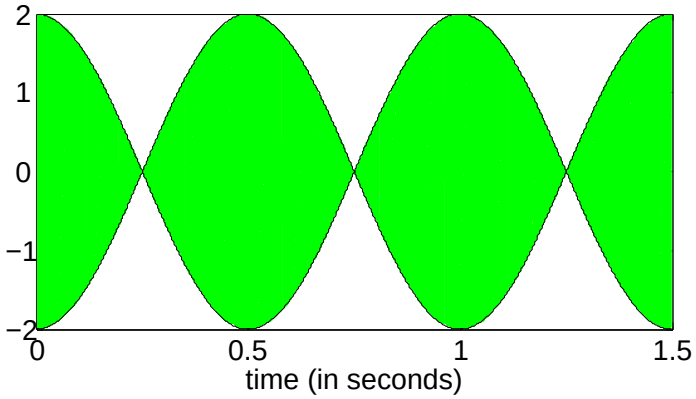

Figure A.2: A 348 Hz signal and a 350 Hz superimposed into one new waveform. The green line is the resultant wave and is plotted over 1.5 seconds. The beat frequency is equal the frequency difference 350 $Hz - 348\ Hz = 2\ Hz$.

Superposition of signals of different amplitude

When both signals have the same amplitude, the resultant wave will beat strongly, and the amplitude will vary from zero to double. However, the beat principle will apply if the amplitudes of the original waveforms are different as well. In Figure A.3 one of the signals are given an amplitude of 6, while the other signal has an amplitude of 1. The 50 Hz signal has the largest amplitude and is drawn in red. The 60 Hz signal has the small amplitude and is blue.

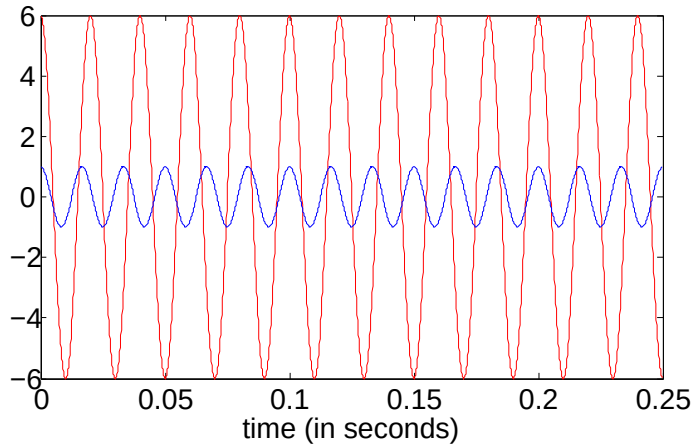

Figure A.3: A 50 Hz signal (red) and a 60 Hz signal (blue) is plotted together over 0.25 seconds. Amplitudes of the 50 Hz signal is 6 times larger than amplitude of the 60 Hz signal. The waves are completely in phase at t=0, but move apart from each other during the 0.25 seconds.

The superposition of these two signals is given as the green line in Figure A.3. An important difference between this signal and the one depicted in Figure A.2 or Figure 4.2, is that the amplitude variation is much smaller, measured in percentage. The blue signal in Figure A.3 does only increase the large red amplitude by a small portion when interfering constructively. Similarly, a destructive interference becomes small relative to the red amplitude, because the blue signal is small. The amplitude will therefore vary between $6 + 1 = 7$ and $6 - 1 = 5$.

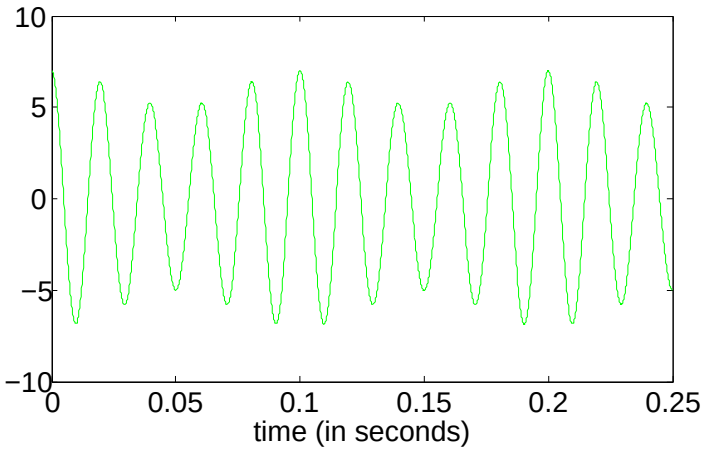

Figure A.4: A signal superimposed of a 50 Hz signal 50 (red) and a 60 Hz signal (blue) plotted over 0.25 seconds. Amplitude of the 50 Hz signal is 6 times larger than the amplitude of the 60 Hz signal.

Superposition of signals of different amplitude around the 7^{th} harmonic frequency

As described in earlier work, and reviewed in chapter 2, data processing of measurements from the hydro pump station shows that it exists a current component

at approximately 348 Hz that is approximately 2.8 times larger than the component occurring at 350 Hz. This is depicted in Figure 2.3 in chapter 2. Therefore, a combination of the two previous superpositions is now performed. A red signal with an amplitude of 2.8 and a frequency of 348 Hz is plotted together with a blue signal with an amplitude of 1 and a frequency of 350 Hz. This is shown in Figure A.5.

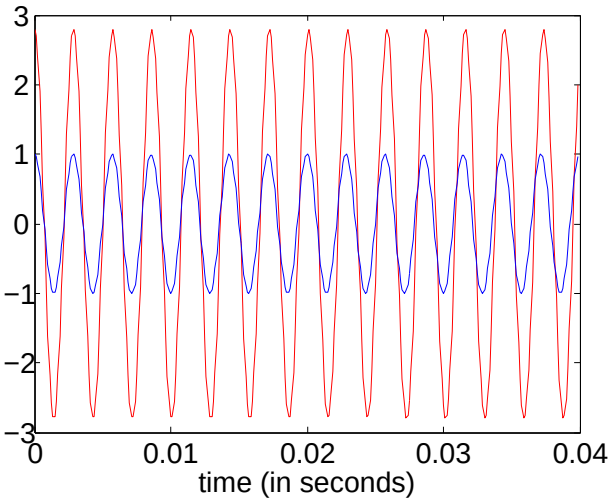

Figure A.5: A 348 Hz signal (red) and a 350 Hz signal (blue) is plotted together over 0.04 seconds. Amplitudes of the 348 Hz signal is 2.8 times larger than amplitude of the 350 Hz signal. This magnitude relationship is very close to what can be seen in the FFT plot created from measurements performed at the hydro pump station, presented in Figure 2.3.

The superposition of these two signals is given as the green line in Figure A.6. The amplitude of the superimposed signal is 2.8 ± 1.

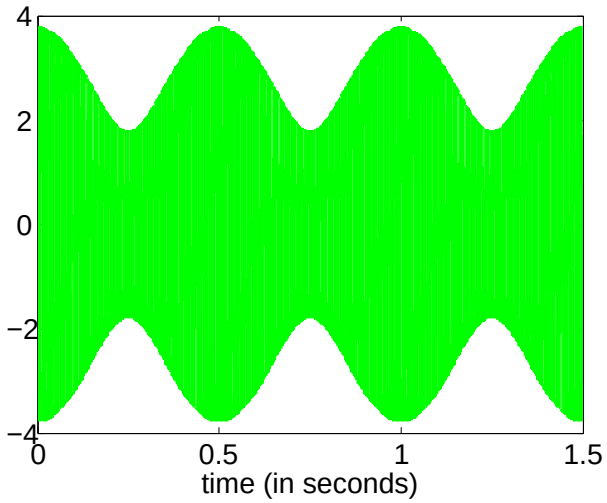

Figure A.6: A signal superimposed of a 348 Hz signal and a 350 Hz signal plotted over 1.5 seconds. Amplitude of the 348 Hz signal is 2.8 times larger than the amplitude of the 350 Hz signal. The green line is the resultant wave and is plotted over 1.5 seconds. The beat frequency is equal the frequency difference 350 $Hz -$ 348 $Hz = 2$ Hz.

If these signals are harmonic components in a signal with a 50 Hz fundamental component, and they are sufficiently large, this beat will manifest itself as a variation in the RMS value of the signal. In Figure 2.4 in chapter 2 the RMS value of the current at the hydro pump station is given for a 3.5 second interval. This shows that the RMS value has a small 2 Hz variation, similar to the envelope of the signal in Figure A.6.

Appendix B

Calculations of interharmonic components

Interharmonic frequency from laboratory tests

The asynchronous machine in the laboratory has the following relevant data necessary for calculations:

- Nominal frequency: 50 Hz
- Nominal rotational speed: 1430 $rpm = 23.83\ rps \Rightarrow s = 4.67\ \%$
- Rotor: wound rotor
- Pole pairs: 2

First, calculations of an interharmonic frequency component during the machine run presented in Figure 12.3 in section 12.3 will be given. In the 10 second interval 15:00:30 - 15:00:40, which the FFT plot presented in Figure 12.12 is based on, the machine rotates at 1450 rpm. In a 4 pole machine and 50 Hz frequency of supply voltage, synchronous speed in 1500 rpm, which gives a slip of 3.33 % and a rotor frequency of $fr_e = fs \cdot slip = 50\ Hz \cdot 0.0333 = 1.665\ Hz$. 1450 rpm equals 24.17 rps. The calculation procedure followed here is explained in section 7.2. In rotor reference frame, fundamental field rotates electrically at 1.665 Hz. Mechanical rotational speed of the field is

$$\frac{1.665\ Hz}{2\ pole\ pairs} = 0.8325$$

full rotations per second. The 7^{th} harmonic field component seen from rotor reference frame will rotate mechanically at

$$\frac{0.8325\ Hz}{7} = 0.1189$$

full rotations per second in forward direction. In stator reference frame, the mechanical rotation is

$$24.17\ rps + 0.1189\ rps = 24.2857\ rps$$

Efficient number of pole pairs are $2 \cdot 7 = 14$. Electrical frequency of 7^{th} harmonic magnetic field, seen from stator reference frame therefore becomes

$$fs_7 = 24.2857 \cdot 14 = 340.0\ Hz. \tag{B.1}$$

Further, considering the time interval from 15:03:00 - 15:03:10, in Figure 12.3. FFT voltage plot created from these data is presented in Figure 12.14. Performing the same calculations for this time interval, the machine rotational speed is 1425 rpm, a slip of 5.0 %. This give a rotor frequency of $fr_e = fs \cdot slip = 50\ Hz \cdot 0.05 = 2.5\ Hz$ and 23.75 rps. In rotor reference frame, fundamental field rotates electrically at 2.5 Hz. Mechanical rotational speed of the field is

$$\frac{2.5\ Hz}{2\ pole\ pairs} = 1.25$$

full rotations per second. The 7^{th} harmonic field component seen from rotor reference frame will rotate mechanically at

$$\frac{1.25\ Hz}{7} = 0.1786$$

full rotations per second in forward direction. In stator reference frame, the mechanical rotation is

$$23.75\ rps + 0.1786\ rps = 23.9286\ rps$$

Efficient number of pole pairs are $2 \cdot 7 = 14$. Electrical frequency of 7^{th} harmonic magnetic field, seen from stator reference frame therefore becomes

$$fs_7 = 23.9286 \cdot 14 = 335.0\ Hz. \tag{B.2}$$

Finally, a calculation for an interharmonic frequency araising from the 5^{th} harmonic is given. The time interval from 15:03:00 - 15:03:10, in Figure 12.3 is considered and conditions are similar as above. The 5^{th} harmonic field component seen from rotor reference frame will rotate mechanically at

$$\frac{1.25\ Hz}{5} = 0.25$$

full rotations per second in negative direction. In stator reference frame, the mechanical rotation is

$$23.75\ rps - 0.25\ rps = 23.50\ rps$$

Efficient number of pole pairs is $2 \cdot 5 = 10$. Electrical frequency of 5^{th} harmonic magnetic field, seen from stator reference frame therefore becomes

$$fs_7 = 23.50 \cdot 10 = 235.0\ Hz. \tag{B.3}$$

Calculation of alternativ motor speed

The interharmonic component at the hydro pump station, depicted in Figure 7.1, occur at approximately 2.1 Hz less than the 7^{th} harmonic component in the same plot. For the machines at the hydro pump station to generate an interharmonic component at 2.1 Hz less than the 7^{th} harmonic component, a specific rotational speed is necessary. This speed can be calculated by assuming the interharmonic component has a frequency of 347.9 Hz, 2.1 Hz less than 350 Hz. Rotational speed of machine rotor measured in rpm is called x in the following calculations.

Slip of the machine is given as

$$s = 1 - \frac{x}{750}$$

,which gives a rotor frequency

$$fr_e = fs \cdot slip = 50 \cdot (1 - \frac{x}{750})$$

This is electrical rotational speed of the fundamental field in rotor reference frame. Mechanical rotational speed of the field is

$$\frac{50 \cdot (1 - \frac{x}{750})}{4\ pole\ pairs}$$

full rotations per second. The 7^{th} harmonic field component seen from rotor reference frame will rotate mechanically at

$$\frac{50 \cdot (1 - \frac{x}{750})}{4} \cdot \frac{1}{7} = \frac{50 \cdot (1 - \frac{x}{750})}{28}$$

full rotations per second in forward direction. Machine rotor speed measured in rps is given as $\frac{x}{60}$. In stator reference frame, the mechanical rotation then becomes

$$\frac{x}{60}\ rps + \frac{50 \cdot (1 - \frac{x}{750})}{28}\ rps$$

Efficient number of pole pairs are $4 \cdot 7 = 28$. Electrical frequency of 7^{th} harmonic magnetic field, seen from stator reference frame therefore becomes

$$fs_7 = \left[\frac{x}{60} + \frac{50}{28} \cdot (1 - \frac{x}{750})\right] \cdot 28$$

This should now equal 347.9 Hz

$$28 \cdot \frac{x}{60} + 50 \cdot (1 - \frac{x}{750}) = 347.9$$

Solving for x

$$\Longrightarrow x = 744.8 \; rpm \tag{B.4}$$

Calculation of interharmonic component using different slip

To examine the calculations sensetivity for slip variations, another calculation of the frequency of the interharmonic component in Figure 12.12 will be given. Again calculations are based on the 10 second interval 15:00:30 - 15:00:40 in Figure 12.3, but it is now assumed that the rotational speed of machine rotor was 1455 rpm, instead of 1450 rpm, as earlier calculations were based on. 1455 rpm gives a slip of exactly 3 % and a rotor frequency of $fr_e = fs \cdot slip = 50 \; Hz \cdot 0.03 = 1.5 \; Hz$. 1455 rpm equals 24.25 rps. In rotor reference frame, fundamental field rotates electrically at 1.5 Hz. Mechanical rotational speed of the field is

$$\frac{1.5 \; Hz}{2 \; pole \; pairs} = 0.75$$

full rotations per second. The 7^{th} harmonic field component seen from rotor reference frame will rotate mechanically at

$$\frac{0.75 \; Hz}{7} = 0.1071$$

full rotations per second in forward direction. In stator reference frame, the mechanical rotation is

$$24.25 \; rps + 0.1071 \; rps = 24.357 \; rps$$

Efficient number of pole pairs are $2 \cdot 7 = 14$. Electrical frequency of 7^{th} harmonic magnetic field, seen from stator reference frame therefore becomes

$$fs_7 = 24.357 \cdot 14 = 341.0 \; Hz. \tag{B.5}$$

Appendix C

ELSPEC plots

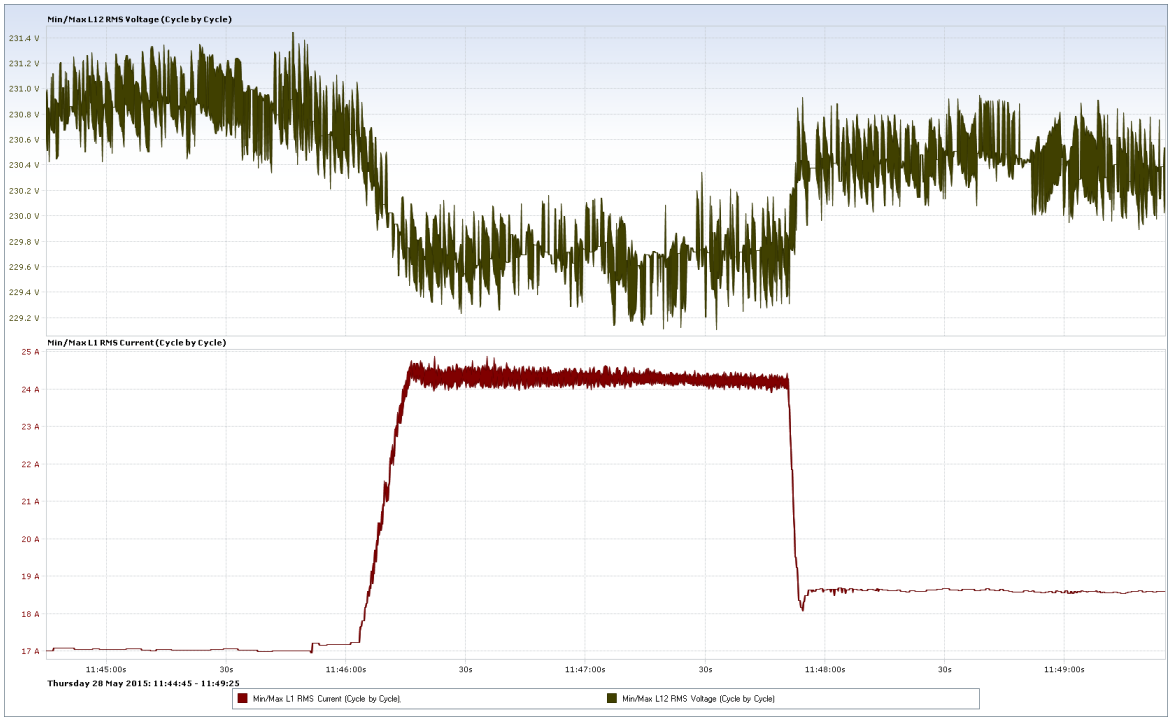

Figure C.1: ELSPEC Investigator time plot. In the upper pane, machine stator voltage V_{12} is plotted, while machine stator current I_1 is given in the lower pane. The machine runs idle until it is gradually loaded from around 11:46:00. This loading is very evident in the current, which increases. Stator voltage is very close to 230 V during the entire machine run, and only drops about 1 V when machine is loaded. That indicates a strong network.

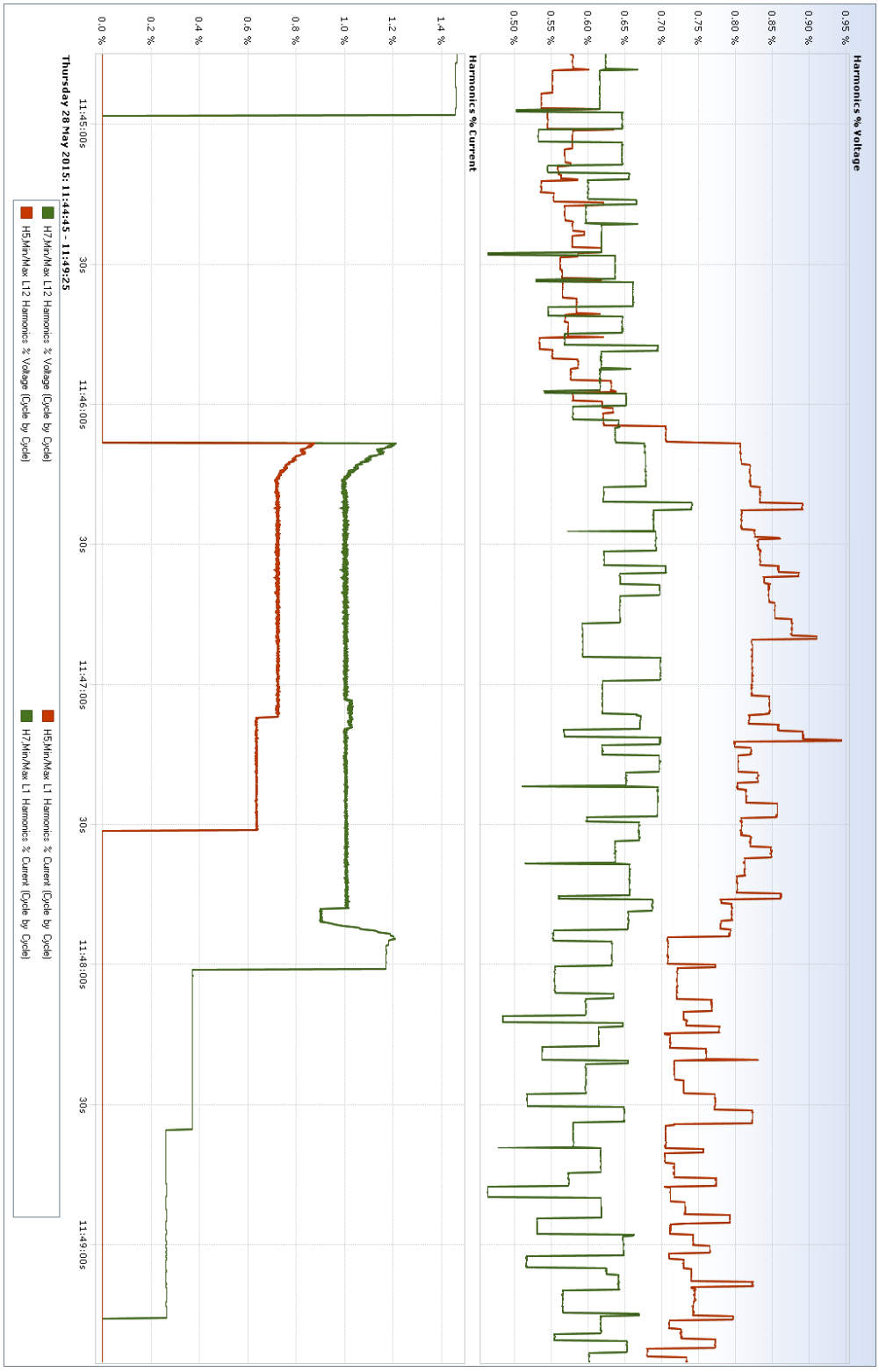

Figure C.2: ELSPEC Investigator time plot for the same time interval as depicted in Figure C.1. In the upper pane, 5^{th} (red line) and 7^{th} (green line) voltage harmonics are plotted. In the lower pane, 5^{th} (red line) and 7^{th} (green line) current harmonics are plotted. Harmonics are given in percentage and voltage harmonics are at all times less than 1 %. Current harmonics are slightly larger, but at all times less than 1.5 %, which is very acceptable values according to FoL [15]. In the one minute interval from 11:45:00 to 11:46:00 both current harmonics are 0. This is a measurement inaccuracy, due to the very small current magnitude, as explained in section 12.4.

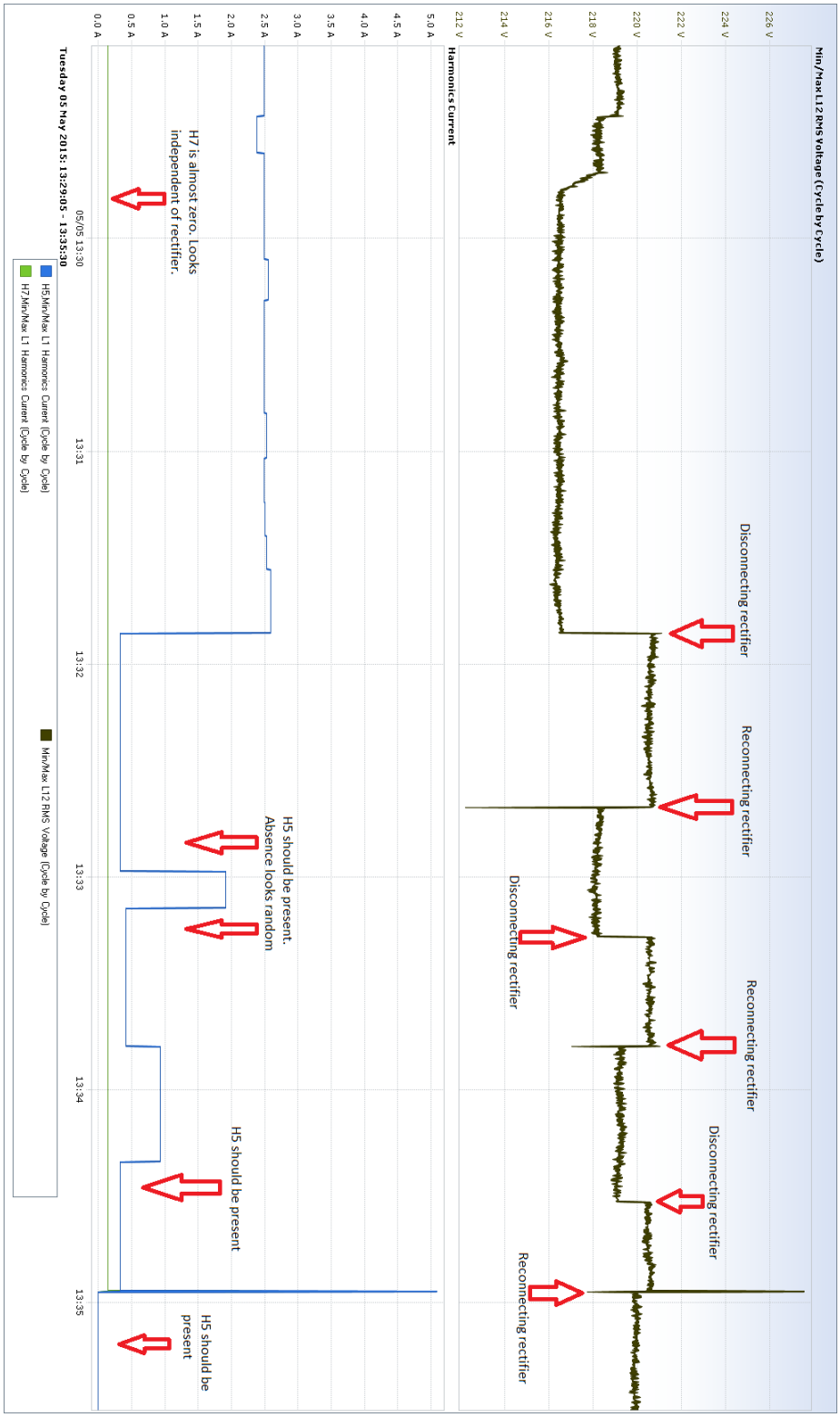

Figure C.3: ELSPEC Investigator plot. $L = 2\ mH$. Upper pane shows the machine stator line voltage V_{12}. The lower pane shows the 5^{th} and 7^{th} harmonic component of stator current in phase 1. The connection and disconnection of the rectifier is indicated in the figure. Rectifier draws less power for every connection, which gives a lower voltage drop in the machine stator and less harmonic content. The 7^{th} harmonic component is almost zero and independent of the rectifier. The 5^{th} harmonic component disappear at random times.

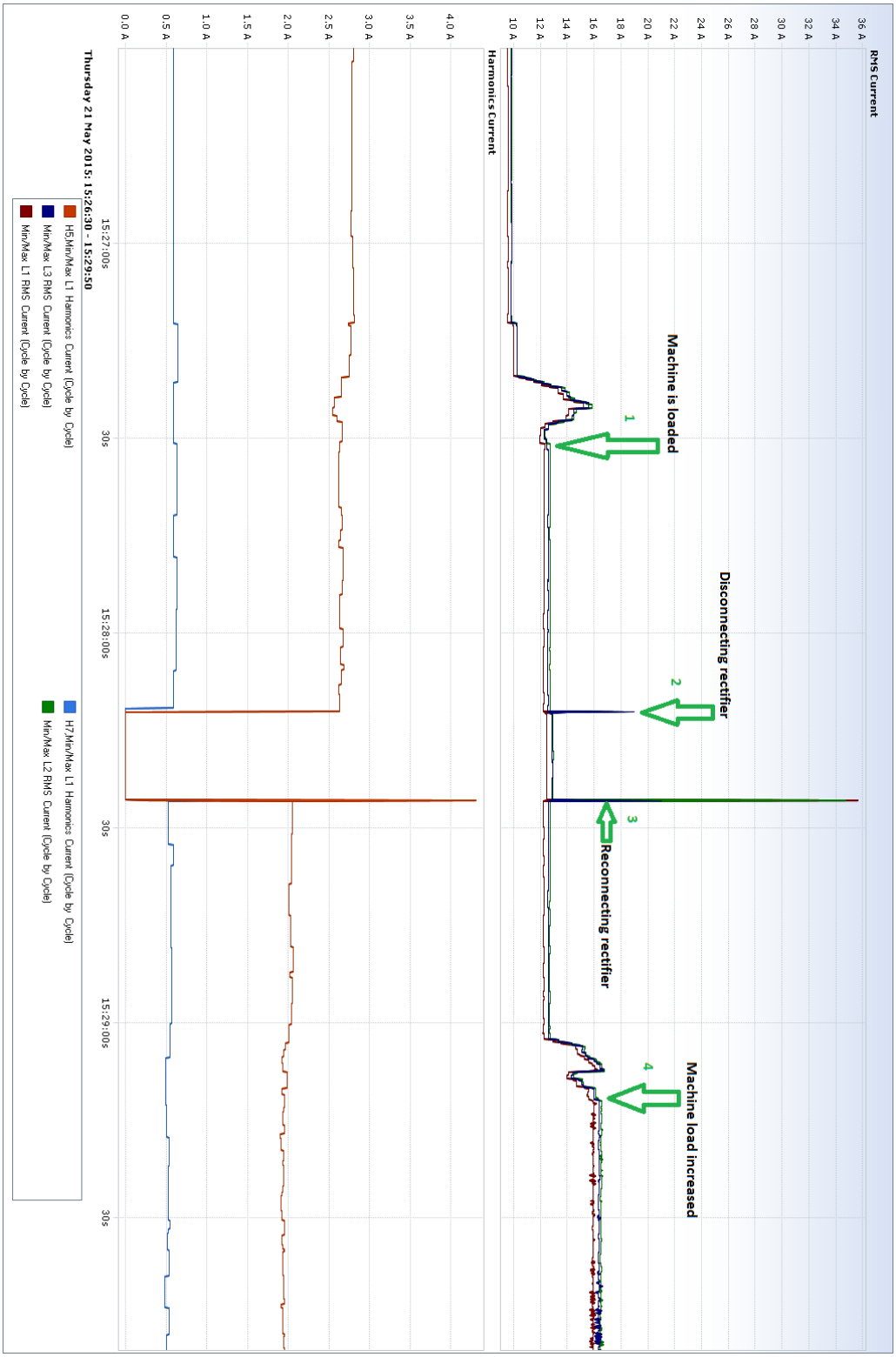

Figure C.4: ELSPEC Investigator time plot, $L = 6\ mH$. In the upper pane, stator current of three phases is plotted. In the lower pane, 5^{th} (red line) and 7^{th} (blue line) harmonics of stator current are given. The connection and disconnection sequence is given in Table 12.2.

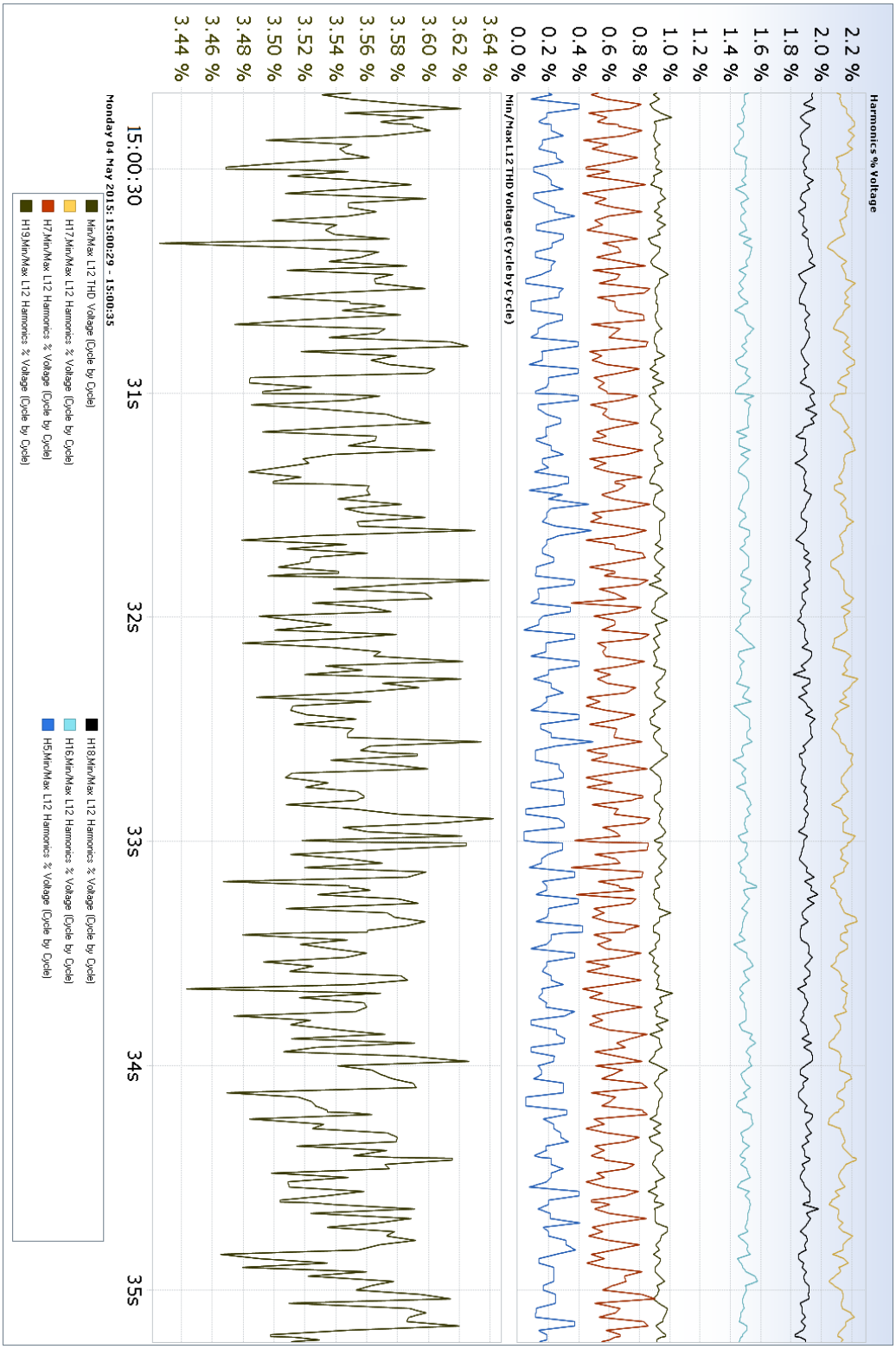

Figure C.5: ELSPEC Investigator time plot from 5 seconds of the machine run given in Figure 12.3, where the rectifier is disconnected. In the upper pane, 5^{th}, 7^{th}, 16^{th}, 17^{th}, 18^{th} and 19^{th} harmonic components in the voltage are given. The harmonics from order 16 to 19 are the largest and are creating the irregularities in the voltage waveform in Figure 12.16. In the lower pane, total harmonic distortion, THD, of voltage is given, confirming the harmonic content.

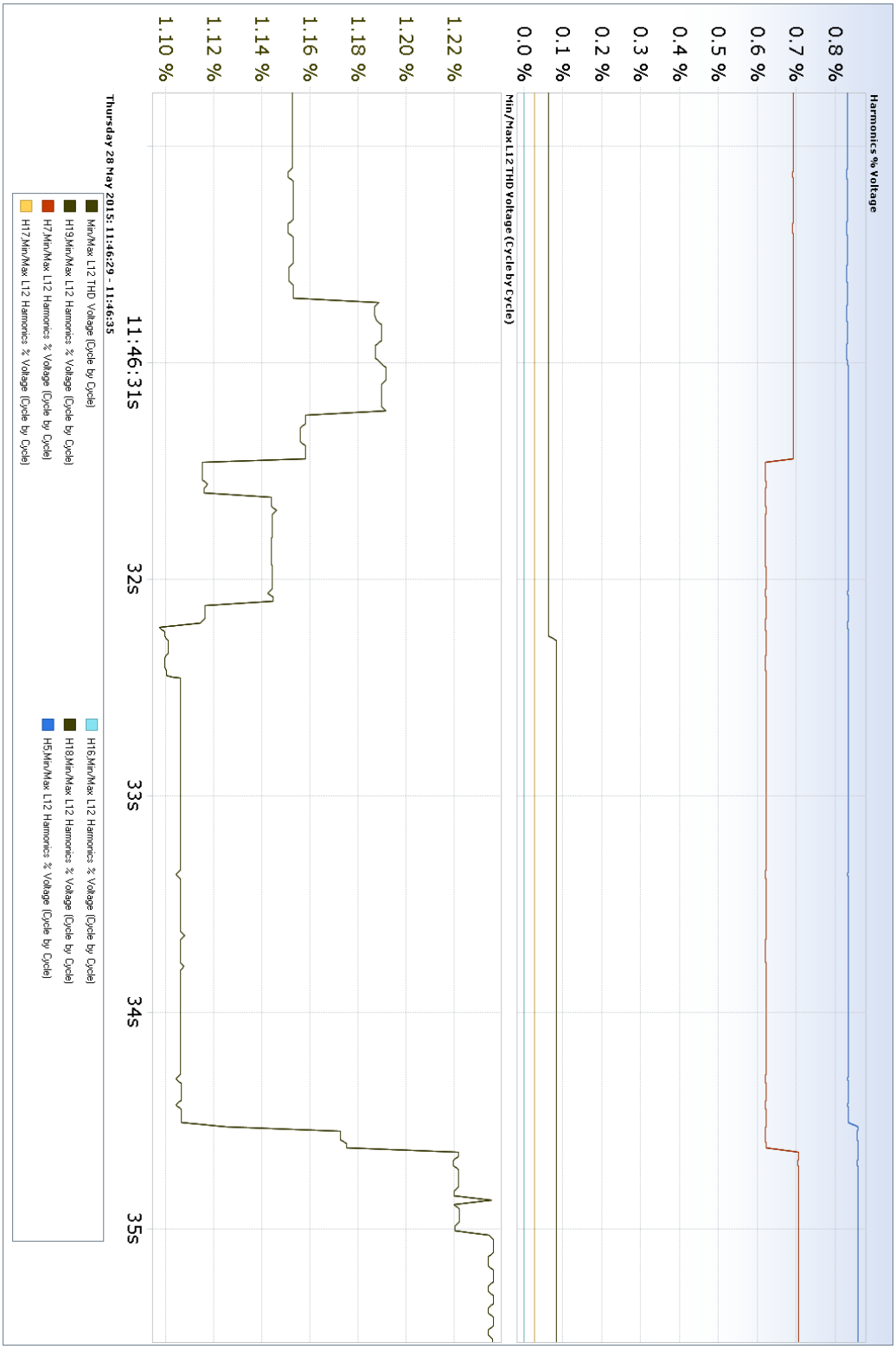

Figure C.6: ELSPEC Investigator time plot from 5 seconds of the base case, when the grid is stiff. In the upper pane, 5^{th}, 7^{th}, 16^{th}, 17^{th}, 18^{th} and 19^{th} harmonic components in the voltage are given. 5^{th} and 7^{th} harmonics are by far the largest. Higher order harmonics are much smaller than in Figure C.5, where the network is soft. In the lower pane, total harmonic distortion, THD, of voltage is given, confirming less harmonic content in the stiff grid than in the soft grid.

Appendix D

Matlab plots

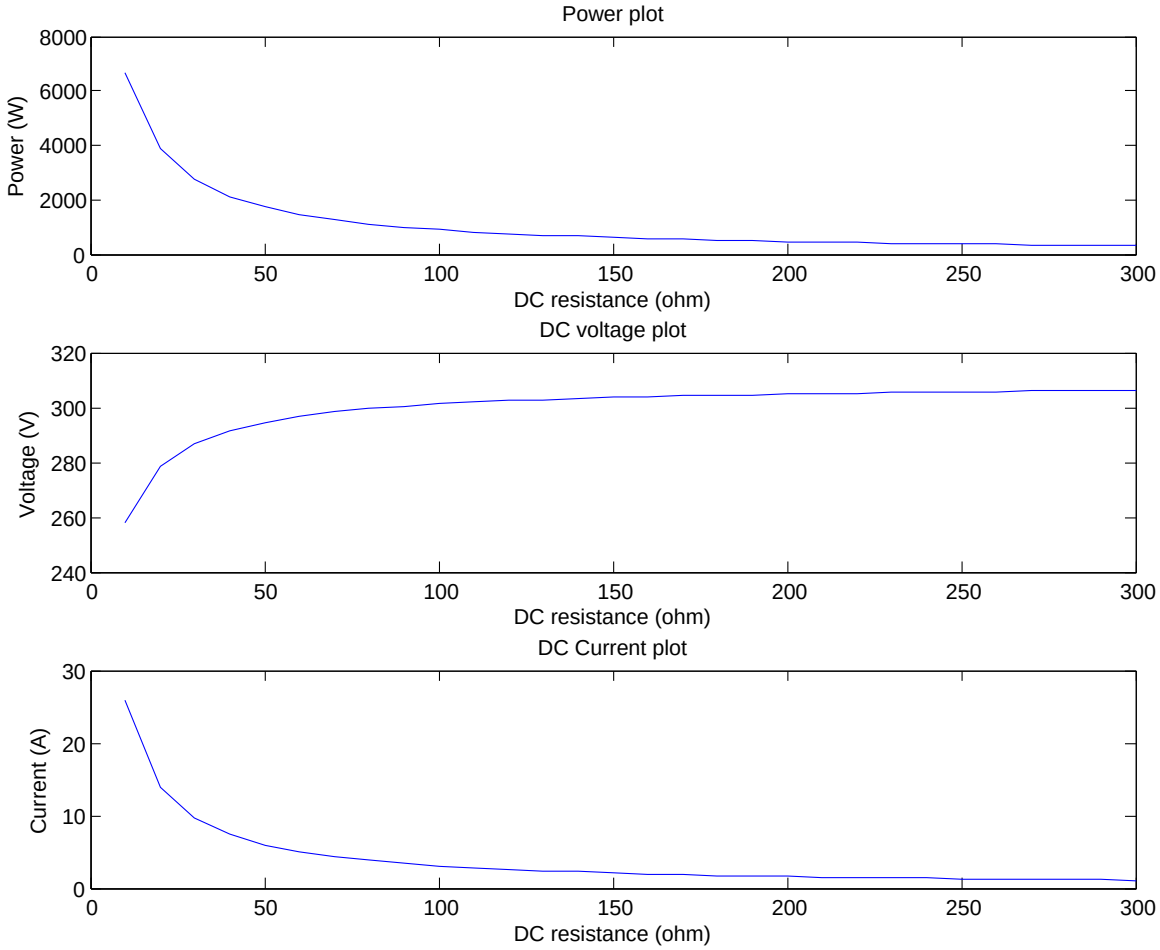

Figure D.1: For a constant value of $Ls = 6.7\ mH$, R is varied from 10 Ω to 300 Ω with increments of 10 Ω. This is plotted against DC power, -voltage and -current respectively.

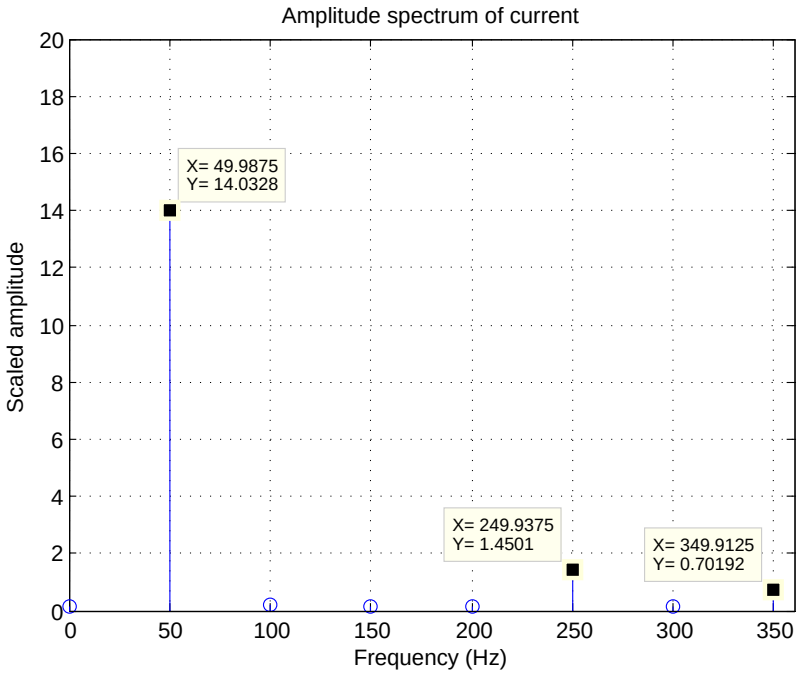

Figure D.2: Amplitude spectrum plot of the current. The FFT analysis is performed on data from period number 6. $Ls = 6.7\ mH, R = 10\ \Omega$ and the filter capacitor $C\_d = 6.0\ mF$. Increasing the capacitance has a very small impact on the system, and this plot is very similar to the one in Figure 11.6.

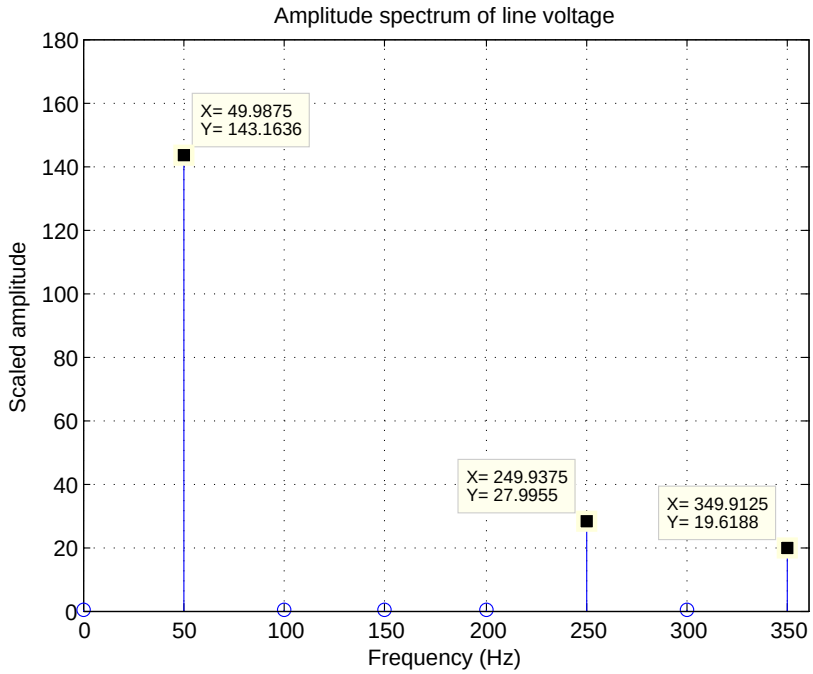

Figure D.3: Amplitude spectrum plot of the voltage. The FFT analysis is performed on data from period number 6. $Ls = 6.7\ mH, R = 10\ \Omega$ and the filter capacitor $C\_d = 6.0\ mF$. Increasing the capacitance has a very small impact on the system, and this plot is very similar to the one in Figure 11.7.

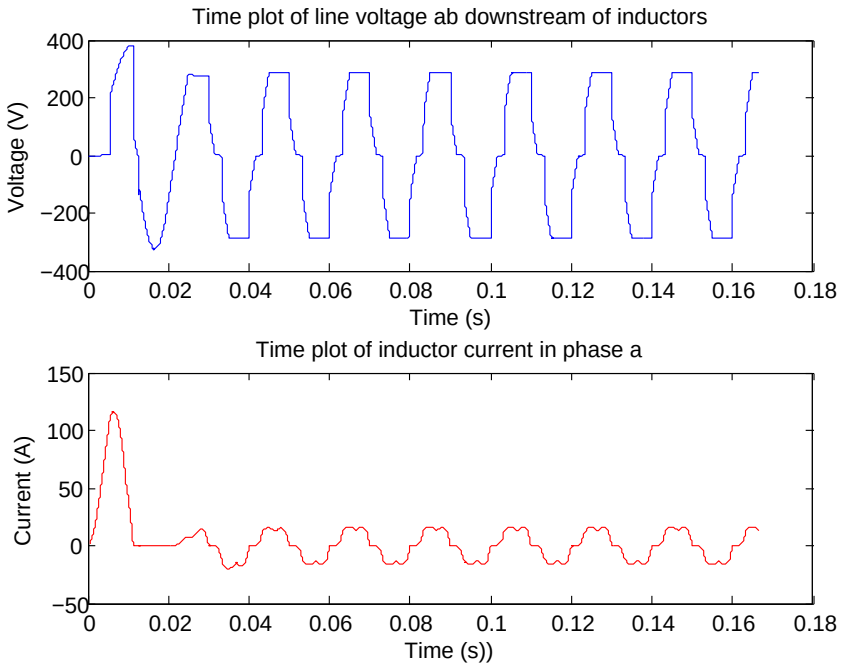

Figure D.4: Time plot of voltage and current for the first eight periods of the simulation. $Ls = 5.05\ mH, R = 20\ \Omega$.

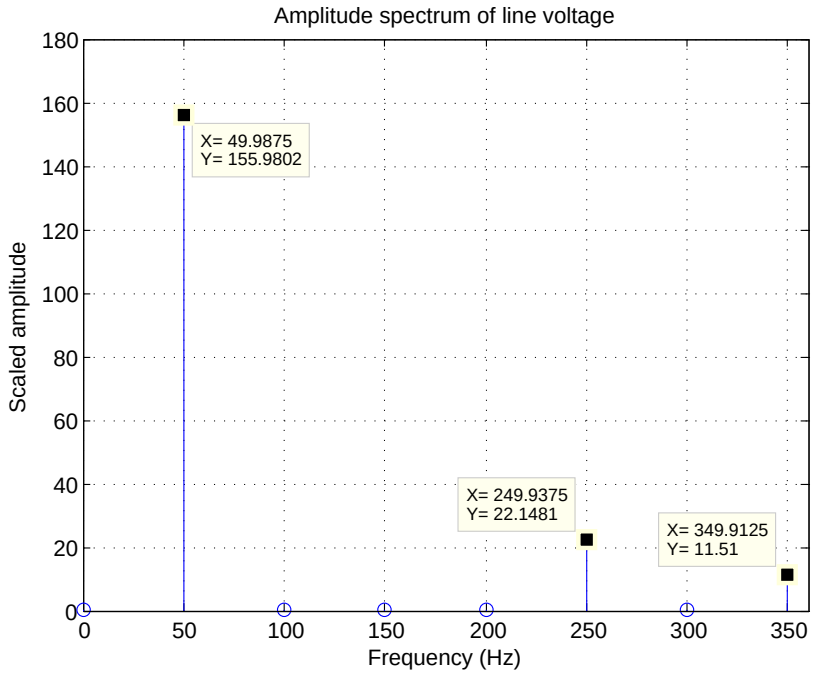

Figure D.5: Amplitude spectrum plot of the voltage. The FFT analysis is performed on data from period number 6 in the signal given in Figure D.4. $Ls = 5.05\ mH, R = 20\ \Omega$.

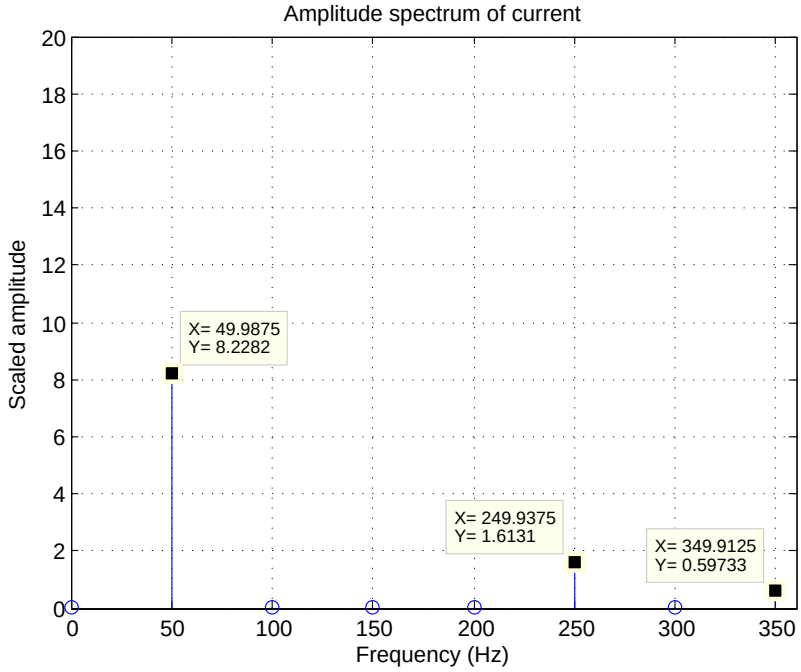

Figure D.6: Amplitude spectrum plot of the current. The FFT analysis is performed on data from period number 6 in the signal given in Figure D.4. $Ls = 5.05\ mH, R = 20\ \Omega$.

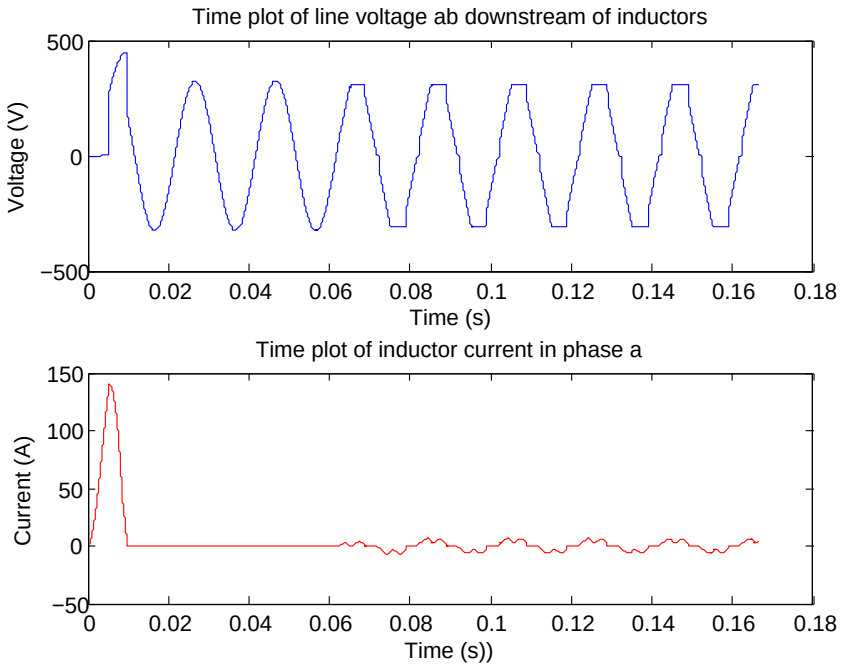

Figure D.7: Time plot of voltage and current for the first eight periods of the simulation. $Ls = 3.37\ mH, R = 80\ \Omega$. In the current waveform an additional startup effect can be seen. From about 10 - 60 ms, the current is zero. The DC load is small (measured in consumed power) and draws a small current. DC side capacitor gets highly charged by the inrush current in the very beginning of the simulation. DC voltage (supported by the capacitance) therefore become higher than AC voltage and rectifier diodes will not conduct current. The capacitor is gradually discharged by the 80 Ω load and when DC voltage drops below AC voltage, AC current starts flowing again. Also, it is worth noting that without AC side current, AC voltage is a clean sinusoidal waveform, not disturbed by the current.

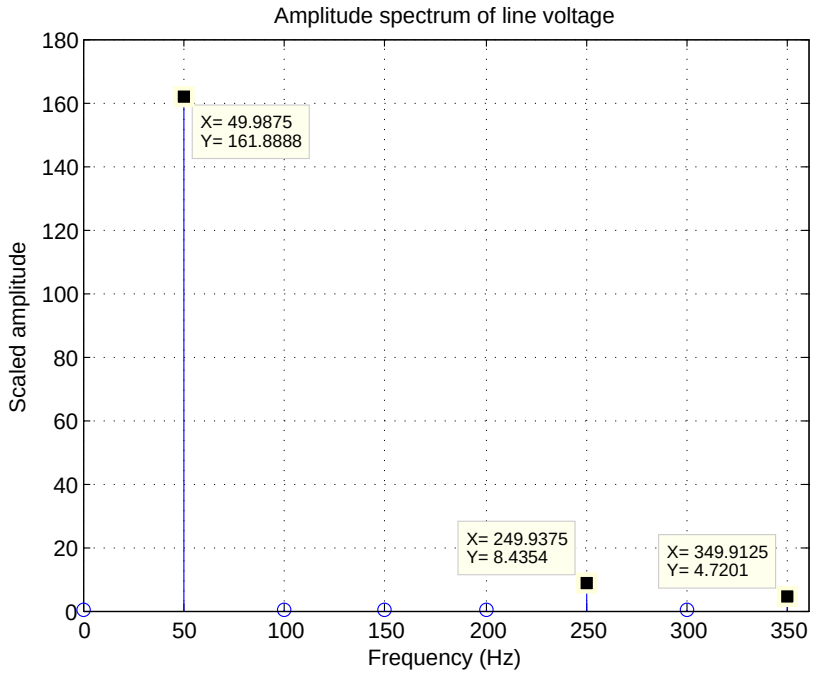

Figure D.8: Amplitude spectrum plot of the voltage. The FFT analysis is performed on data from period number 6 in the signal given in Figure D.7. $Ls = 3.37\ mH, R = 80\ \Omega$.

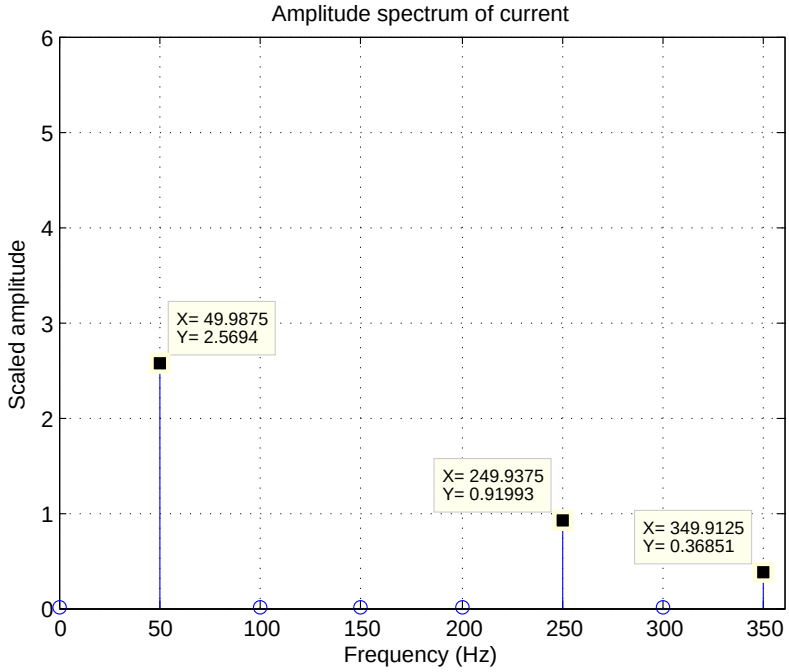

Figure D.9: Amplitude spectrum plot of the current. The FFT analysis is performed on data from period number 6 in the signal given in Figure D.7. $Ls = 3.37\ mH, R = 80\ \Omega$.

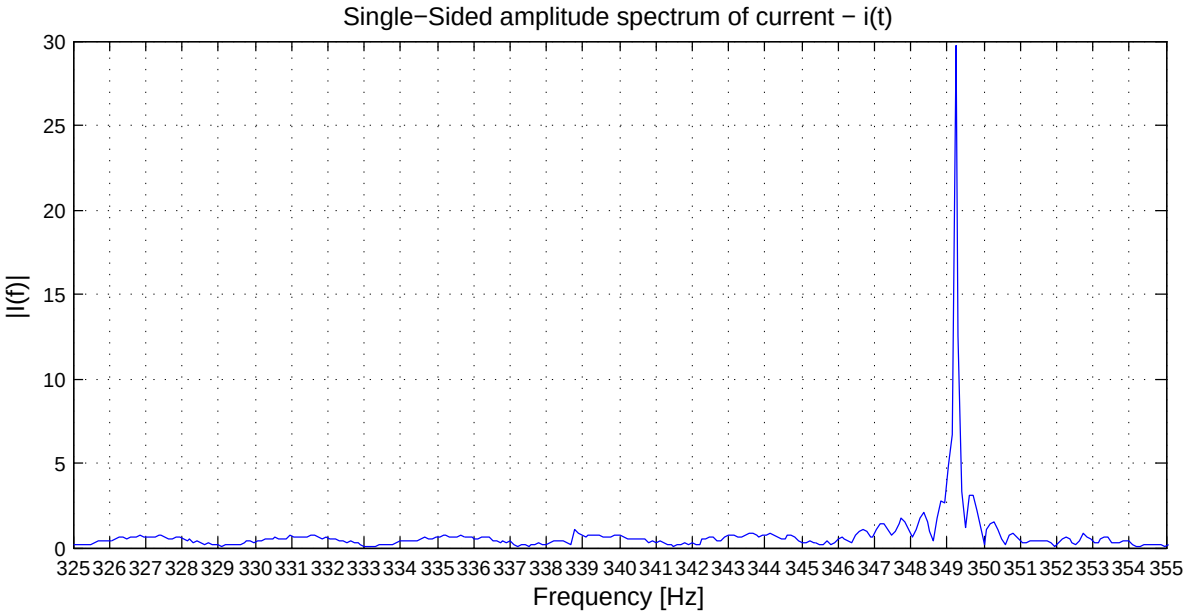

Figure D.10: Amplitude spectrum of machine stator current I_1 for frequencies around the 7^{th} harmonic frequency for the base case. Data is taken from the 10 second interval 11:46:30 - 11:46:40, in Figure C.1. The machine is loaded and run at 1450 rpm, a slip of 3.33 %.

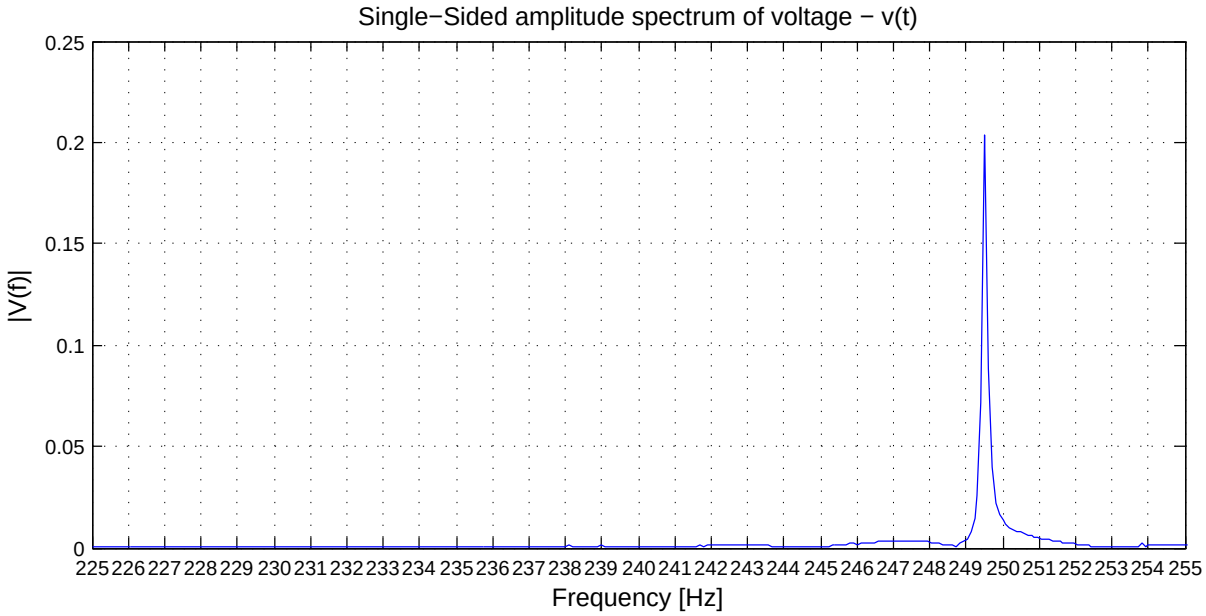

Figure D.11: Amplitude spectrum of machine stator voltage V_{12} for frequencies around the 5^{th} harmonic frequency. Data is taken from the 10 second interval 14:31:30 - 14:31:40, in Figure 12.9, where the rectifier is connected. The machine is loaded and run at 1450 rpm, a slip of 3.33 %. The shunt connected rectifier has a resistance of $R = 12.4\ \Omega$.

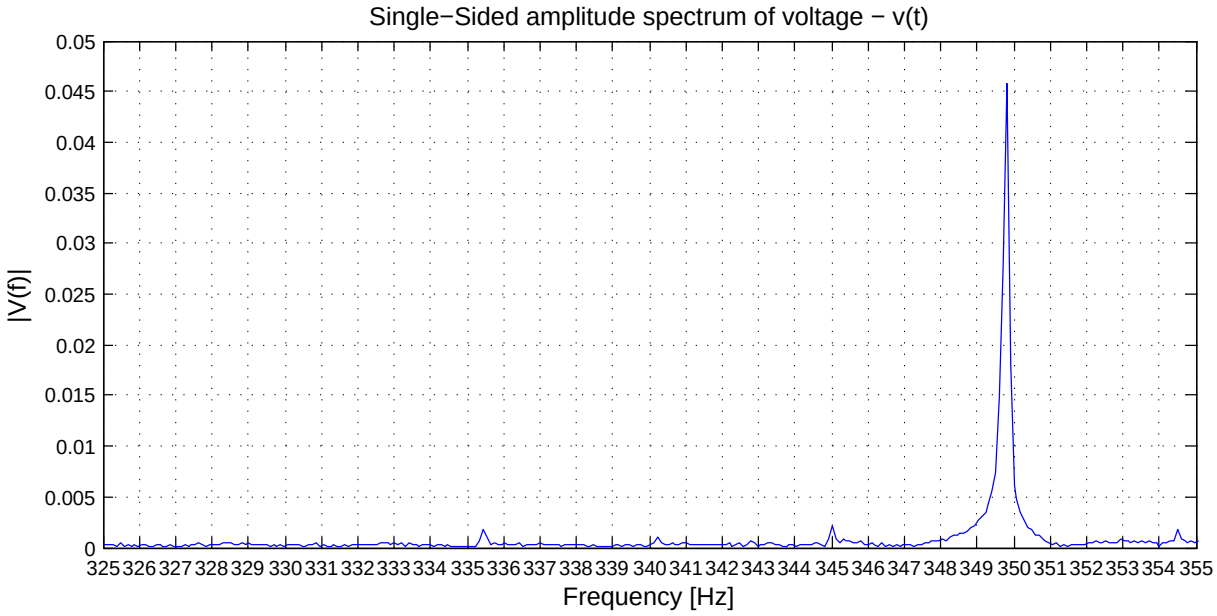

Figure D.12: Amplitude spectrum of machine stator voltage V_{12} for frequencies around the 7^{th} harmonic frequency. Data is taken from the 10 second interval 15:29:30 - 15:29:40, in Figure C.4, where the rectifier is connected. The machine is loaded and run at 1430 rpm which is the rated machine speed and gives a slip of 4.67 %. The shunt connected rectifier has a resistance of $R = 22\ \Omega$.

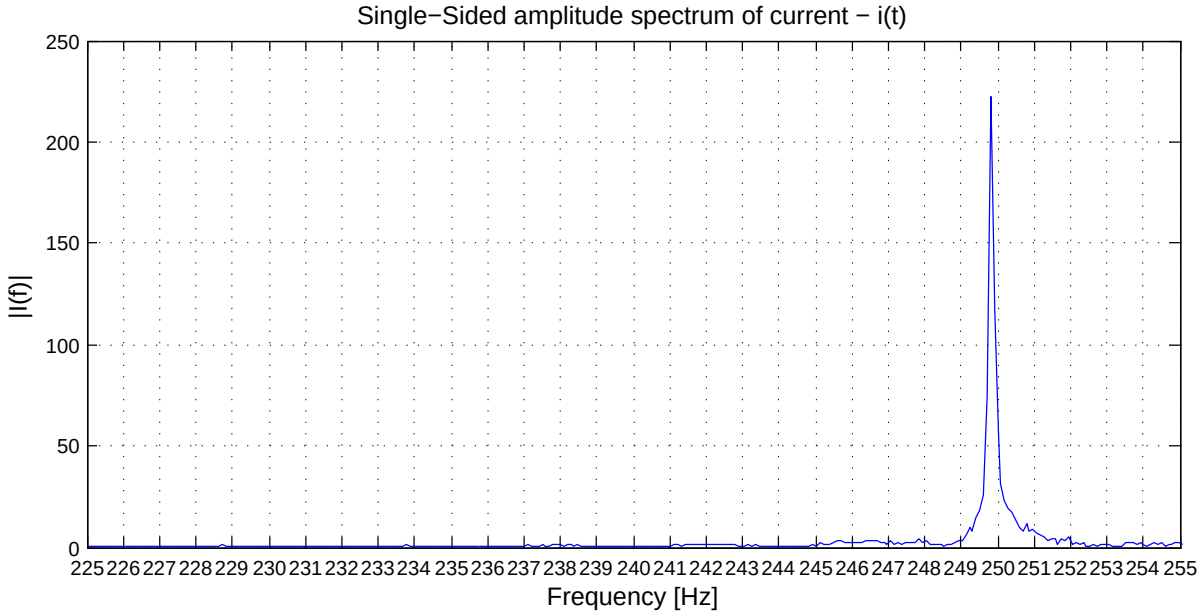

Figure D.13: Amplitude spectrum of machine stator current I_1 for frequencies around the 5^{th} harmonic frequency. Data is taken from the 10 second interval 15:29:30 - 15:29:40, in Figure C.4, where the rectifier is connected. The machine is loaded and run at 1430 rpm which is the rated machine speed and gives a slip of 4.67 %. The shunt connected rectifier has a resistance of $R = 22\ \Omega$.

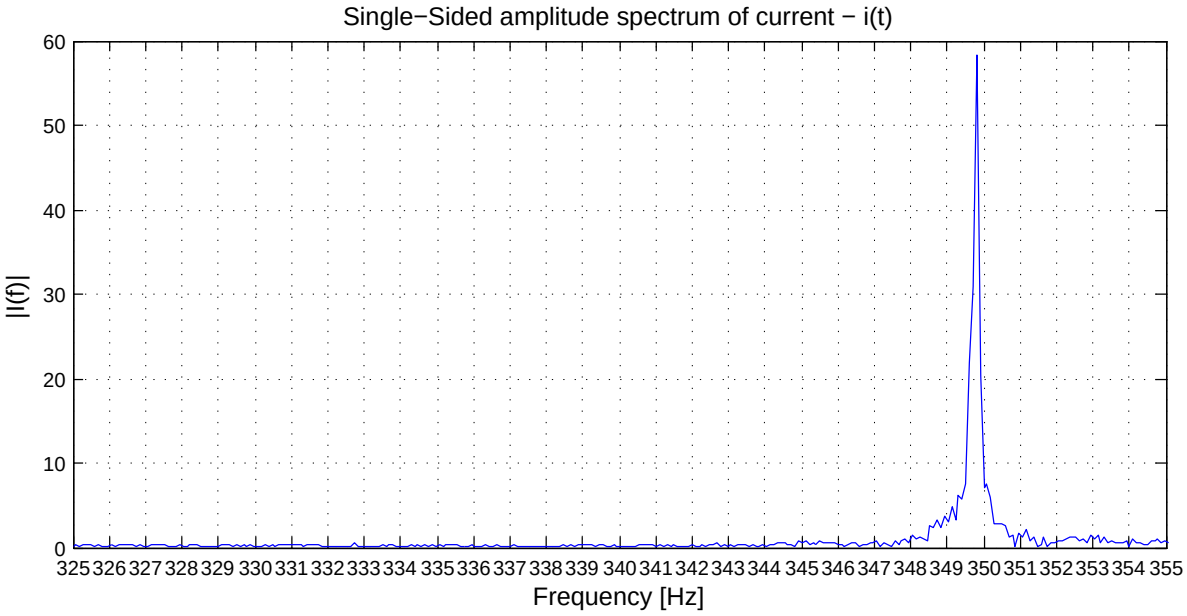

Figure D.14: Amplitude spectrum of machine stator current I_1 for frequencies around the 7^{th} harmonic frequency. Data is taken from the 10 second interval 15:29:30 - 15:29:40, in Figure C.4, where the rectifier is connected. The machine is loaded and run at 1430 rpm which is the rated machine speed and gives a slip of 4.67 %. The shunt connected rectifier has a resistance of $R = 22\ \Omega$.

Appendix E

Another case in Norway

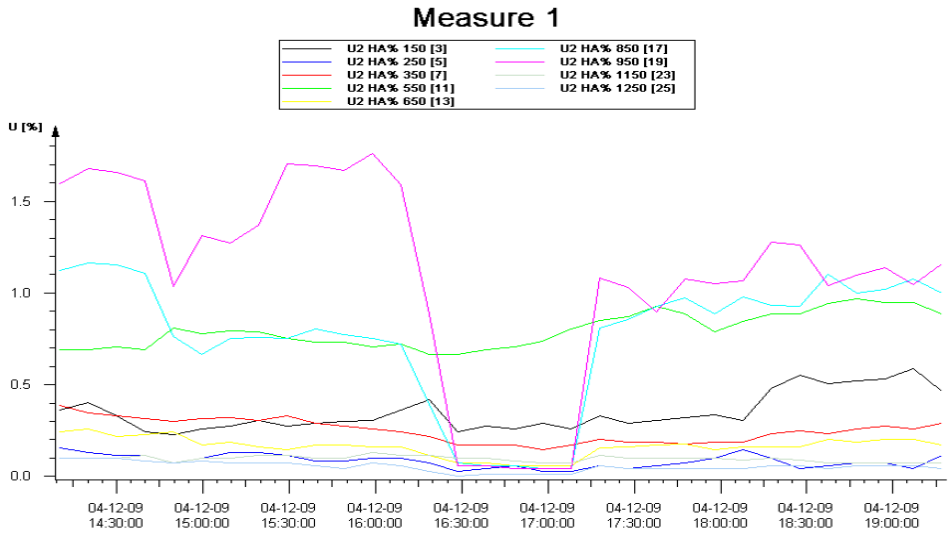

Figure E.1: Image acquired from SINTEF Energy Reaserch. The figure shows harmonic content in a measurement performed somewhere in western Norway. The 19^{th} (magenta colored) and the 17^{th} (turquoise) harmonic are the once causing flicker. An interharmonic component close to the 17^{th} harmonic frequency is expected. [1]

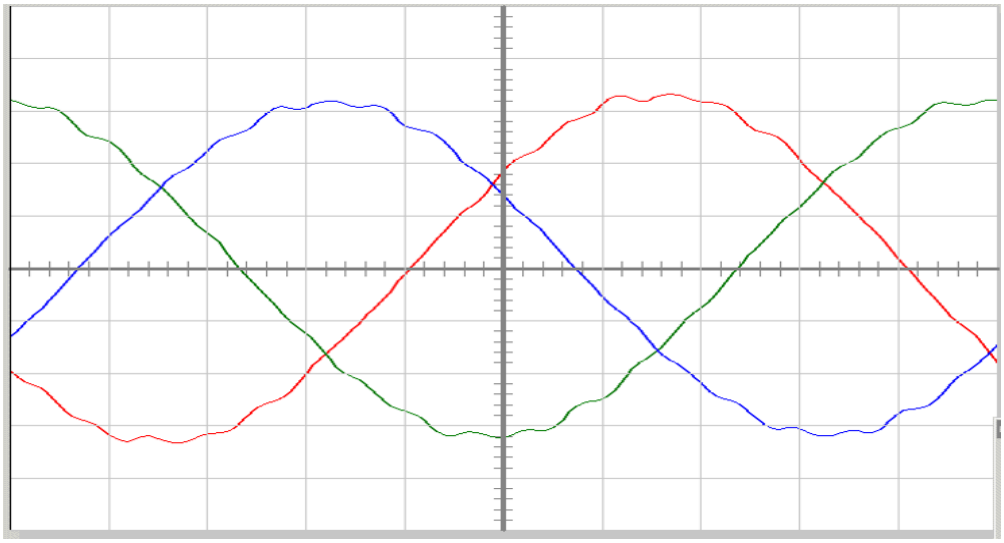

Figure E.2: Image acquired from SINTEF Energy Reaserch. The figure shows the voltage waveforms. The small waves creating the bumpy surface on the sine-waves are the 19^{th} and the 17^{th} harmonics. When monitoring waveforms over time, the small waves move across the sinusoid. This movement indicate an interaction between two different frequency components in close frequency proximity. [1]

Appendix F

Photographies of laboratory set up

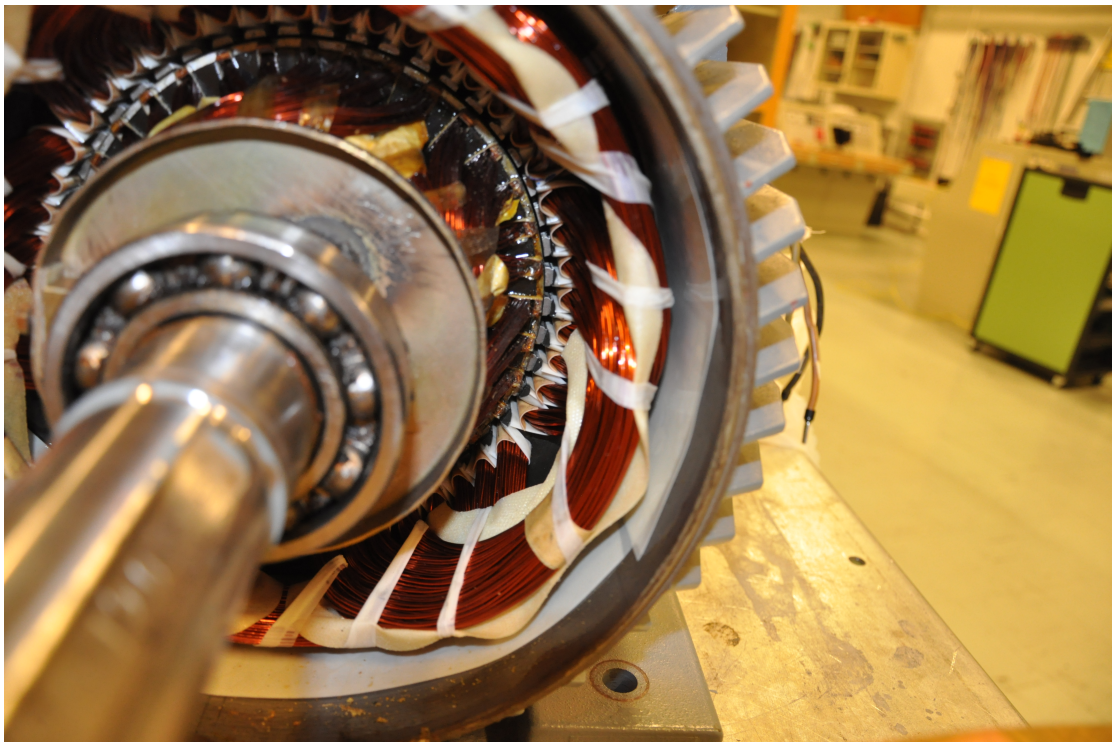

Figure F.1: Picture of open induction machine used for the laboratory exercice.

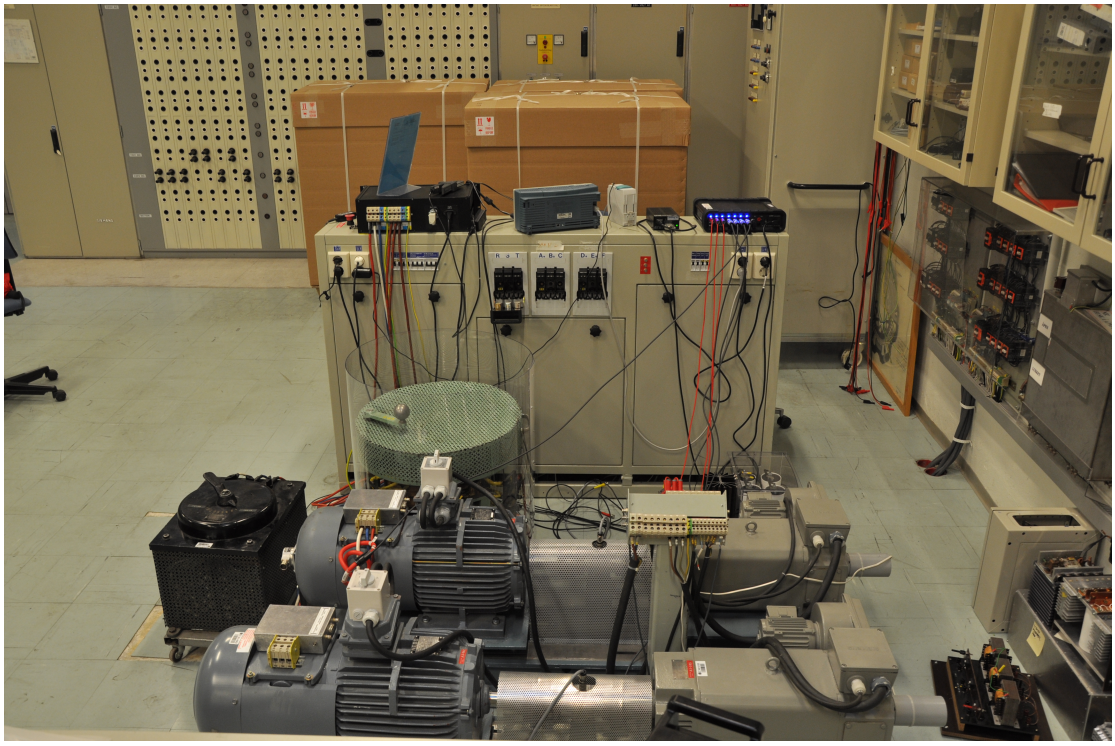

Figure F.2: A view of the complete laboratory set up.

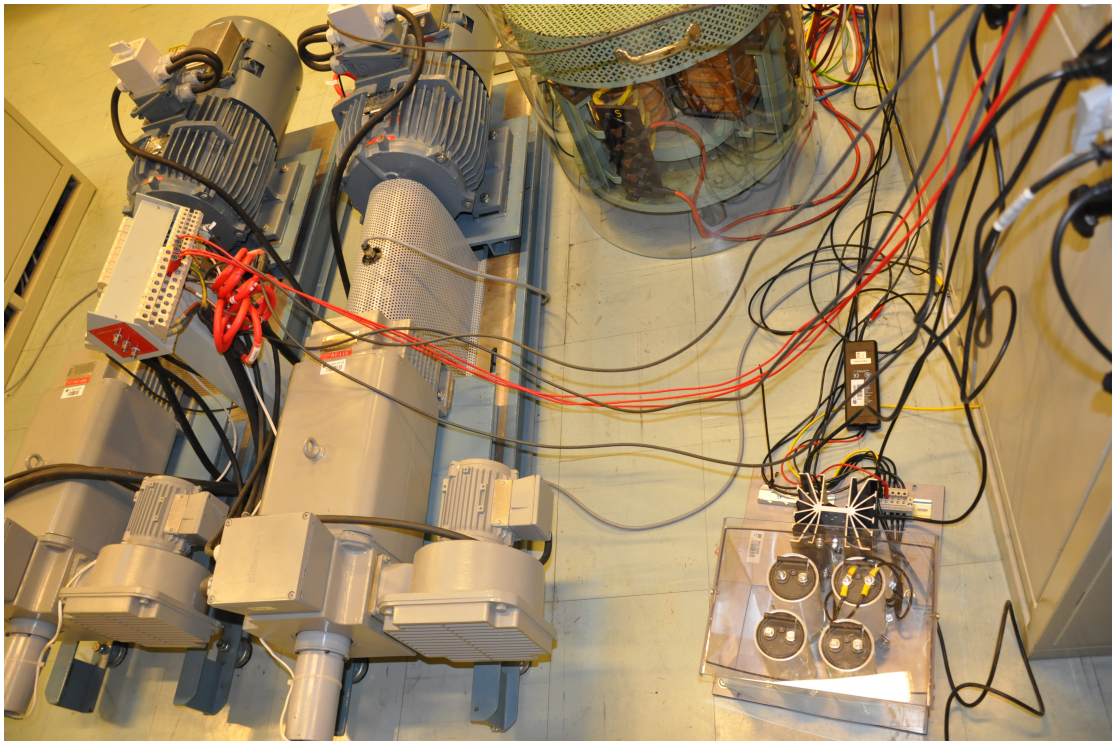

Figure F.3: Laboratory set up from another angle.

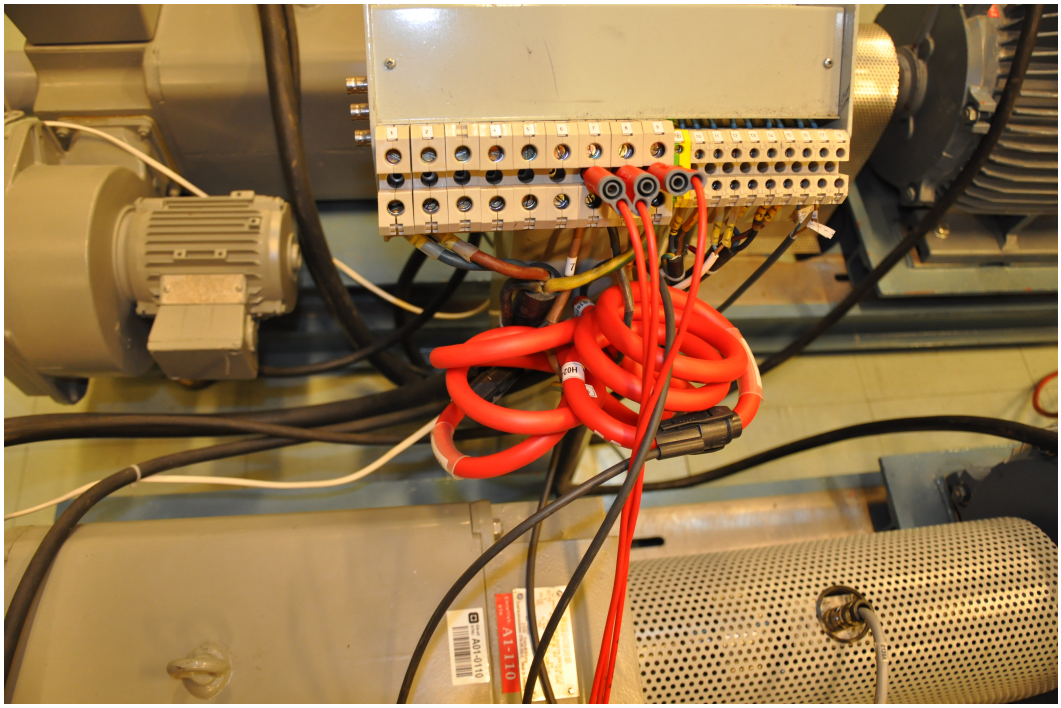

Figure F.4: Measurement arrangement. Three Rogowski coils measureing current, each entangled three turns around one of the conductors feeding the machine stator via the control tower. Also, voltage are measured by the use of banana plugs in the control tower. Measurement data is collected by the ELSPEC instrument.

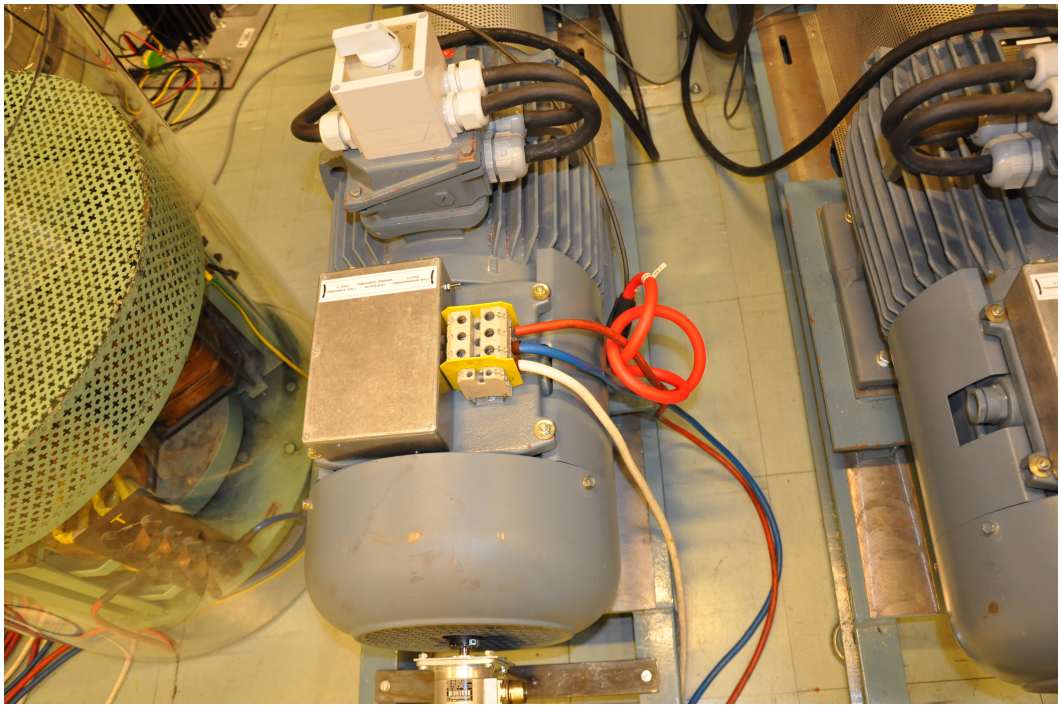

Figure F.5: Induction machine. Red, blue and white wire is connected to the rotor via slip rings, and rotor resistance is connected in the other end. One Rogowski coil is entangled three turns around the red conductor, as a control fr rotor current.

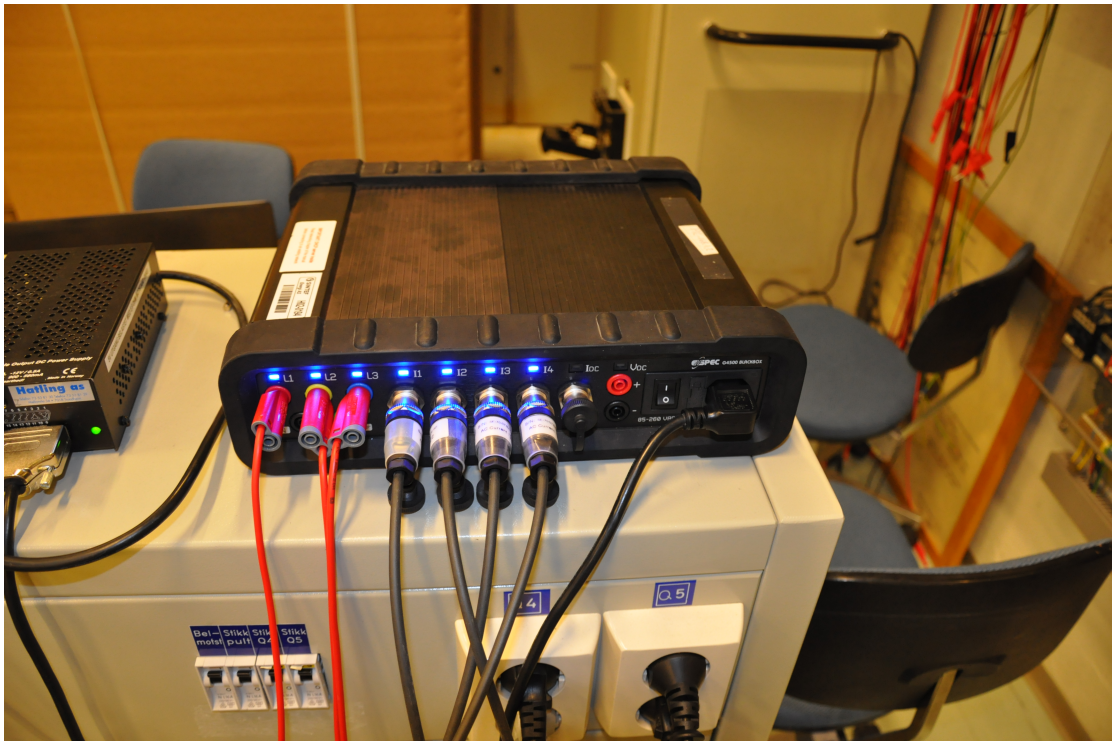

Figure F.6: Measurement equipment delivered by ELSPEC. All measuring wires are connected.

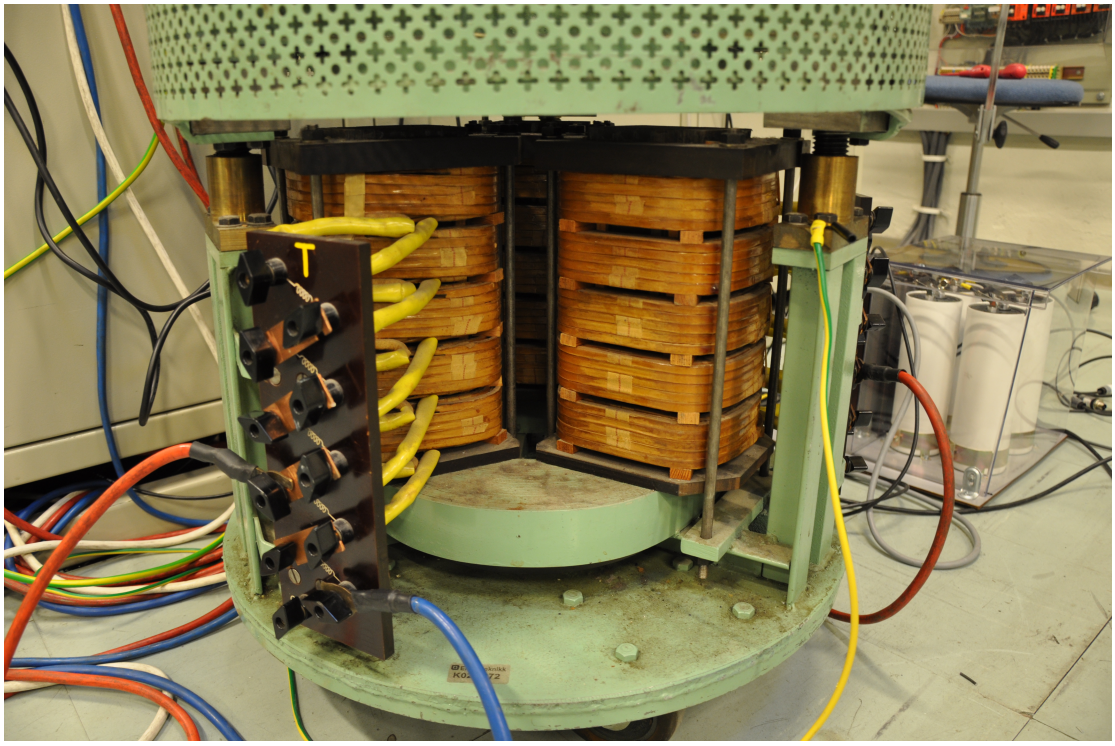

Figure F.7: Variable inductance. Between one and five coils can be connected in series. Adjustable air gap.

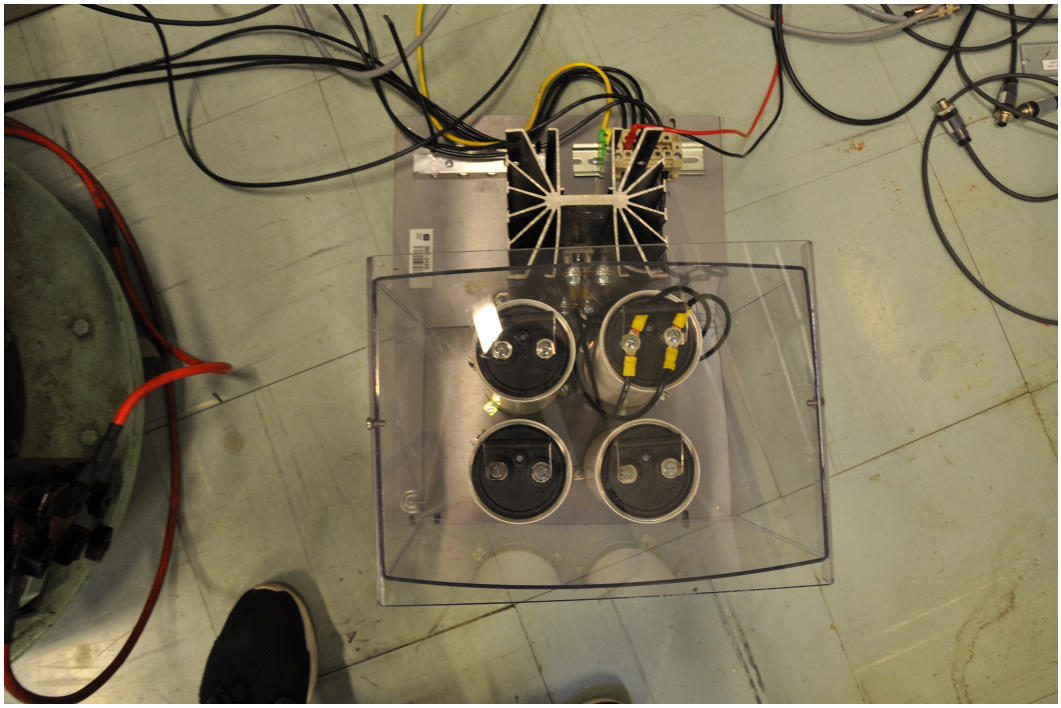

Figure F.8: Three-phase, six-pulse, full-bridge diode rectifier. Four capacitors available to connect as desired at DC side. A heat sink is connected to avoid rectifier overheating.

Figure F.9: Main fuse connecting laboratory circuit to the mains. 36 A fuses are used.

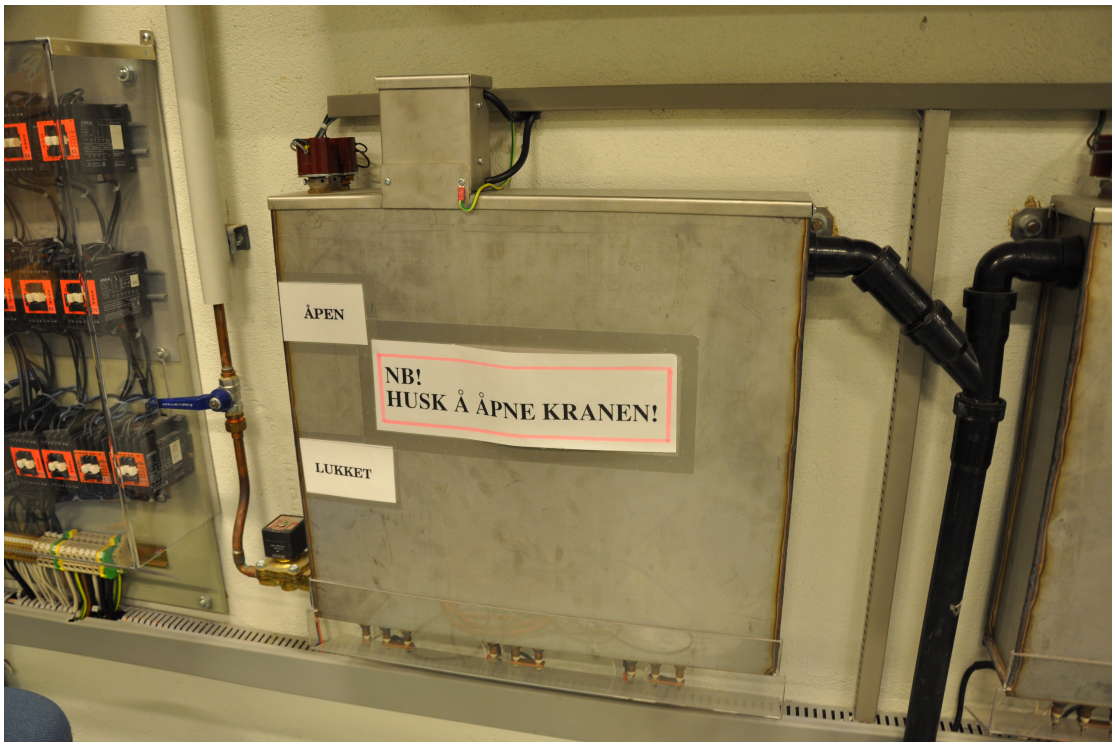

Figure F.10: Water cooled resistance consuming power drawn by rectifier.

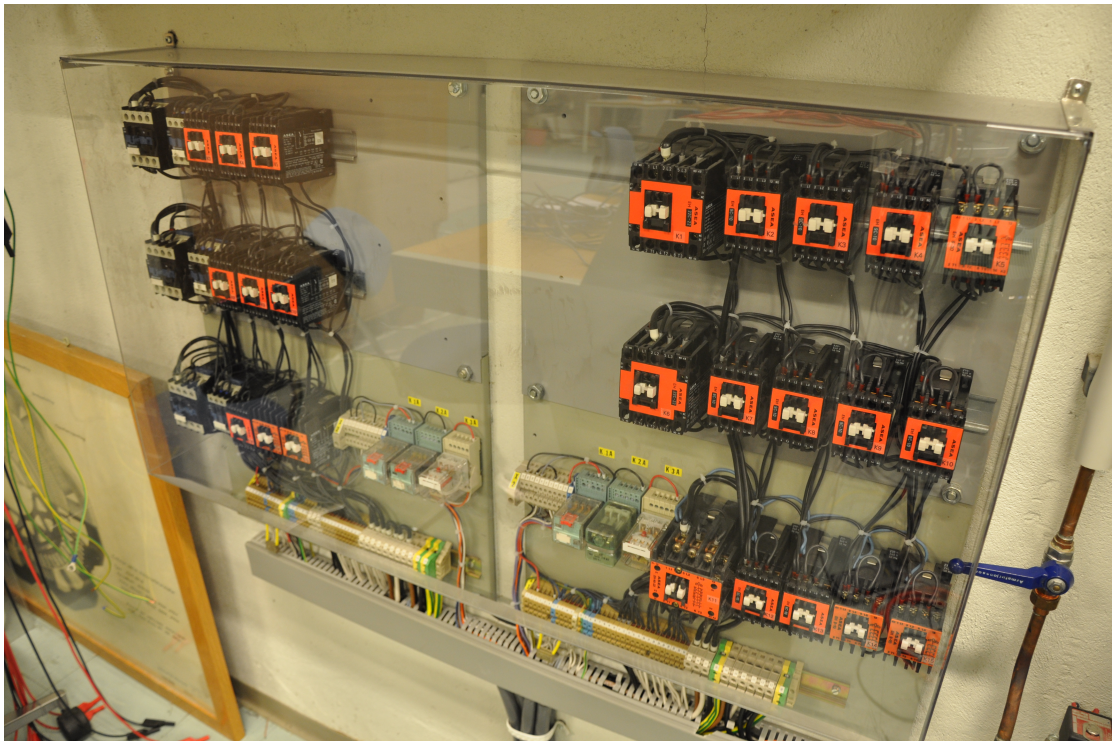

Figure F.11: Switchboard for water cooled resistance, used to connect and disconnected resistances from the circuit.

Figure F.12: Soft start equipment. An internal circuit containing resistance reduce in rush current, and disconnect the resistance after a few periods.

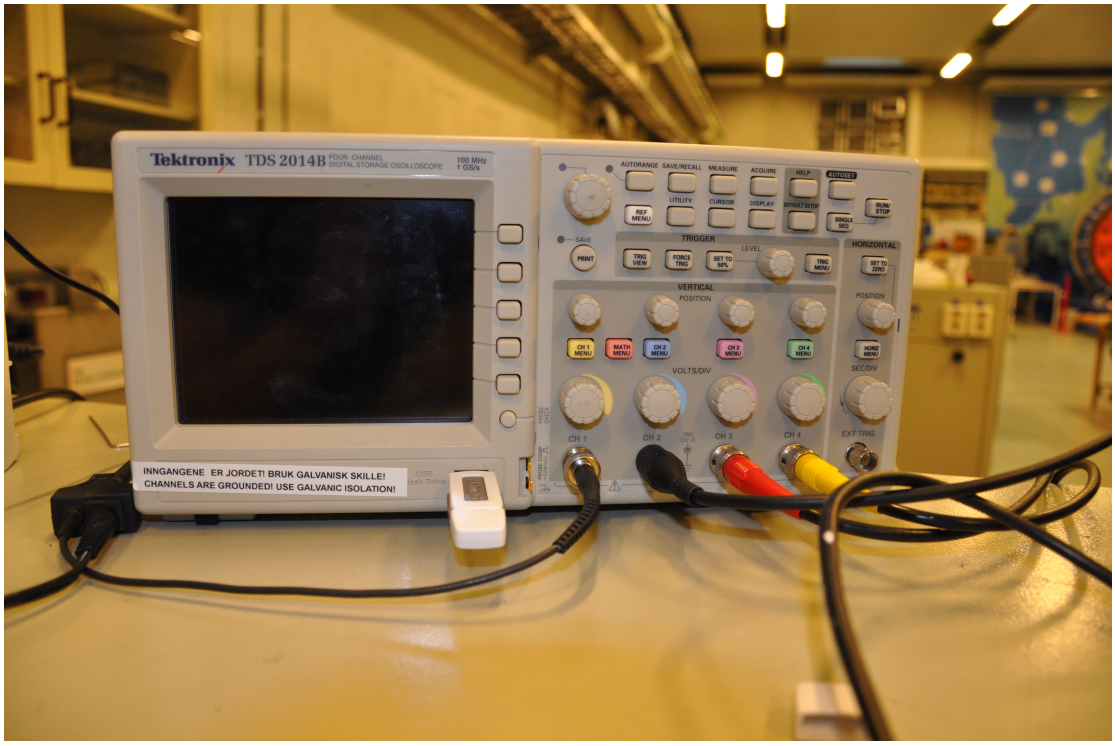

Figure F.13: Oscilloscope. Used for live stream of current and voltage waveforms as well as verification of current and voltage magnitude.

Figure F.14: Current clamp used for current measurements with oscilloscope and FLUKE.

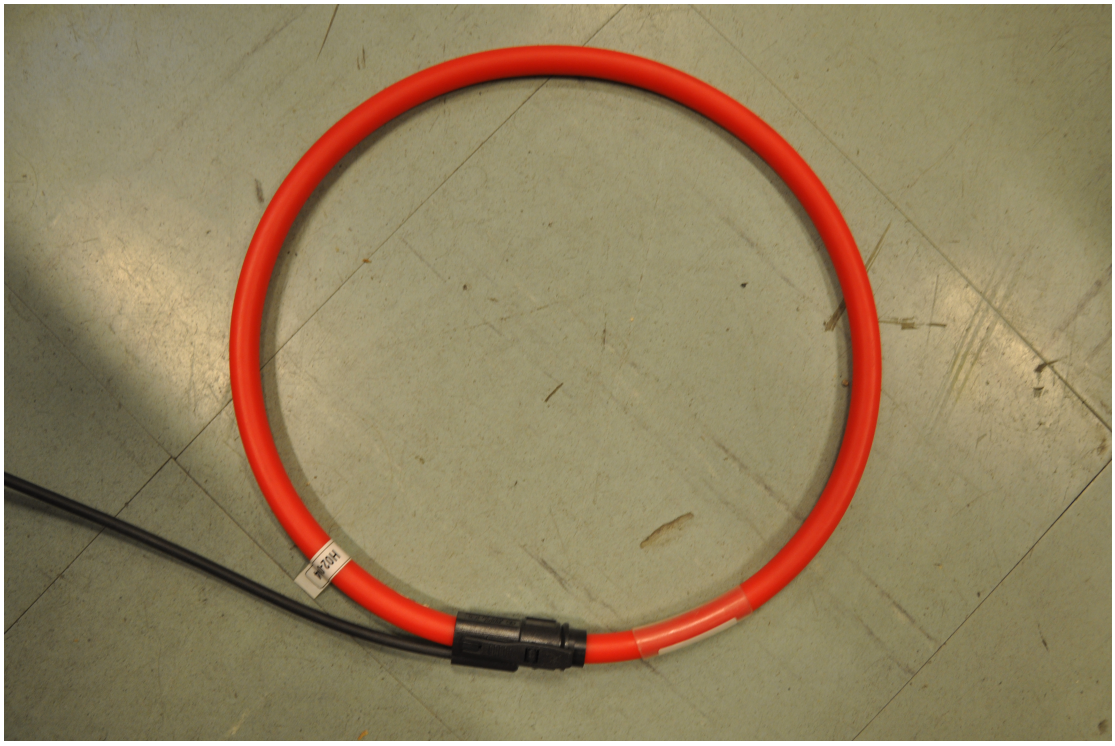

Figure F.15: One of the Rogowski coils used for current measurements with ELSPEC.

Figure F.16: Single phase Power Harmonic Analyzer by FLUKE.

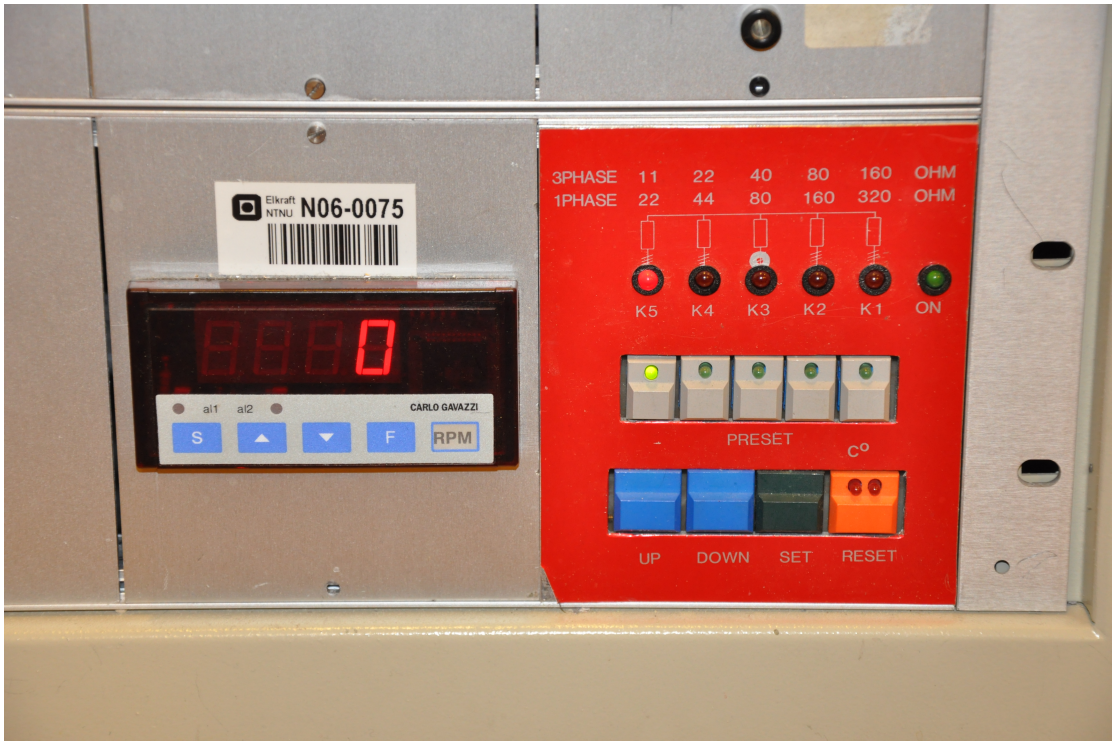

Figure F.17: Speed measurement of machine shaft and console for controlling water cooled resistance.

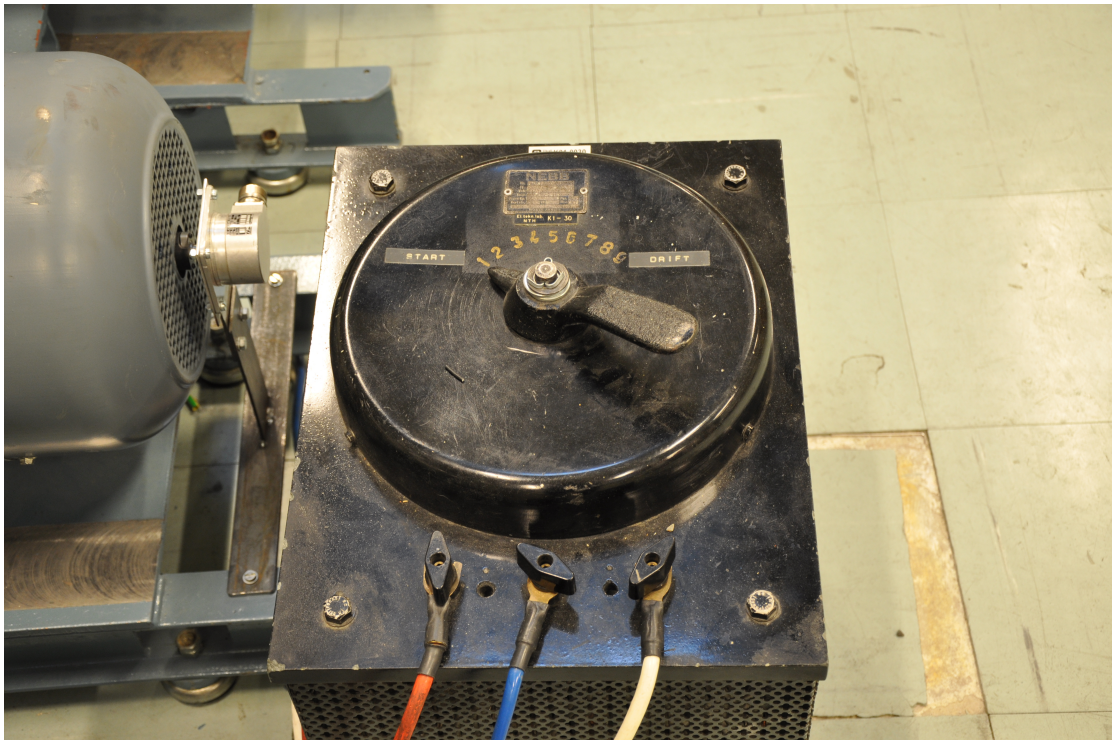

Figure F.18: Variable rotor resistance.

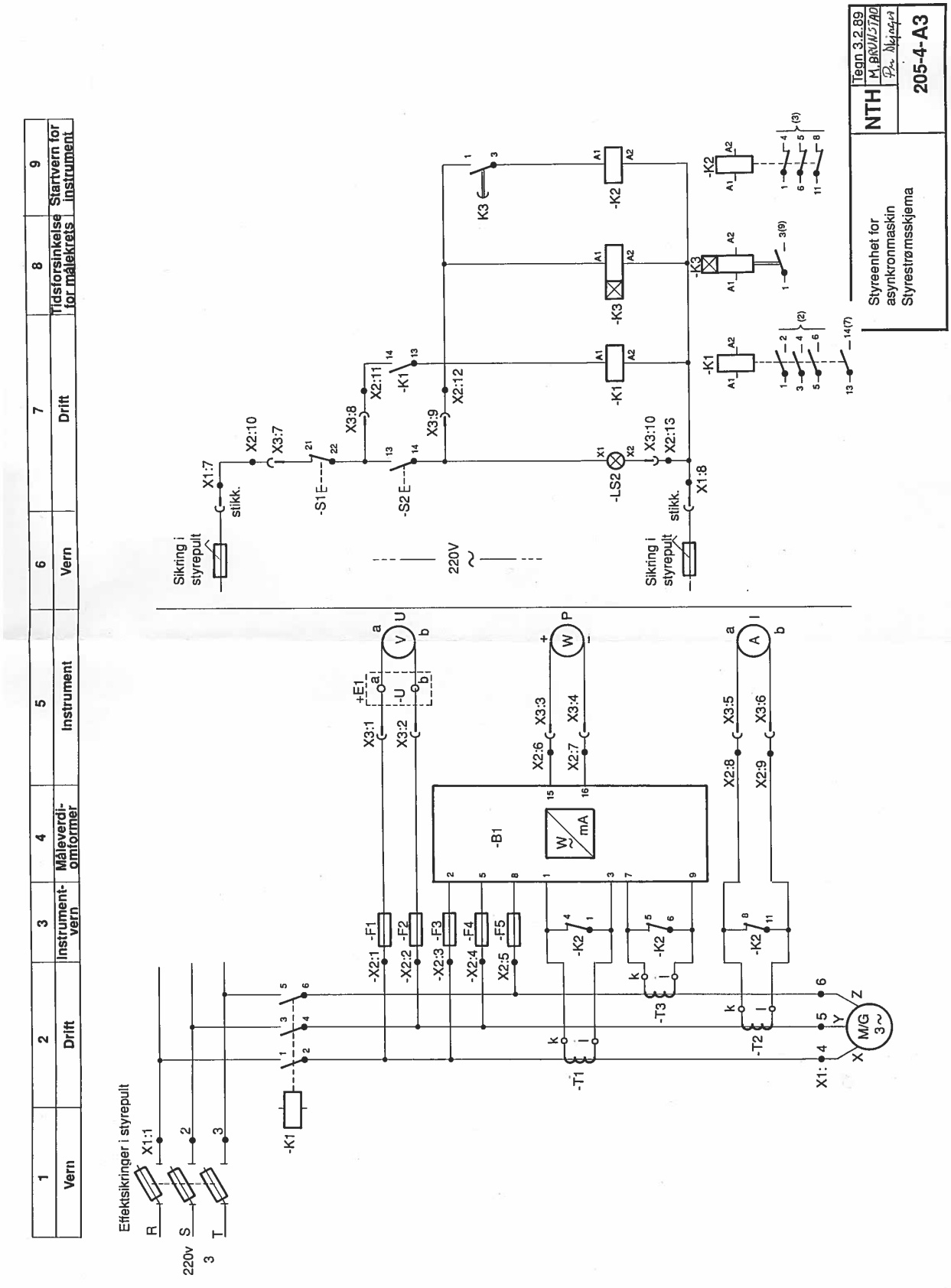
1 Vern
2 Drift
3 Instrument-vern
4 Måleverdi-omformer
5 Instrument
6 Vern
7 Drift
8 Tidsforsinkelse for målekrets
9 Startvern for instrument
Effektsikringer i styrepult
220v 3
R S T
X1:1 X1:2 X1:3
-K1
-F1 -F2 -F3 -F4 -F5
-X2:1 -X2:2 -X2:3 -X2:4 X2:5
-T1 -T2 -T3
M/G 3~
X1: 4 5 6
+E1
X3:1 X3:2
X3:3 X3:4
X3:5 X3:6
X2:6 X2:7
X2:8 X2:9
-B1
W/mA
Sikring i styrepult
X1:7 stikk.
X2:10 X3:7
-S1 -S2
X3:8 X2:11 X3:9 X2:12
-K1 -K2 -K3
K3
220V
-LS2
X3:10 X2:13
X1:8
Styreenhet for asynkronmaskin
Styrestrømsskjema
NTH
Tegn 3.2.89
M.BRUVSTAD
205-4-A3

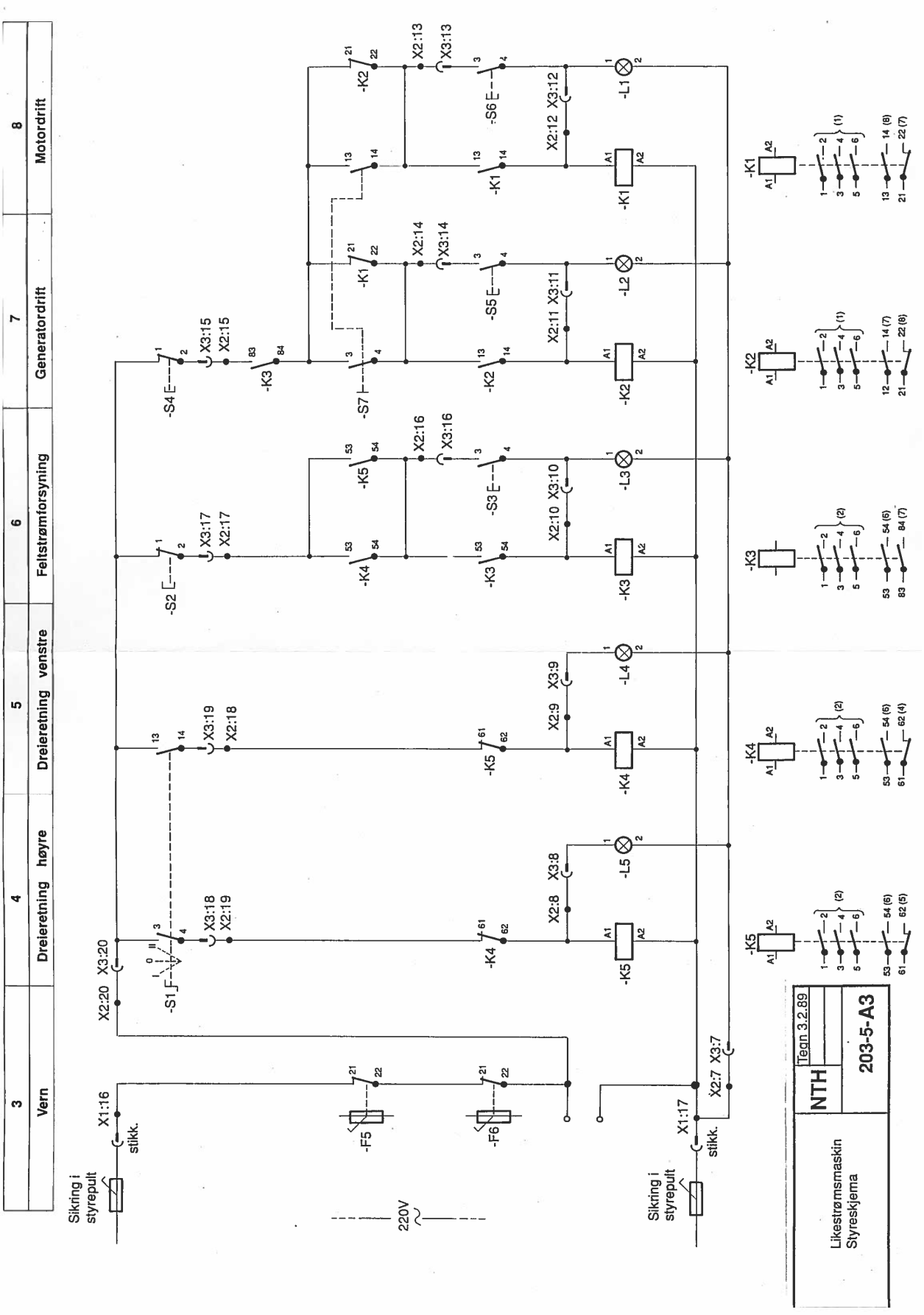
3 Vern
4 Dreieretning høyre
5 Dreieretning venstre
6 Feltstrømforsyning
7 Generatordrift
8 Motordrift
Likestrømsmaskin
Styreskjema
NTH
Tegn 3.2.89
203-5-A3
Sikring i styrepult
stikk.
220V
-S1
-S2
-S3
-S4
-S5
-S6
-S7
-K1
-K2
-K3
-K4
-K5
-L1
-L2
-L3
-L4
-L5
-F5
-F6

Appendix G

MATLAB code

Matlab script running Simulink simulation and post processing data:

```
%Script that run Simulink simulation

clear all
close all
clc

%Set values of variable parameters
V_l=188;                    % Amplitude of phase voltage in IT network.
                            % RMS line voltage is 230 V
freq=50;                    % System frequency
Ls=3.37e-6;                 % Upstream inductance
C_d=2.07e-3;                % DC side filter capacitor
%R_load=10;                 % DC side resistance
%Ls_2=0.4e-3;               % Size of second inductance. Only used in one
                            % version of the Simulink model

%Diode values
Ron=0.001;
Lon=0;
FV=1;
Snubb_res=1e3;
Snubb_cap=inf;

%Simulink simulation

power_vector=[];
counter=0;

min_r=2;        % Input parameters.
max_r=24;
step=2;
points=(max_r-min_r)/step +1;

% This part is included to plot circuit parameters for variabel R_load
for variable_r=min_r:step:max_r
```

```
36      R_load=variable_r;    %Makes R_load variable to allow plotting
37
38  sim('rectifier')
39
40  time=multi.time;
41
42  % Extract data from the simulations. Not all of this is used.
43
44  %Voltages from simulations
45
46  L_sa_v=multi.signals.values(:,1);       % Voltages over inductance
47  L_sb_v=multi.signals.values(:,2);
48  L_sc_v=multi.signals.values(:,3);
49  ACa=multi.signals.values(:,4);          % Voltages measured at the source
50  ACb=multi.signals.values(:,5);
51  ACc=multi.signals.values(:,6);
52  R_load_v=multi.signals.values(:,7);     % Voltage across resistive load
53  v_d=multi.signals.values(:,8);          % Voltage across capacitor
54  V_ab=voltage.signals(1,1).values;       % Line voltage ab
55  V_bc=voltage.signals(1,2).values;
56  V_ac=voltage.signals(1,3).values;
57
58  v_tot=L_sa_v+L_sb_v+L_sc_v;
59  v_d_avg=mean(v_d);
60  v_d_rms=rms(v_d);
61
62  v_d_ripple=v_d-v_d_avg;                          % ripple voltage
63  V_ripple=(max(v_d_ripple)-min(v_d_ripple))/2     % ripple amplitude
64
65  v_line_rms=rms(V_ab);                            % RMS of line voltage
66
67  voltage_percent=v_line_rms/(V_l*sqrt(3)/sqrt(2))*100
68
69  %Currents from simulations
70
71  L_sa_i=multi.signals.values(:,9);       % Current in inductor
72  L_sb_i=multi.signals.values(:,10);
73  L_sc_i=multi.signals.values(:,11);
74  R_load_i=multi.signals.values(:,12);    % Current in load
75  C_d_i=multi.signals.values(:,13);       % Current in capacitor
76  i_d=id.signals(1,1).values;             % Current at DC side
77
78  i_tot=L_sa_i+L_sb_i+L_sc_i;
79  i_d_avg=mean(i_d);                      % average output current
80  i_d_rms=rms(i_d);                       % RMS of output current
81
82  i_d_ripple=i_d-i_d_avg;                          % ripple current
83  I_ripple=(max(i_d_ripple)-min(i_d_ripple))/2     % ripple amplitude
84
85  i_L_rms=rms(L_sa_i);                    % RMS of inductor current
86
87  % Power
88
89  P_in_inst=i_tot.*v_tot;
90  P_in_avg=mean(P_in_inst);
```

```
91
92  P_out_inst=R_load_v.*R_load_i;
93  P_out_avg=mean(P_out_inst);
94
95
96  P_in_ac=3*i_L_rms*(v_line_rms/sqrt(3));   % Power at AC side after inductor
97
98  end
99  % power_vector
100 R_DC=linspace(min_r,max_r,points);
101
102 % Plotting figures. Some are commented out, depending on the simulation
103
104 % figure;
105 % subplot(3,1,1)
106 % plot(R_DC,power_vector)
107 % xlabel('DC resistance (ohm)')
108 % ylabel('Power (W)')
109 % title('Power plot')
110 %
111 % subplot(3,1,2)
112 % plot(R_DC,voltage_vector)
113 % xlabel('DC resistance (ohm)')
114 % ylabel('Voltage (V)')
115 % title('DC voltage plot')
116 %
117 % subplot(3,1,3)
118 % plot(R_DC,current_vector)
119 % xlabel('DC resistance (ohm)')
120 % ylabel('Current (A)')
121 % title('DC Current plot')
122 %
123 % figure;
124 % subplot(3,1,1)
125 % plot(R_DC,voltage_vector_ac)
126 % xlabel('DC resistance (ohm)')
127 % ylabel('Voltage (V)')
128 % title('RMS AC voltage plot')
129 %
130 % subplot(3,1,2)
131 % plot(R_DC,voltage_vector)
132 % xlabel('DC resistance (ohm)')
133 % ylabel('Voltage (V)')
134 % title('DC voltage plot')
135 %
136 % subplot(3,1,3)
137 % plot(R_DC,v_rel_vector)
138 % xlabel('DC resistance (ohm)')
139 % ylabel('V_D_C/V_R_M_S')
140 % title('Relationship between RMS voltage and DC voltage')
141
142 m =length(V_ab);          % Number of data points. m=2000001
143 dt=5e-06;                 % Time step defined in Simulink
144 fs=1/dt;                  % Sampling frequency
145
```

```
146 time=(0:m-1)*dt;          % Time vector
147
148 %Plot current and voltage for the first 8 periodes of the simulation
149
150 figure;
151 subplot(2,1,1)
152 plot(time(1:m/60),V_ab(1:m/60))    % m/60=3.3333e+04 data points. 4000 data
153                             % points per period. 3.3333e+04/4000=8.33 periods
154 xlabel('Time (s)')
155 ylabel('Voltage (V)')
156 title('Time plot of line voltage ab downstream of inductors')
157 %legend('Line voltage')
158
159 subplot(2,1,2)
160 plot(time(1:m/60),L_sa_i(1:m/60),'r')
161
162 xlabel('Time (s))')
163 ylabel('Current (A)')
164 title('Time plot of inductor current in phase a')
165 %legend('Inductor current')
166
167 %FFT plot with data from all 10 seconds of simulation
168
169 %[YfreqDomain,frequencyRange] = positiveFFTtest(L_sa_i,fs);
170
171 % figure;
172 % %subplot(2,1,1)
173 % stem(frequencyRange,abs(YfreqDomain));
174 % xlabel('Freq (Hz)')
175 % ylabel('Amplitude')
176 % title('Amplitude spectrum of current')
177 % grid
178 % axis([0,360,0,25])
179
180 % Set data points used for fft plot generation. 4000 data points are one
181 % periode of fundamental frequency of 50 Hz. In total 2000001 datapoints
182 % (incl. t=0) constitute all 10 seconds.
183
184
185 % Inductor current fft
186 new=L_sa_i(8000:12000); %Data point 50000 corresponds to 0.25 sec. dt*50000=0.25
187 [YfreqDomain,frequencyRange] = positiveFFTtest(new,fs);
188
189 figure;
190 stem( frequencyRange,abs(YfreqDomain));
191
192 xlabel('Frequency (Hz)')
193 ylabel('Scaled amplitude')
194 title('Amplitude spectrum of current')
195 grid
196 axis([0,360,0,20])
197
198 %-----Another FFT plot - Line voltage at induction machine connection point
199 newvolt=V_ab(20000:24000); %Data point 50000 corresponds to 0.25 sec. dt*50000=0.25
200 [YfreqDomain,frequencyRange] = positiveFFTtest(newvolt,fs);
```

```
201
202 figure;
203 stem(frequencyRange,abs(YfreqDomain));
204
205 xlabel('Frequency (Hz)')
206 ylabel('Scaled amplitude')
207 title('Amplitude spectrum of line voltage')
208 grid
209 axis([0,360,0,180])
210
211 %Plot DC voltage for 17ms
212 % figure;
213 % plot(time(1:m/60),R_load_v(1:m/60));
214 % title('Voltage across resisitve load')
```

Matlab script performing the FFT of the signal. A part of post processing data form the Simulink simulation:

```
1  function [X,freq]=positiveFFTtest(x,Fs)
2  N=length(x);     % get the number of points
3  k=0:N-1;         % create a vector from 0 to N-1
4  T=N/Fs;          % get the frequency interval
5  freq=k/T;        % create the frequency range
6  X=fft(x)/N;      % normalize the data
7
8  % Only want the first half of the FFT, since it is redundant
9  length(X);
10 cutOff = ceil(N/2);
11
12 % take only the first half of the spectrum
13 X = X(1:cutOff);
14 length(X);
15 freq = freq(1:cutOff);
```